To the Graduate Council:

I am submitting herewith a dissertation written by Ramzi Behnam Abdul-Ahad entitled "Effects of Restrained Thermal Movement in a Continuous, Prestressed Concrete Bridge without Interior Expansion Joints." I recommend that it be accepted in partial fulfillment of the requirements for the degree of Doctor of Philosophy, with a major in Civil Engineering.

Edwin G. Burdette

Edwin G. Burdette, Major Professor

We have read this dissertation and recommend its acceptance:

Jerry E. Stoneking

W. W. Goodpasture

Harry L. Johnson

Accepted for the Council:

L. Evans Roth

Vice Chancellor
Graduate Studies and Research

EFFECTS OF RESTRAINED THERMAL MOVEMENT IN A CONTINUOUS, PRESTRESSED CONCRETE BRIDGE WITHOUT INTERIOR EXPANSION JOINTS

A Dissertation

Presented for the

Doctor of Philosophy

Degree

The University of Tennessee, Knoxville

Ramzi Behnam Abdul-Ahad

June 1981

ACKNOWLEDGMENTS

The writer wishes to express deep appreciation to the Iraqi government for their encouragement and support throughout the course of the study.

Special appreciation is due to Dr. Edwin Burdette for his advice and encouragement which contributed greatly to this dissertation.

The author also wishes to acknowledge the Tennessee Department of Transportation for providing the facilities which made this research possible.

The author also acknowledges Dr. David Goodpasture for his guidance and suggestions on this study. Also a special word of thanks to Dr. J. E. Stoneking and Prof. H. L. Johnson who served on the graduate committee and assisted in the review of the manuscript.

Special thanks are due to Bill Long, Jim Frei and Sherman Green for their help in the laboratory work and collection of data.

Gratitude is expressed to Abdallah Jubran for his encouragement, to Scott Wilhoite for his help in preparing the figures, to Mrs. Vikki Webb for her assistance in typing the first draft.

The assistance of Mrs. Maxine Martin, who typed the final draft of this dissertation, is appreciated.

Finally, the author wishes to express to his wife, Araksi, his sincere appreciation and gratitude for her constant encouragement and her enthusiasm during his study at The University of Tennessee, Knoxville.

ABSTRACT

In their standard practice for the design of bridges for thermal effects, the AASHTO Specifications call for expansion devices to be taken into consideration in design. In recent years, the Tennessee Department of Transportation has taken the lead in the omission or reduction in the number of expansion joints in designing bridges for temperature effects. This reduction in expansion devices decreases the maintenance and construction costs as well as improves the riding quality. The bridge which is the subject of this investigation is 2700 feet long and has no expansion joints except at the abutments. Strains and movements will be induced due to the continuity and restraint of the structure.

An understanding of bridge behavior due to thermal effects is needed for the designer. Most of the existing codes have no direct provisions which guide the designer on how to calculate the thermally induced stresses and movements.

The purposes of this dissertation are manifold. Its primary purpose was to develop and present a theoretical method for calculating thermal stresses and movements in continuous bridge structures. Another objective of this research was to collect and analyze experimental data obtained from strain gages and thermocouples that have been placed in the piers and deck. A third purpose was to compare the field data obtained with those predicted from theory.

The nonlinear distribution of temperature throughout the depth of superstructure, which was obtained from measurements, was divided

into two parts: a linear temperature distribution which causes deformation and another part which is nonlinear and results in self-equilibrating stresses which do not cause any deformation of the structure.

From the comparisons made between the data obtained from field measurement and the method presented in this research, a good agreement was achieved for stresses and movements.

It was also shown that the thermal stresses were typically greater than dead load stresses, and that the movements of the deck were proportional to mid-deck temperature.

TABLE OF CONTENTS

PAGE

LIST OF TABLES

LIST OF FIGURES

FIGURE PAGE

NOTATION

A = total area of the cross section

At = area of the top slab

b_y = total width of the section, exclude voids, at distance y from the origin

C_t = distance from centroid of the composite section to the top of the slab

e = distance from centroid of the top slab to the top of the section

E = modulus of elasticity

f_b = thermal stress in the bottom flange of the girder

f_{c1} = concrete stress in the top slab

f_{c2} = stress due to axial force

f_{c3} = stress due to moment at the top fiber

f_{c4} = stress due to moment at the bottom fiber

f_y = eigenstress

h = depth of the section

I = moment of inertia of the section

k = stiffness of the member

L = solar radiation received on a horizontal surface

L = span length

n = constant depending on the section depth

p = total force at the top slab

R_1, R_2 = resistances in Wheatstone bridge

R_c = calibration resistor

S_g = gage factor

T = temperature which is uniform across the depth of the section

T_a = average daily air temperature, in degrees Fahrenheit

T_m = maximum surface temperature, in degrees Fahrenheit

T_r = daily range in air temperature, in degrees Fahrenheit

T_s = temperature difference between the top and bottom of the slab

T_1 = temperature at the top fiber of the section

T_2 = temperature at the bottom fiber of the section

t_y = temperature at distance y from the bottom of the section

y = vertical distance from bottom of the section to fiber in question

$\bar{y}$ = the vertical distance of the centroid from the bottom of the section

α = coefficient of thermal expansion

α_g = coefficient of thermal expansion of gage material

β = coefficient of thermal expansion of base material

γ = temperature coefficient of resistivity of gage material

Δt = change in temperature at any section

ΔT = change in temperature between the top and bottom of the section

ΔTm = maximum temperature differential between the top and bottom of the deck

$(\frac{\Delta R}{R})_{\Delta t}$ = change in gage resistance due to temperature change Δt

ε = strains due to applied load

ε_{app} = apparent strain

ε_c = calibration strain

ε_R = indicated strain

ε_s = strain produced by stress

λ = lag factor

σ = stress

ϕ = curvature

CHAPTER I

INTRODUCTION

1.1. THE PROBLEM

Bridge structures are affected by daily and yearly temperature changes. These temperature changes cause longitudinal movement, and when these movements are restrained, they can produce large thermal stresses.

The American Association of State Highway and Transportation officials in their specifications state that "in continuous bridges provision should be made in the design to resist thermal stresses induced or means should be provided for movement caused by temperature changes".[16] Expansion devices and joints used as standard practice in bridge design frequently cause serious problems because of their high construction and maintenance cost. Most of the existing codes do not offer the designer any direct method or information on how to convert temperatures to stresses upon which the design will then be used.[22]

The use of prestressed concrete bridges has become more popular for long span bridges. Because of more efficient distribution of moments, it is preferable for long structures to be continuous over the supports. A recent innovation in Tennessee has been the use of expansion devices only at the two abutments, with the result being a shallower construction depth, lower maintenance costs, and improved riding quality due to the absence of expansion joints in the bridge deck. Little information presently exists to provide guidance as to whether or not the omission of expansion devices will cause problems in bridges longer than some particular value and, if so, what that limiting length is.

1.2. DESCRIPTION OF THE PROJECT

The Department of Civil Engineering at The University of Tennessee, Knoxville, under a research grant from the Tennessee Department of Transportation, is currently investigating a prestressed concrete bridge recently completed on State Route 137 over the Holston River at Kingsport, Tennessee. This bridge was monitored to find the magnitude of the stresses and strains induced by temperature changes. What makes this bridge the subject of a research project is the fact that even though it is a long structure which, under standard practice procedures, calls for many expansion joints, none was provided except at abutments. Some Tennessee bridges have been constructed without expansion joints in recent years, but none of them is as long or as important as the bridge now under investigation at Kingsport.

The bridge, approximately 2700 feet long, consists of 29 spans. The cross section of the bridge for each of the two roadways consists of four prestressed concrete box girders for most spans, and five box girders for some spans. A typical cross section of the bridge with four girders are shown in Figure 1.

In this research project both internal stresses (and strains) and external deformations due to thermal load effects will be studied. Test data were obtained by placing instrumentation in the bridge during its construction.

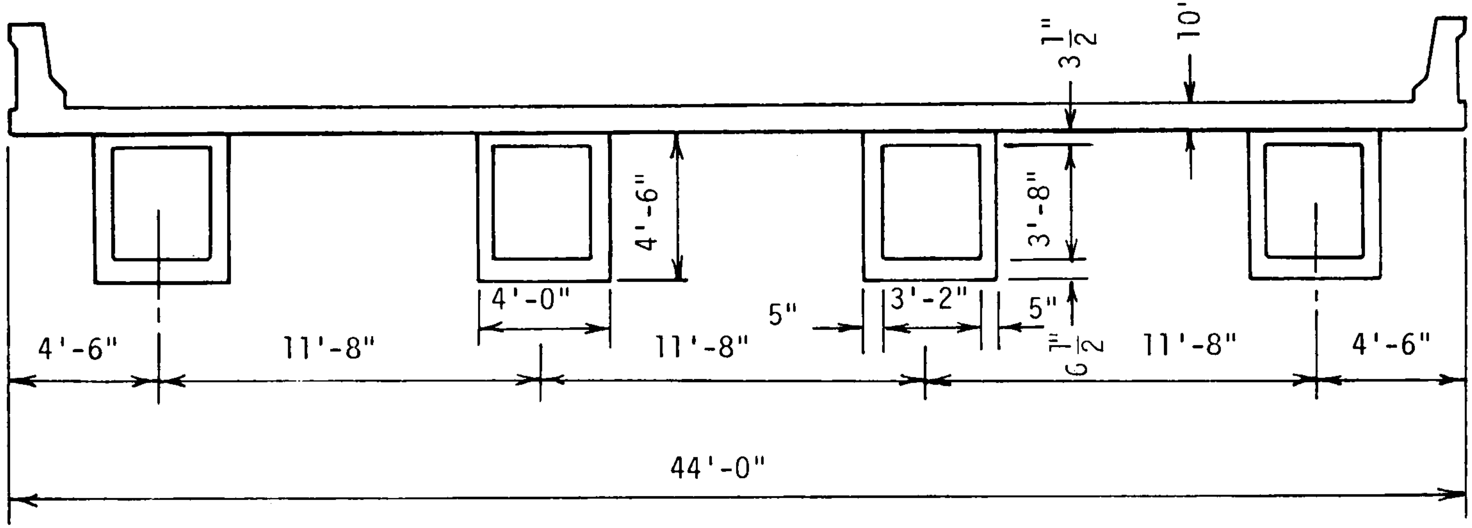

Figure 1. Typical deck cross section.

1.3. INSTRUMENTATION

Two types of instrumentation were used on this project. The first includes electronic devices such as resistance strain gages, Carlson stress meters, and thermocouples. The second type of instruments used are mechanical measuring devices consisting of scales, levels, and a Whittemore strain gage. These devices are placed at selected locations in the piers and deck of the bridge. The uses and application of the measuring devices used on this project are explained in a report by Terry Scholes[15] and are explained later in this report.

1.4. PURPOSE

The purpose of the research reported in this dissertation is threefold: The first objective is to develop and present a theoretical method for calculating thermal stresses induced in continuous bridge structures.

The second objective is to analyze experimental data obtained from strain gages that have been placed in the piers and deck. The measured results will then be compared with analytical and computer results for different models devised. The model will then be modified and improved, if need be, to achieve agreement with field data.

Finally, from the comparison of field and theoretical results, it is hoped that useful information will be provided for designers of this type of bridge.

1.5. BRIDGE TEMPERATURE

The fact that concrete has low heat conductivity creates a difference of temperature between the upper and lower surfaces of the structure. The temperature at the bottom elements of the bridge is usually that of the surrounding atmosphere.[22] The temperature of the upper elements and the exterior beams will vary depending upon the amount of solar radiation received, the wind, and the amount of precipitation.[2] When the sun shines on the deck of the bridge, the top of the deck slab is warmer than the bottom of the bridge. The top of the deck slab will cool faster than the girders when a rain or snow storm first begins. Thus, a variety of temperature distributions across the depth of a bridge are possible.[19] The study of these temperature gradients and their effects will be undertaken in this research through the use of thermocouples located throughout the depth of the structure to measure the temperatures.

1.6. THERMAL STRESS AND STRAIN

The vertical gradients through the depth of the structure can be nonlinear and result in nonlinear stress distributions. The most difficult problem in the study of thermal effects is that either strain or stress, or both strain and stress, can result.[17] If the material is free to expand and the distribution of temperature varies linearly across the depth of the structure, a thermal strain with no thermal stress will exist. On the other hand, if the material is completely restrained from movements at its ends, thermal stresses will exist which result no thermal strains.[13] Most structures are never completely free to move nor are they completely restrained; therefore, a combination of strain and stress is usually present. The presence of strain resulting from creep, shrinkage, and humidity further complicates the study of thermal strains. Thermal stresses have significant values compared to the live and dead load stresses.[7]

CHAPTER II

REVIEW OF LITERATURE

2.1. IMPORTANCE OF THERMAL LOADING CONSIDERATION IN BRIDGES

The use of prestressed concrete as a material for building large bridges has increased because it has allowed the designer greater scope in the choice of cross section, span lengths and structural articulation.[9] However, this added choice of alternatives is not problem-free and introduces new problems not hitherto encountered. Thermal effects become more apparent than ever before when long spans are being considered. Bridge behavior under thermal loading needs further investigation. This was expressed editorially in 1960.[20] The following points were especially emphasized: (1) Neglecting the thermal effects in the design of structures has caused many damages previously; (2) Thermal strains have values comparable to live and dead load strains as obtained from measurements, and adequate provisions should be made for them; (3) To keep thermal strains under control, close consideration should be given to preventing structural damage; (4) In some cases, it may prove to be more feasible and economical to design the structure to resist the thermal strains rather than to make provisions for free movement.

2.2. REVIEW OF RELATED RESEARCHES

2.2.1. W. Zuk[20]

Since 1960, considerable work to calculate the thermal stresses and strains of continuous structures has been done. Zuk recorded the daily and yearly temperature distributions and found that thermal stresses were affected by air temperature, wind, humidity, radiation, and type of material. In a composite bridge structure, the upper elements of the deck are heated by solar radiation from the top down through the slab. The bottom elements are shaded most of the day and maintain the same temperature as that of the air. Thus, nonlinear temperature distributions are possible throughout the depth.

A sixty-six foot composite steel girder and concrete slab was studied by Zuk for temperature effects. Twenty-four iron-constantan thermocouples were placed at various points throughout the depth and width of the bridge to record temperatures on an hourly basis. A 10-in Whittemore strain gage was used in obtaining strain readings. All the thermally-induced strain readings were taken only under dead load and constant slab moisture conditions in an attempt to isolate the thermal strains from other strains. The temperatures in the composite bridge were recorded for one year, then a 1-in thick coating of sprayed foam urethane insulation was applied underneath the concrete deck and the exposed portion of the steel beams in the middle portion of the bridge. Temperature readings were taken for both cases, the gray-white concrete and black-gray bituminous concrete. The color effects make the darker surface to absorb more short-wave solar radiation, thus raising the bituminous temperature approximately 15°F higher than that of the normal concrete on a sunny summer afternoon.

Barber[1] developed an equation relating weather factors to a maximum surface temperature of the bridge. Zuk developed coefficients for use in Barber's equation for two conditions. One, for normal concrete deck in the Middle Atlantic States, the maximum surface temperature in degrees Fahrenheit is:

$$T_m = T_a + 0.18L + 0.667\ (0.50\ T_r + 0.054L)$$

where

T_m = maximum surface temperature, in degrees Fahrenheit,

T_a = average daily air temperature, in degrees Fahrenheit,

T_r = daily range in air temperature, in degrees Fahrenheit, and

L = solar radiation received on a horizontal surface, in gram-calories per square centimeter per day (Langleys).

Two, the maximum surface temperature of a bridge deck covered with a thin bitumen would be:

$$T_m = T_a + 0.027L + 0.65\ (0.50\ T_r + 0.081L)\ .$$

For other regions, the constants would vary depending on the local conditions. The value of L (Langleys of solar radiation) can be determined from U.S. Weather Bureau maps.

For sunny summer afternoons, the maximum surface temperature of a black-topped deck was found to be about 15°F higher than for the normal gray-white concrete deck. A temperature differential between the top and bottom of the deck (ΔT_m) was found to occur, and its exact calculation is a complex matter. The following simplified equation was developed:

$$\Delta T_m = T_m - T_a - \lambda T_r$$

in which λ = the lag factor indicating the phase lag between the maximum surface temperature and the maximum ambient temperature, varying from 1/4 in the summer to 1/2 in the winter. The results obtained from the above equation were compared with the measured temperatures and showed a fair agreement.

From the one-year test data for the 66-ft composite bridge, it was found for the uninsulated bridge that the high temperature was 123°F on the top surface of the deck with an air temperature of 97°F, and the low temperature was -6°F at the bottom of steel beam with air temperature also of -6°F. For the uninsulated bridge, the maximum temperature differential was 37°F for interior beams and 42°F for exterior beams. For the insulated bridge the temperature differentials were 25% greater than those of the uninsulated deck. On sunny days the temperature at the top surface of the deck was 20°F to 30°F higher than the ambient air temperature by mid-afternoon.

For the composite bridge, it was concluded that there was interface slip between the steel and the concrete deck. This caused several of the 1-in anchor bolts at supports to bend. A large temperature differential would induce higher thermal stresses than a large overall temperature change. So, it was concluded by Zuk that a temperature differential of 40°F to 50°F was capable of stressing the members beyond the allowable when combined with dead load and live load stresses.

Zuk derived two sets of equations to determine the stresses and deflection for the composite steel beam bridge with concrete deck and for the composite prestressed concrete beam with concrete deck. Divergent results were obtained between the theoretical and the measurement stress distribution.

In 1965, six simple span composite steel girder bridges ranging in span from 47 ft 3 in to 71 ft 5 in were tested.[22] A 10-in Whittemore gage was used to measure the strain at the upper and lower part of the girder flanges. Several strain and temperature readings were recorded under dry, zero line-load conditions. A simple empirical formula relating thermal stresses at the bottom of the flange to the temperature difference between the top and bottom of the slab and the depth of the bridge was obtained as follows:

$$f_b = 2500 \frac{T_s}{h}$$

in which f_b = the thermal stress in the bottom flange of the girder (positive if tension, negative if compression), in psi;

T_s = the temperature difference between the top and bottom of the slab (positive if the temperature at the top of the slab is greater than at the bottom, and negative if the temperature at the top is less than the temperature at the bottom), in degrees Fahrenheit; and

h = the total section depth of the bridge, in inches.

The above equation must be tested for different climatic conditions. For bridges in the region of Charlottesville, Va., where the tests were made, it was found that maximum temperature differences of +40°F and -10°F occur in summer and winter, respectively.

Three years later, the end movements of various types of highway bridges were studied for a period of one year.[21] Four types and different span lengths of bridges were included in this investigation: (1) simply supported composite bridge with steel girders and concrete deck having a span of 62 ft-7 in; (2) simply supported composite bridge of prestressed concrete beams and concrete deck having a span of 72 ft-1 in with a skew of 20 deg-12 min-16 sec; (3) simply supported reinforced bridge of span 72 ft-1 in with a skew of 29 deg-30 min; (4) a noncomposite, continuous, steel beam and concrete deck bridge, with three spans of 170 ft-3 in long and a skew of 2 deg-15 min. (A zero skew is a right angle crossing.)

The ambient air temperature, the movement at the top joint of the girder, the movement at the bearing of the girder, and the rotation at the end of the girder were recorded for each hour. It was found that an inexact relationship existed between the air temperature and the movements and that the movement was subject to a lag time from one to seven seven hours. It was also observed that the movements at the top and bottom of the bridge were different, due to the rotation of the end of the girder. Zuk recommended that in design it was practical to assume that the end movements were equal to about twice the theoretical movement. The theoretical values of the movement were equal to the product of the span of the bridge, the ambient temperature change, and the coefficient of expansion of the material.

2.2.2. Liu and Zuk[8]

In 1963, Liu and Zuk investigated thermoelastic effects in prestressed flexural members. Four types of prestressed concrete members were studied: (1) a simply supported prestressed beam with straight tendons; (2) a simply supported prestressed beam with parabolic tendons; (3) a simply supported prestressed beam with straight tendons, composite with a concrete slab; and (4) a simply supported prestressed beam with draped tendons, composite with a concrete slap. The temperature was assumed to vary in any manner across the depth of the member, nevertheless, it was assumed constant at any given horizontal layer. Many simplifying assumptions such as neglecting the effects of creep, shrinkage and the interface slip between the beam and the slab were made. Theoretical concepts involved the separation of the flexural members into their basic elements of beam, slab, and tendon, subjected to their temperature. Then, proper restraining forces were applied to these elements in order to make all strains compatible with actual combined forms. The force in the tendon, the deflection, the moment, and the interface shear force between the beam and the slab caused by temperature changes were determined by solving four equations.

Liu and Zuk solved numerical examples for the four different cases of prestressed members. It was found that a temperature differential of 25°F with a parabolic distribution across the depth induced thermal stresses and deflection in the beam within the allowable design limit. Nevertheless, two special observations were made relating to interface forces and transverse stresses. Large interface shearing forces and moments up to 30434 lb and 122877 in-lb, respectively, for typical simply supported beams used in highway bridges were found. High transverse stresses in the slab where the slab spans many beams were observed. In the examples solved by Zuk and Liu, values from 800 psi in compression to about 1000 psi in tension were calculated as transverse stresses. Thus, some cracking may occur if no provisions are made for temperature reinforcement. The deflections were about 0.04% of the span length. Liu and Zuk concluded a good agreement between the experimental data which were mentioned in Buyon's book and their theoretical result for the deflection of prestressed beam for temperatures up to 175°F at the bottom of the beam.

2.2.3. C. P. Worth[18]

The Hammersmith Flyover is a four-lane viaduct that was built in Britain in 1961. It is a precast, prestressed concrete, continuous structure spanning 2043 ft. The Flyover consists of 16 spans, most of which are 140 ft in length. The major structural element is a continuous, hollow-spine beam 26 ft wide, with depth varying from 6 ft-6 in to 9 ft and supported by central columns. The columns are supported on roller bearings which allow for 10-in of longitudinal movement caused by temperature change, creep, and shrinkage of the concrete. During the construction of the Flyover, many problems occurred as a result of the expansion and contraction of the bridge. These special problems were solved by leaving the abutment end free to move on its bearing until the completion of the conforming section of the structure. One expansion joint was provided to take all the longitudinal movement of the superstructure. The designers provided a total allowance of 14-in movement at the expansion joint. These 14 in included an 8.85-in allowance for temperature movement due to an effective range of 60°F and coefficient of expansion of 6×10^{-6} per °F and 1.85 in for humidity movement, corresponding to a maximum strain of 25×10^{-6}, and 2.75 in for residual creep and shrinkage. Measurements of longitudinal movements and the air temperature inside the structure were made, and it was found that there was no time-lag between the two measurements. The actual temperature range in the concrete was from 31.8°F to 81.5°F, while the external air temperature had a range of 20°F to 92°F.

From the measured values, a set of linear relationships were found between the internal air temperature of the deck and the movements at different periods. The effective coefficient of thermal expansion was then evaluated by drawing an additional straight line representing the means of the straight lines previously obtained. A value of effective coefficient of thermal expansion of 6.25×10^{-6} per °F was obtained, compared to the assumed design value of 6×10^{-6} per °F.

2.2.4. C. F. Steward[17]

In 1969, a study of annual movement of 231 bridge deck expansion joints in 80 bridges was conducted throughout California over a three-year period. Bridge deck expansion joint movements were recorded on an aluminum tube attached to the barrier rail by using a sharp pointed metal scribe. The scribe was fixed to the rail on one side of the expansion joint. When the joint moved, the metal scribe traced a mark on a painted target on the other side. Then, a graduated scale with 0.01-in divisions and a 10X magnifying glass were used to measure the scribe mark. The average movements per unit length for concrete bridges were found to be: 0.00027 (Coast), 0.00034 (Valley), 0.00041 (Desert) and 0.00046 (Mountain). For steel structures, the average values were: 0.00041 (Coast), 0.00042 (Valley), 0.00048 (Desert) and 0.00060 (Mountain). California uses the movement per unit length criteria in designing for thermal movement of highway structures. The type of expansion bearing and joint skew had no significant effect on the joint movements due to temperature changes. The movement of the reinforced concrete box girder structures was found to be less than the movement of the other concrete structures; this was due to insulating effects of the air trapped inside the box section. The movements at the expansion joints were found to vary even though the expansion joints were uniformly spaced along the structure. Average apparent thermal coefficients of expansion of 0.0000065/°F and 0.0000053/°F for steel and concrete superstructures, respectively, were found. These values for thermal coefficient were determined based on using the highest movement and temperature range at the bridge location.

From the study made in California, the following recommendations were made in designing for thermal expansion movement: (1) for concrete bridges, the movement per unit length should increase to 0.00032, 0.00026, 0.00021 for temperature range changes of 60°F, 50°F, and 40°F, respectively, for different bridge sites from the values mentioned by the Bridge Planning and Design Manual; (2) for steel structures, the movement per unit length should be based on a coefficient of expansion of 0.0000065; (3) for bridges with one or two expansion joints and diaphragm type abutments, reduce the total length of the structure by

25% of the length between abutments and adjacent joints for designing the expansion joint movement.

2.2.5. D. R. Maher[9]

In Australia, a study of the effects of temperature differential on continuous prestressed concrete bridges was made. From the measurements of temperatures on bridges it was found that the daily maximum temperature differential occurred in the early afternoon and that the minimum gradient across the structure took place in the late evening and in the early morning. Due to this differential in temperature, the structure had a tendency to bend between the end supports with a constant radius if the structure is unrestrained. For continuous structures, moments and strains would exist due to fixity of internal spans. These stresses and strains were dependent upon temperature difference, coefficient of linear expansion, depth of cross section and the degree of indeterminancy of the structure.

For hollow prestressed concrete box sections, a linear temperature distribution across the top slab was assumed. This assumption was consistent with previous measurements taken on the Victoria and West Gate Bridge in Australia. The temperature on the sides and bottom of the box was assumed to be constant. It was concluded from the study that in continuous bridge structures, a large value of tensile stress is produced due to differential thermal effects. The expansion movement along the hollow box section bridge was found to be proportional to the internal air temperature.

2.2.6. M. T. N. Priestley[12]

An analytical study on thermal gradients in bridges was made. In New Zealand, damage to bridges due to thermal stresses has forced engineers to study the effect of temperature on prestressed box-girder bridges. Bending and axial stresses can be induced due to a temperature difference between the top and bottom of a box bridge.

The major objective in the study was to use the basic equilibrium phenomenon to derive simple equations for determining thermal stresses for any cross section under an arbitrary vertical temperature distribution. Four assumptions were made: (1) plane section remains plane; (2) the temperature varies through the depth of the bridge only; (3) the principal of superposition holds; and (4) the material properties are not altered by temperature.

Two equilibrium conditions for a simply supported beam were used in the development of the equations for stresses. First, the total axial force due to temperature variations through the depth of a beam should equal to zero. Second, the moment on the section due to any temperature induced stresses must be zero.

For the temperature distributions, the following form was found:

$$t_y = \frac{\Delta T\ y^n}{h^n}$$ (Varying from a maximum value at the top of the deck slab to zero at the bottom of the beam.)

where:

t_y = temperature at distance y from the bottom of the section;

y = vertical distance from bottom of section to fiber in question;

h = depth of the section;

ΔT = temperature differential between the top and bottom of the section;

n = 2,4,6, ... (depending on the section depth, n = 6 for a section of 4 to 5 ft in depth, n > 6 for a greater depth, n < 6 for a lesser depth).

A value of 60°F for the temperature differential was used to calculate the thermal stresses. This value of temperature agreed with peak temperatures recorded on Australian bituminous concrete surface.[5]

For continuous structures the effect of thermal loading caused major thermal stresses. The following steps were suggested:

1. Calculate the curvature induced by thermal loading.
2. Calculate the deflected shape of the bridge from the curvature calculated in Part 1 by assuming the bridge supported only at the extreme ends.
3. Calculate the reactions at the internal supports which are required to reimpose compatibility at supports.
4. Calculate the bending moments and stresses due to these reactions.

The above theoretical study was followed by a model study of a simply supported prestressed box-girder bridge under thermal loading.[11] A quarter-scale model symbolizing a typical trapezoidal box-grider simply supported beam of 30.5 m (100 ft) was selected. The model consisted of six segments of 1.22 m (4.0 ft) and two solid 0.305 m (1.0 ft) end diaphrams. These segments were prestressed by ten draped tendons, five in each web. An epoxy mortar was used to bond the precast concrete segments. The mortar had a high compressive strength and a high modulus of elasticity, it gained strength rapidly, and its color was close to that of concrete. Electrical resistance strain gages, thermocouples, and strain-gaged deflectometers were installed in the model to determine strain, temperature, and deflection. One-quarter of the model was gaged because of its symmetry. For the thermal load tests, one hundred, 375 watt infrared light bulbs were fixed to the ceiling of the box. From the test of the model bridge, the following results were found for a temperature change of 60°F between the deck slab top and the soffit: (1) upward deflection of 0.67 in at the center of the beam; (2) a compressive stress of 725 psi in the deck slab; (c) a tensile stress of 290 psi in the web; and (4) a compressive stress of 145 psi in the soffit. A comparison between theoretical and experimental results was made, and good agreement between theoretical stresses, deflections and the test results was found.

2.2.7. Reynolds and Emanuel[14]

The problem of thermal stresses and movements in bridges were discussed in general terms, and it was concluded that considerable research was needed to fully understand the actual bridge temperature distributions and the thermally induced stresses.

Reynolds and Emanuel mentioned the German bridge specifications (DIN 1078, 1958) for thermal stress effects in composite construction which states as follows:

> A. Indeterminate structure: A temperature difference of ± 27°F (± 15°C) between the top of the concrete slab and the bottom of steel beam with a straight linear variation shall be considered for thermal effects.

B. Statically determinate structures: The thermal strain effect shall be considered by adding a shrinkage of 10×10^{-15}. These stresses shall be combined with stresses from live load as follows: (a) Full live load + half temperature difference. (b) Full temperature variation and live load reduced by 1% per meter of span to 40 meters span, then constant 40% reduction.

C. Shearing forces due to thermal effects may be distributed as maximum at the end of the girder to zero at a distance equal to the effective width of the slab.

Some other countries such as Austria, Sweden, and Japan considered the effects of thermal stresses in their specifications, but all their provisions essentially based on the German Code.[14]

2.2.8. Emanuel and Hulsey[6]

Emanuel and Hulsey, in 1978, described how the ambient air temperature controlled the distribution of temperature in composite bridges at Columbia, Mo. They found that on a hot day the maximum deck top temperature was 150°F at 2:00 P.M., and the bottom of the bridge deck was 120°F at 4:00 P.M., about 2 hours after the deck top reached its maximum temperature. The maximum temperature differential in the deck was 39°F which occurred at 2:00 P.M. on a hot day for a bridge total depth of 50 in. For a cold day, the minimum temperatures were -8°F for the top deck and -5°F for the bottom deck, and both were measured at 4:00 A.M. The maximum differential in temperature was 18°F and occurred at 2:00 P.M. The study also showed that for a composite bridge, the magnitude of the stresses was influenced by the temperature variation through the depth, the internally induced forces due to difference in coefficients of thermal expansion, and the boundary conditions of the supports.

2.3. POST-TENSIONING INSTITUTE AND PRECAST CONCRETE INSTITUTE PROCEDURE[10]

In 1978, the Post-Tensioning Institute (PTI) and the Prestressed Concrete Institute (PCI) published a manual dealing with precast segmental box girder bridges. The analysis for temperature effects on a precast bridge superstructure was discussed. The temperature changes cause the structure length to increase or decrease in the longitudinal direction. Due to the temperature difference between the top slab and bottom of the box girder, bending moments will result. For the changes in the longitudinal direction of the structure, expansion joints, and/or flexure of piers may be provided.

To study the effects of temperature differential, a simply supported beam with a temperature difference ΔT between the top and bottom of the cross section is shown in Figure 2.

For the purpose of the analysis, the total force P at the top slab required to prevent the top slab from deforming is:

$$P = f_{c1} A_t$$

where $f_{c1} = E \alpha \Delta T$ in which

α = coefficient of thermal expansion,

ΔT = change in temperature,

A_t = area of the top slab, and

f_{c1} = concrete stress in the top slab.

External equilibrium was restored by applying a force P' which is equal in magnitude to force P but opposite in direction. The force P'

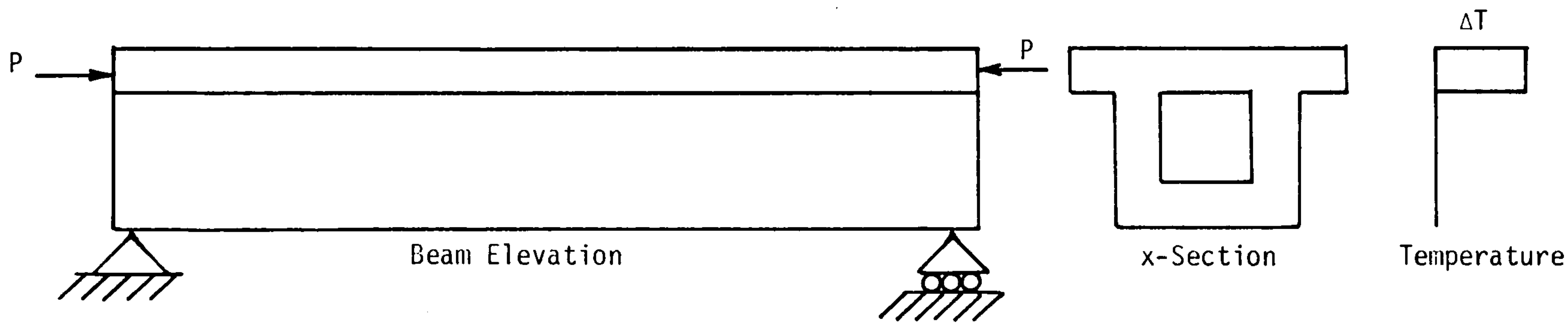

Figure 2. Beam with uniform deck temperature.

can be transmitted to the centroid of the full section by introducing a moment (M) as shown in Figure 3.

$$P' = E\,\alpha\,\Delta T\,A_t$$

$$M = P'\,(C_t - e)$$

where:

C_t = distance from centroid of the composite section to the top of the slab,

e = distance from centroid of the top slab to the top.

The stress in the section due to P' and M will be:

stress due to P': $f_{c2} = \dfrac{P'}{A} = \dfrac{E\alpha\Delta T\,A_t}{A}$

stress due to M at the top fiber: $f_{c3} = \dfrac{MC_t}{I} = E\alpha\Delta T\,A_t(C_t - e)\,\dfrac{C_t}{I}$

stress due to M at the bottom fiber: $f_{c4} = \dfrac{MC_b}{I} = E\alpha\Delta T\,A_t(C_t - e)\,\dfrac{C_b}{I}$

where:

A = total area of the cross section,

I = moment of inertia of the section.

The resulting stresses and the final stress are shown in Figure 4.

For continuous bridges, the following steps were followed to calculate the thermal stresses:

1. Cut the continuous structure over the supports into simply supported beams. Then, calculate the thermal stresses and rotations at supports for simple spans as described before.

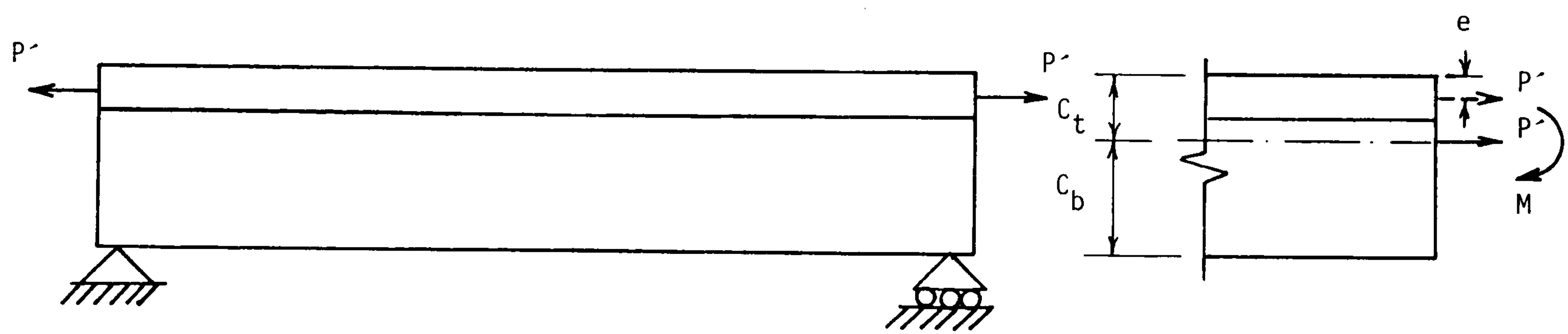

Figure 3. Analysis for thermal load.

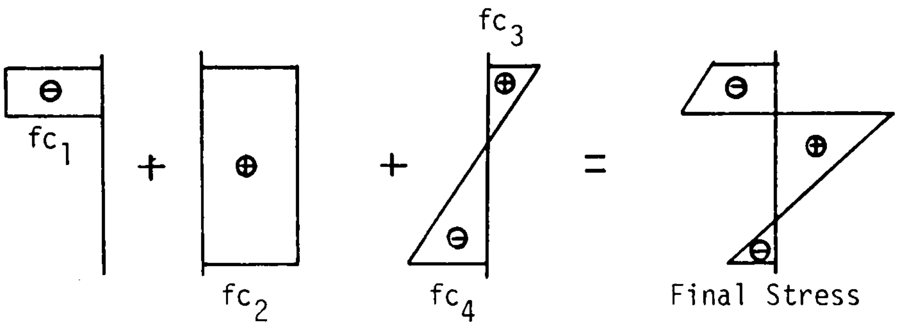

Figure 4. Thermal stresses for the P.C.I. procedure.

2. Calculate the restraint moments required to rejoin the ends of the beams over the supports.

3. The final stresses due to temperature can be obtained by adding the stresses from steps 1 and 2.

2.4. AASHTO CODE PROVISIONS[16]

The 1977 Specifications of the American Association of State Highway and Transportation officials state two sections concerning thermal forces and expansion joints.[16]

Thermal Forces

Provision shall be made for stresses or movements resulting from variations in temperature. The rise and fall in temperature shall be fixed for the locality in which the structure is to be constructed and shall be figured from an assumed temperature at the time of erection. Due consideration shall be given to the lag between air temperature and the interior temperature of massive concrete members of structures. The range of temperature shall generally be as follows:

Metal Structures

Moderate climate, from 0 to 120°F (-17.8 to 48.9°C)
Cold climate, from -30 to 120°F (-34.4 to 48.9°C)

Concrete Structures

	Temperature rise	Temperature fall
Moderate climate	30°F (16.7°C)	40°F (22.2°C)
Cold climate	35°F (19.4°C)	45°F (25.0°C)

Expansion and Contraction

1. In general, provision for temperature changes shall be made in simple spans when the span length exceeds 40 feet (12.192 m).
2. In continuous bridges, provision shall be made in the design to resist thermal stresses induced or means shall be provided for movement caused by temperature changes.
3. Movements not otherwise provided for shall be provided by rockers, sliding plates, elastometric pads or other means.

CHAPTER III

METHOD OF CALCULATION OF THERMAL STRESSES

3.1. FUNDAMENTAL CONCEPTS AND ASSUMPTIONS

It is well known by structural engineers that temperature changes can induce significant stresses in some types of structures. The presence of temperature gradients across the depth of a structure makes the problem relatively complex. The basic assumptions in beam theory are assumed to be applicable. Those assumptions are:[3]

1. Lateral contraction is small in comparison to the depth of the member (i.e., Poisson's ratio may be taken equal to zero).
2. Plane sections remain plane (i.e., strain is proportional to the depth from the neutral axis).

The behavior of a structure due to thermal loading is different from its behavior caused by strain accompanied by stress which results from load application.[13]

The stresses in a structure when thermal loads are present are given as follows:[3]

$$\sigma = E(\varepsilon - \alpha \Delta t) \tag{3.1}$$

where:

σ = stress,

E = modulus of elasticity,

ε = strains due to applied load,

α = coefficient of thermal expansion,

t = change in temperature at any location.

The stresses induced by temperature change are affected by the temperature gradients through the depth of the structure and by the support conditions of the structure. As a general rule, as the order of restraint on the structure increases, the stresses, induced by temperature, also increase.

3.2. CASES OF BEAM END CONDITIONS WITH VARIOUS TEMPERATURE GRADIENTS

3.2.1. Case A: Simply Supported Beam with Constant Temperature

For the uniform temperature, T, through the depth of the beam, a uniform strain, αT, results with no stress as shown in Figure 5.

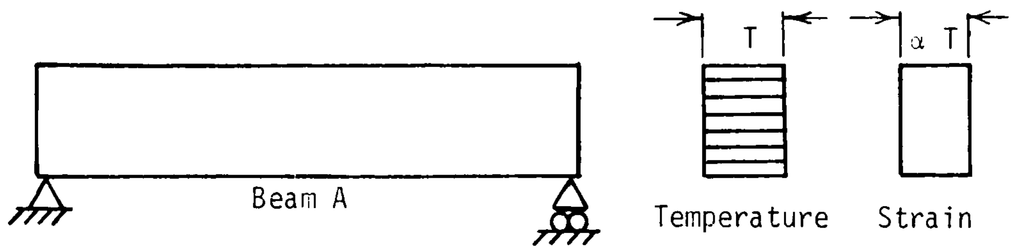

Figure 5. Beam for Case A.

3.2.2. Case B: Simply Supported Beam with Linear Temperature Distribution

Figure 6 shows the beam B will be used to illustrate the stresses induced by a linear temperature differential across the beam depth.

Beam B is simply supported. Let us assume that a change of temperature between the top and bottom of the section, ΔT, takes place across the depth of beam B, with the top at a higher temperature than the

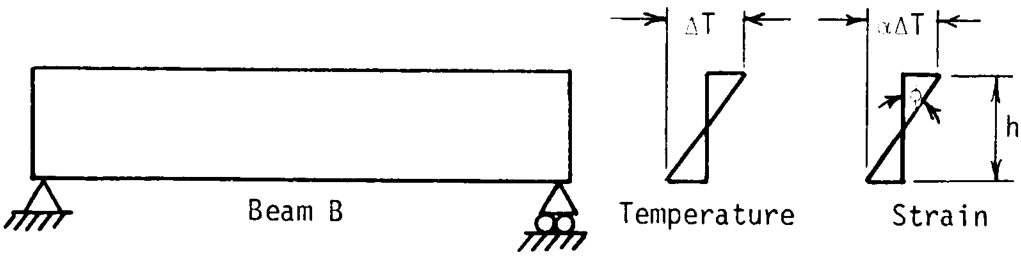

Figure 6. Beam for Case B.

bottom. The increase in the length of the top fiber of the beam will be given by $\alpha \frac{\Delta TL}{2}$ where α is the coefficient of thermal expansion, L is the length of the beam, and ΔT is the change in temperature. By dividing this change in length over the total length, the strain in the top fiber is given by:

$$\varepsilon = \frac{\alpha \Delta TL}{2L} = \frac{\alpha \Delta T}{2} . \tag{3.2}$$

The curvature at any section is given by the gradient of the strain diagram, and as shown in Figure 6, the curvature, ϕ, is as follows:

$$\phi = \frac{\frac{\alpha \Delta T}{2}}{\frac{h}{2}} = \frac{\alpha \Delta T}{h} \tag{3.3}$$

where: h = depth of the section.The conjugate beam method to calculate deflection is well known to structural engineers. In this method the conjugate beam is loaded with the curvature induced by the applied moment. In this case there are no applied moments, but the curvature at all points along the beam is given by Eq. (3.3). The maximum deflection which in this case occurs at mid-span is given by $\frac{\phi L^2}{8}$.

Therefore, the maximum deflection at the mid-span of the beam is equal to

$$\text{deflection at mid-span} = \frac{\alpha \Delta T L^2}{8h} \tag{3.4}$$

For this beam there are no stresses induced but the deflection at mid-span is given by Eq. (3.4).

3.2.3. Case C: Fixed End Beam with Linear Temperature Distribution

Let us now consider the beam C with fixed supports and a linear temperature variation ΔT throughout its depth as illustrated in Figure 7. Since this structure is indeterminate we must first define the primary structure. If we select the end moments as redundants, the primary structure is identical to the case analyzed in beam B. The slope at the two ends can be calculated from the conjugate beam to be equal to $\frac{\phi L}{2}$ (Figure 8).

The redundant moments must induce a slope of equal magnitude to those in the primary structure but opposite in direction as shown in Figure 9. It is apparent that the slopes induced at the support by two equal moments M are given by $\theta = \frac{M}{EI}\frac{L}{2} = \frac{\phi L}{2}$. Solving for M:

$$M = \frac{\phi L}{2}\frac{EI2}{L} = \phi EI \tag{3.5}$$

but $\phi = \dfrac{\frac{\alpha \Delta T}{2}}{\frac{h}{2}} = \dfrac{\alpha \Delta T}{h}$

substitute the value of ϕ into Eq. (3.5) get

$$M = \frac{\alpha \Delta T}{h} EI \ . \tag{3.6}$$

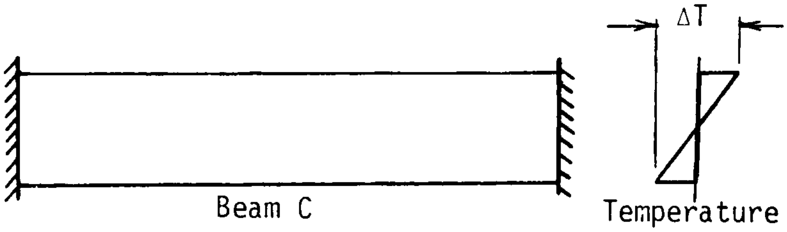

Figure 7. Beam for Case C.

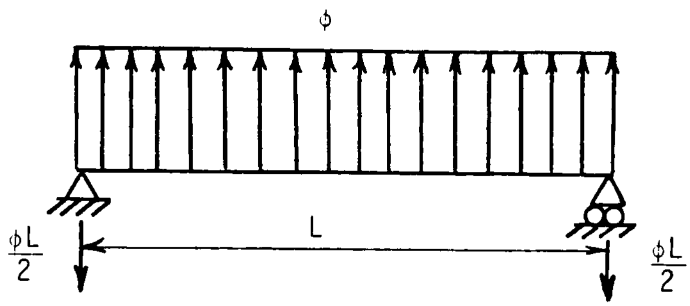

Figure 8. Primary structure for Beam C.

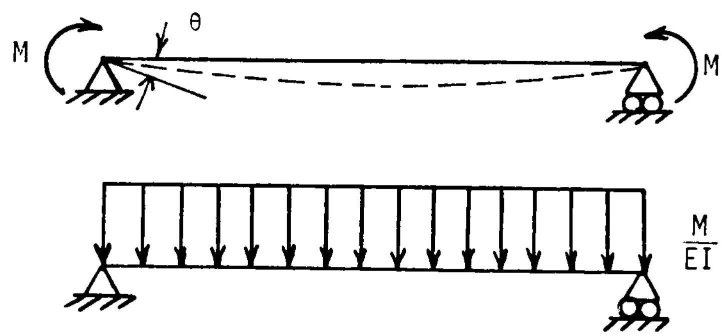

Figure 9. Structure with redundants for Beam C.

Therefore the final moment in beam C due to temperature change (ΔT) will be equal to the value in Eq. (3.6). This moment is constant all over the beam. The stress at any location throughout the depth of the structure due to this moment is equal to:

$$\sigma = \frac{My}{I}$$

$$= \frac{\alpha \Delta T E I y}{hI} .$$

But $\frac{y\Delta T}{h} = \Delta t$ (temperature change at any section)

$\therefore$ the stress due to temperature = $-E\alpha\Delta t$.

In beam C, the deflection at the mid-span of the primary structure is equal to the moment in the conjugate beam = $\frac{\phi L}{2} \cdot \frac{L}{2} - \frac{\phi L}{2}\frac{L}{4} = \frac{\phi L^2}{8}$ (downward). The deflection at the mid-span due to the redundant = $\frac{M}{EI}\frac{L^2}{8}$. But, from Eq. (3.5)

$$M = \phi EI .$$

Thus, the deflection at mid-span due to the redundant is equal to $\frac{\phi EI}{EI}\frac{L^2}{8} = \frac{\phi L^2}{8}$ (upward).

We can see that the final deflection is equal to zero, since the final deflection is the sum of the deflection of the primary structure due to thermal loads and the deflection of the primary structure due to the redundants.

As we can see, this beam has a moment which is proportional to ΔT but has no deflection. This example demonstrates the importance of the boundary conditions in the stresses induced. Beam B has no stresses but has deflection, and beam C has stresses but no deflection.

3.2.4. Case D: Simply Supported Beam with Nonlinear Temperature Distribution

The cross section of the simply supported beam is shown in Figure 10(a) where:

h = depth of the section,

b_y = total width of the section, excluding voids, at a distance (y) from the origin,

$\bar{y}$ = the vertical distance of the centroid from the origin.

The nonlinear temperature distribution is shown in Figure 10(b), where:

t_y = temperature at distance (y) from the bottom of the section.

Since the beam is simply supported, two equilibrium conditions must be satisfied:

1. The total axial force due to thermal load must be zero.
2. The final moment on the section due to this thermal load must be zero.

The final strain diagram is shown in Figure 10(c). It satisfies the Euler-Bernoulli condition (plane section remains plane). At any point throughout the section, due to thermal load (t_y) the section will attempt to obtain a strain of (αt_y), however since the plane section remains plane the final strain is (e_y). Therefore, a difference in strain between the final strain (e_y) and the free thermal strain will induce stress, f_y, which is:

$$f_y = E\,(e_y - \alpha t_y)$$

but from Figure 10(c) $e_y = e_1 + e_2 \frac{y}{h}$

$$\therefore\ f_y = E\,(e_1 + e_2 \frac{y}{h} - \alpha t_y) \qquad (3.7)$$

in which compressive strains are taken as positive. Apply the first

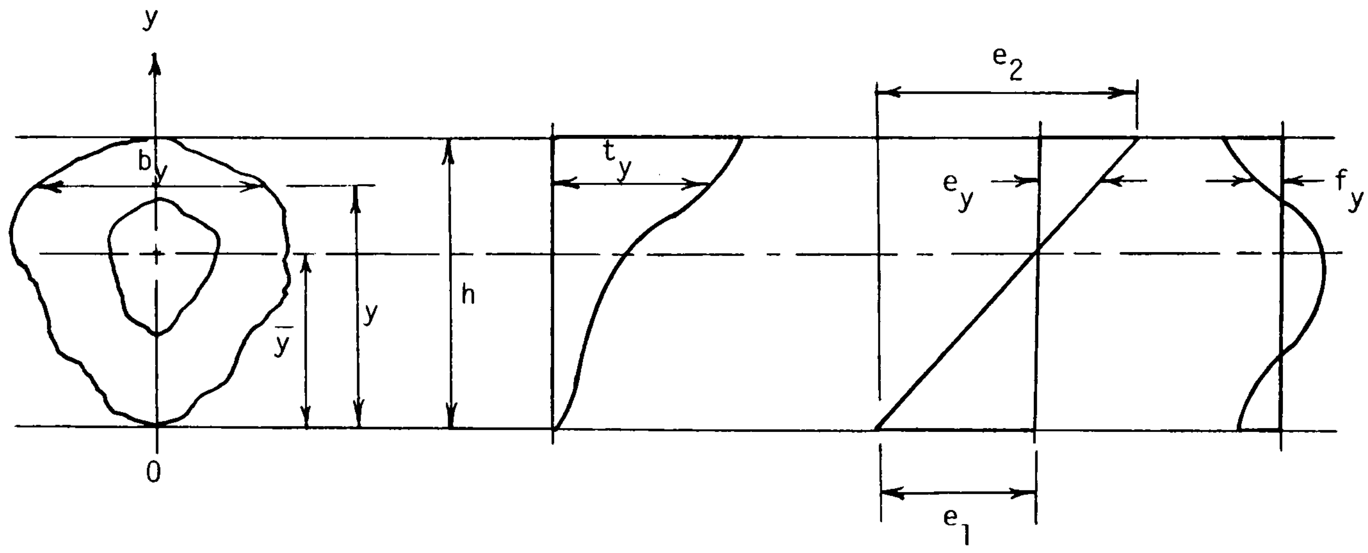

(a) x-Section (b) Temperature (c) Strain (d) Stress

Figure 10. Beam properties for Case D.

condition for the force:

$$ {}_0\int^{h} f_y\, b_y\, dy = 0 $$

$$ E\, {}_0\int^{h} (e_1 + e_2 \tfrac{y}{h} - \alpha t_y)\, b_y\, dy = 0 $$

$$ e_1\, {}_0\int^{h} b_y\, dy + \frac{e_2}{o}\, {}_0\int^{h} y\, b_y\, dy - \alpha\, {}_0\int^{h} b_y\, t_y\, dy = 0 $$

But ${}_0\int^{h} b_y\, dy$ = area of the cross section = A and

${}_0\int^{h} y\, b_y\, dy$ = moment of the area about the bottom = $\bar{y}$ A

$$ \therefore\ e_1 A + \frac{e_2}{h}\, \bar{y}\, A = \alpha\, {}_0\int^{h} b_y\, t_y\, dy $$

$$ e_1 + \frac{e_2}{h}\, \bar{y} = \frac{\alpha}{A}\, {}_0\int^{h} b_y\, t_y\, dy \qquad (3.8) $$

Apply the second condition for moment:

$$ {}_0\int^{h} f_y\, (y - \bar{y})\, b_y\, dy = 0 $$

substitute f_y from Eq. (3.7)

$$ E\, {}_0\int^{h} (e_1 + e_2 \tfrac{y}{h} - \alpha t_y)(y - \bar{y}) b_y\, dy = 0 $$

$$ {}_0\int^{h} e_1 (y - \bar{y}) b_y\, dy + \frac{e_2}{h}\, {}_0\int^{h} y (y - \bar{y}) b_y\, dy - \alpha\, {}_0\int^{h} t_y (y - \bar{y}) b_y\, dy = 0 $$

$$ e_1\, {}_0\int^{h} y\, b_y\, dy - e_1\, \bar{y}\, {}_0\int^{h} b_y\, dy + \frac{e_2}{h} \left[{}_0\int^{h} y^2\, b_y\, dy - \bar{y}\, {}_0\int^{h} y\, b_y\, dy \right] $$

$$ -\alpha\, {}_0\int^{h} t_y (y - \bar{y}) b_y\, dy = 0 $$

But ${}_0\int^{h} y\, b_y\, dy = \bar{y}\, {}_0\int^{h} b_y\, dy$ (moment of the area about bottom)

$$ \therefore\ \frac{e_2}{h}\, {}_0\int^{h} y^2\, b_y\, dy - \frac{e_2}{h}\, \bar{y}\, {}_0\int^{h} y\, b_y\, dy = \alpha\, {}_0\int^{h} t_y (y - \bar{y}) b_y\, dy $$

But ${}_0\int^h y^2\, b_y\, dy$ = moment of inertia of the section about origin which is also equal to $I + \bar{y}^2 A$ where I is equal the moment of inertia of the section about the centroidal axis.

$$\therefore \frac{e_2}{h} (I + \bar{y}^2 A) - \frac{e_2}{h} \bar{y} (\bar{y} A) = \alpha \, {}_0\int^h t_y(y - \bar{y})\, b_y\, dy$$

or:

$$\frac{e_2}{h} = \frac{\alpha}{I} \, {}_0\int^h t_y(y - \bar{y}) b_y \, dy \; . \tag{3.9}$$

Substitute the value of e_2 from Eq. (3.9) into Eq. (3.8),

$$e_1 + \frac{\bar{y}\,\alpha}{I} \, {}_0\int^h t_y(y - \bar{y}) b_y \, dy = \frac{\alpha}{A} \, {}_0\int^h b_y\, t_y\, dy$$

or:

$$e_1 = \frac{\alpha}{A} \, {}_0\int^h b_y\, t_y\, dy - \frac{\bar{y}\alpha}{I} \, {}_0\int^h t_y(y - \bar{y}) b_y \, dy \; . \tag{3.10}$$

Put the value of e_1 from Eq. (3.10) and e_2 from Eq. (3.9) into Eq. (3.7) get

$$f_y = E[\frac{\alpha}{A} \, {}_0\int^h b_y\, t_y\, dy - \frac{\bar{y}\,\alpha}{I} \, {}_0\int^h t_y(y - \bar{y}) b_y \, dy + \frac{\alpha y}{I} \, {}_0\int^h t_y(y - \bar{y}) b_y \, dy - \alpha t_y]$$

$$f_y = E\alpha[-t_y + \frac{{}_0\int^h b_y\, t_y\, dy}{A} + \frac{(y - \bar{y}) \; {}_0\int^h t_y(y - \bar{y}) b_y \, dy}{I}] \tag{3.11}$$

or

$$f_y = - E\alpha \; t_y + \frac{P}{A} + \frac{(y - \bar{y}) \; M}{I} \tag{3.12}$$

where:

$$P = E\alpha \int_0^h b_y\, t_y\, dy \;,\quad M = E\alpha \int_0^h t_y(y - \bar{y})b_y\, dy$$

$y - \bar{y}$ = distance from neutral axis to fiber in question.

The above equation was derived also by Radolli and Green.[13] The stresses in Eq. (3.11) are called eigenstresses[13] since they are self-equilibrating stresses as shown in Figure 10(c). Those stresses are dependent on the gradient of temperature. For a linear temperature distribution the eigenstresses are zero.

A computer program to evaluate the eigenstresses for any cross section and temperature distribution is shown in Appendix B.

3.2.5. Case E: Fixed End Beam with Nonlinear Temperature Distribution

When a fixed end beam is subjected to nonlinear temperature distribution across its depth as illustrated in Figure 11, the following stresses develop:[13]

1. Axial stress due to the axial end restrained of the member.
2. Bending stress due to the rotational restrained of the member.
3. A self-equilibrating eigenstress due to the nonlinearity of the temperature distribution.

From Cases D and E, it has been shown that eigenstresses are independent of the support conditions of the structure.

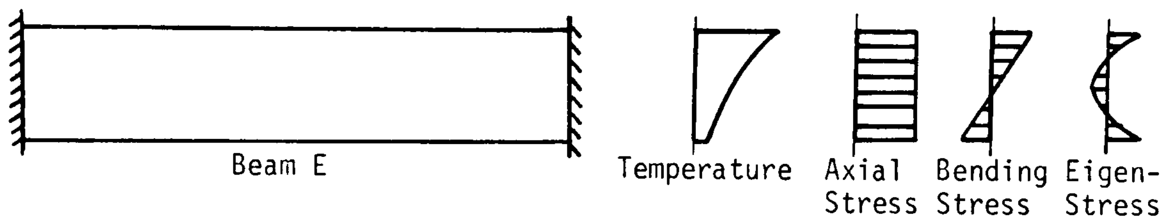

Figure 11. Beam for Case E.

3.3. METHOD FOR CALCULATING STRESSES INDUCED IN CONTINUOUS BEAMS BY NONLINEAR TEMPERATURE VARIATIONS

From Eq. (3.1) since the strain (E) is linear (plane sections remain plane) and the change in temperature (Δt) is nonlinear, therefore the final stress (σ) will be nonlinear. The final stresses can be divided into a linear and a nonlinear portion (for nonlinear temperatures). If the nonlinear portion of the stresses is chosen such that it has a zero moment and a zero resultant force (i.e., eigenstresses), then all deformations are the result of the linear portion.

The eigenstresses are independent of the boundary or support conditions of a structure.[13] Therefore, the temperature required to produce these stresses is:

Temperature required to produce eigenstresses

$$= - \frac{E\alpha\left[-t_y + \frac{\int_0^h b_y t_y dy}{A} + \frac{(y - \bar{y}) \int_0^h t_y (y - \bar{y}) b_y dy}{I}\right]}{E\alpha} . \qquad (3.13)$$

The linear portion of temperature which will induce the linear stress is equal to: linear temperature = actual temperature-temperature required to produce eigenstress, or:

$$\text{linear temperature} = \frac{\int_0^h b_y t_y dy}{A} + \frac{(y - \bar{y}) \int_0^h t_y (y - \bar{y}) b_y dy}{I} \qquad (3.14)$$

i.e., $T = D + (y - \bar{y})E$ in which

$$D = \frac{\int_0^h b_y t_y dy}{A}$$

$$E = \frac{\int_0^h t_y (y - \bar{y}) b_y dy}{I}$$

where D and E depend on properties of the cross section of the beam and on the temperature distribution at $y = h$; $T = T_1$ = temperature at the top fiber of the section at $y = 0$; $T = T_2$ = temperature at the bottom fiber of the section. Therefore, T_1 and T_2 will be applied linear temperature load. So, at least for a fixed beam with any nonlinear temperature distribution, one can calculate the total stresses by computing the eigenstresses from Eq. (3.11) and adding the thermal stresses from the linear temperature distribution from Eq. (3.14).

Of course for the fixed beam, this is no advantage since we know that these stresses are simply equal to $(E\alpha t_y)$. However, for a more general case, if the method is applicable and can be extrapolated, it means that the structural analysis needs to be carried out only for $T = D + (y - \bar{y})E$ and then the eigenstresses from Eq. (3.11) added where applicable.

To demonstrate the validity of this extrapolation, the following examples were selected and the results compared with the worked examples given in the precast segmental box girder bridge manual.[10]

EXAMPLE 1.

A simply supported beam with a cross section as shown in Figure 12 was chosen. The top slab temperature increased by 18°F, $\alpha = 5.5 \times 10^{-6}$ in/in/°F, $E = 4 \times 10^{6}$ psi. Calculate the stresses due to temperature changes.

Cross sectional area $A = 3600$ in.^{2}

Moment of inertia of the cross section = 55.1 ft.^{4}

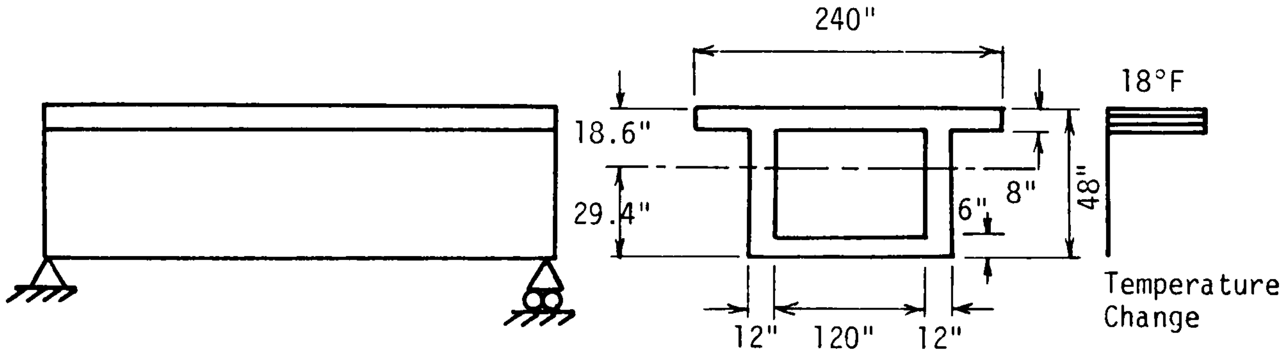

Figure 12. Dimensions and temperature for beam of Example 1.

Solution:

$$f_y = E\,[-\,t_y + \frac{\int_0^d b_y t_y dy}{A} + \frac{(y - n)\int_0^d t_y (y - n) b_y dy}{I}$$

$$\int b_y t_y d = 240(18 \times 8) = 34560 \ °F\ in^2$$

$$\int t_y (y - n) b_y dy = 18(44\text{-}29.4)(240 \times 8) = 504576 \ °F\ in^3$$

$$f_y = 4 \times 10^6 \times 5.5 \times 10^{-6}[-t_y + \frac{34560}{3600} + \frac{504576}{55.1 \times 144 \times 144}(y - 29.4)]$$

$$= 22[-t_y + 9.6 + 0.4416\,(y - 29.4)]$$

At top	$y = 48$; $t_y = 18°F$	$f_y = -4.1$ psi
At flange bottom	$y = 40"$; $t_y = 18°F$	$f_y = -81.8$ psi
	$y = 40"$; $t_y = 0$	$f_y = 314.2$ psi
At bottom	$y = 0$; $t_y = 0$	$f_y = -74.4$ psi

The final stresses are shown below in Figure 13. Those stresses agree exactly with those given in the PCI precast segmental box girder manual for the same beam.[10]

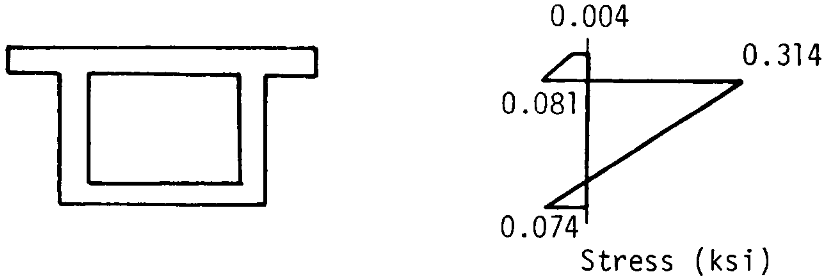

Figure 13. The final stress for Example 1.

EXAMPLE 2.

A five-span continuous superstructure as shown in Figure 14 with the same information in Example 1. Calculate the stresses in span 3-4 due to a temperature differential of 18°F between the top and the bottom slabs.

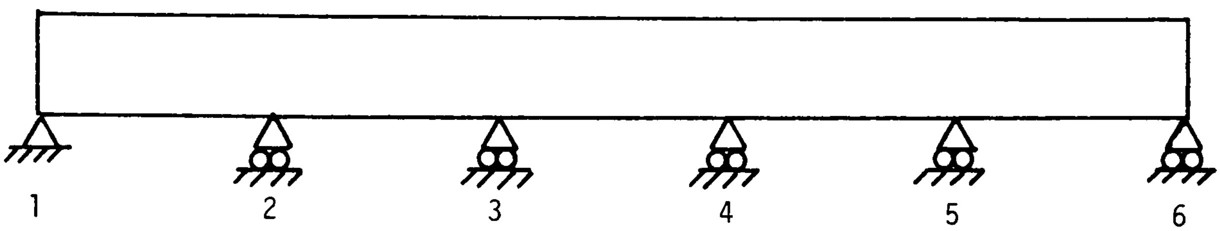

Figure 14. Beam for Example 2.

The stresses in span 3-4 consist of two parts:

1. The eigenstresses which are the same as in Example 1.
2. The stresses due to linear temperature distribution which is calculated by using Eq. (3.14).

Applying Eq. (3.14),

$$T = \frac{34560}{3600} + \frac{504576}{55.1 \times 144 \times 144} (y - 29.4)$$

$$T = 9.6 + 0.4416\ (y - 29.4)$$

At top: $y = 48$ $\quad T_1 = 17.81$

At bottom: $y = 0$ $\quad T_2 = -3.38$

The linear temperature variation can be divided into two parts: (1) which gives pure bending and (2) which gives pure axial load as shown in Figure 15.

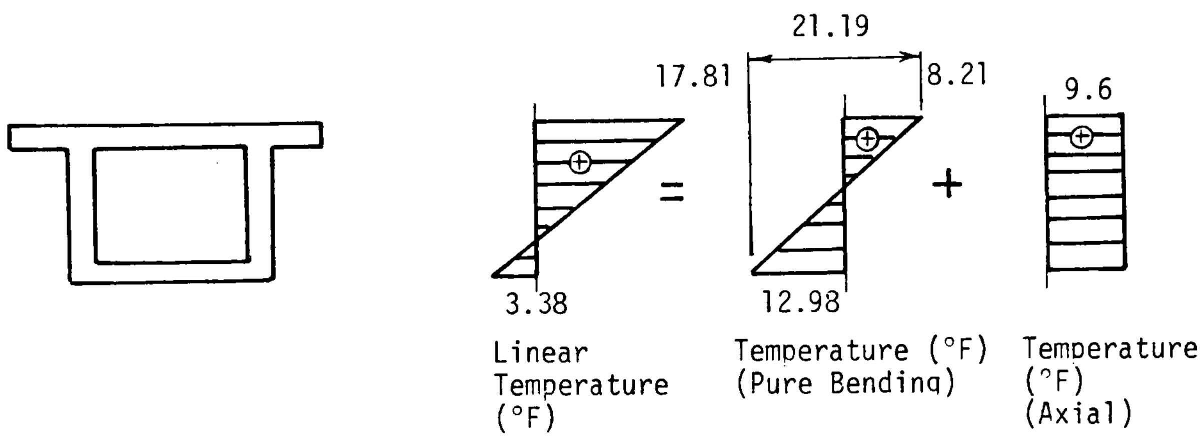

Figure 15. Cross section with temperature distribution for Example 2.

(1) <u>FOR BENDING</u> Applying Eq. (3.6)

$$\text{F.E.M.} = \frac{EI\alpha\Delta t}{h} = \frac{4 \times 10^{6} \times 55.1 \times 144 \times 144 \times 5.5 \times 10^{-6} \times 21.12}{48 \times 1000}$$

$$= 11096 \text{ K in.}$$

Using Symmetry:

Where K = stiffness of the member

K = 1, KR = .75		K = 1		K = 0.5
	.43	.57	.67	.33
+11096	-11096	+11096	-11096	+11096
-11096	- 5548			
0	+ 2386	+ 3162	+ 1581	- 527
		- 527	+ 1054	
	+ 227	+ 300	+ 150	
		- 50	- 100	- 50
	+ 21	+ 29	+ 14	
		- 5	- 9	- 5
	+ 2	+ 3	+ 1	
	-14008	14088	- 1	
			-10514	10514

The final moment diagram due to temperature is shown below in Figure 16.

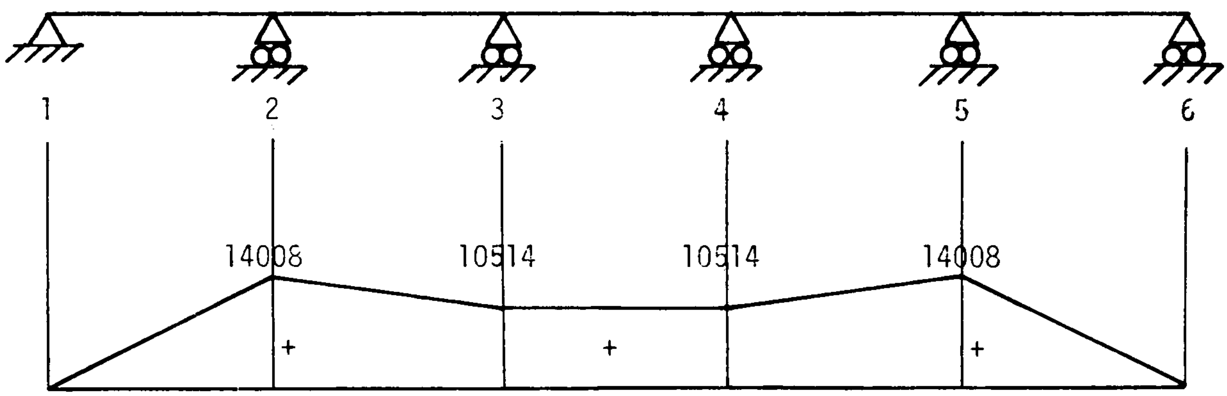

Figure 16. Moment diagram for Example 2 due to 18°F temperature change.

The stresses in panel 3-4 due to bending moments are:

$$\text{Stress at top} = \frac{10514 \times 18.6}{55.1 \times 144 \times 144} = -0.171 \text{ ksi}$$

$$\text{Stress at bottom} = \frac{10500 \times 29.4}{55.1 \times 144 \times 144} = 0.271 \text{ ksi}$$

$$\text{Stress at flange} = \frac{10500 \times 10.6}{55.1 \times 144 \times 144} = -0.097 \text{ ksi}$$

(2) Pure axial

By applying a constant temperature of 9.6°F on the continuous beam, the axial force in the beam becomes zero since all supports are free to move in the horizontal direction except support 1. The final stress in panel 3-4 is equal to the sum of eigenstresses, bending stress and axial stress, as shown in Figure 17.

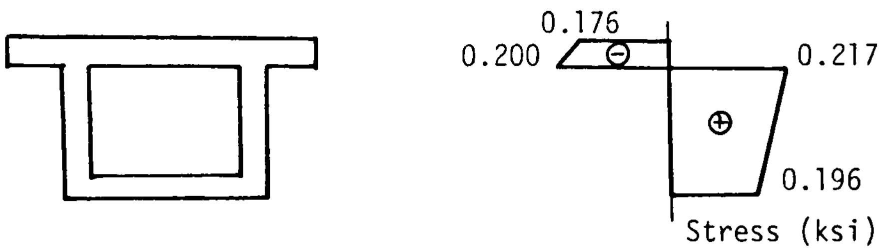

Figure 17. Final stress diagram in Panel 3-4 for Example 2.

The final stresses in Figure 17 for example (2) have exactly the same values as those given in precast segmental Box girder bridge manual.[10] The method cited in Ref. 10 is applicable for linear temperature differential across the slab thickness and becomes cumbersome and involved for nonlinear temperatures. However, the approach followed in the aforementioned examples is applicable to any thermal gradient.

CHAPTER IV

INSTRUMENTATION AND TEST DATA

4.1. DESCRIPTION OF THE BRIDGE

The bridge consists of two separated, almost identical roadways (right and left) a clear distance of 40 ft apart. Each roadway is approximately 2700 ft long. The superstructure of the bridge is supported by 28 piers and two abutments with the north abutment 60 ft higher than the south abutment. The abutments and some of the piers have skews from the longitudinal axis of the bridge. The elevation and plan of the bridge are shown in Figure 18 with the numbering of the piers progressing from south to north.

The bridge deck consists of prestressed concrete box girders acting compositely with both precast and reinforced concrete slab as shown in Figure 1 (p. 3). The deck slab has an asphalt topping 3 in in thickness. The reinforced concrete piers are rectangular in plan and vary in height from 15 ft to 46 ft. The elevation and side view for a typical pier are shown in Figure 19. The prestressed beams in adjacent spans are connected by casting 9 in diaphragms that are attached to the piers through three, 1-in. diameter dowel bars as shown in Figure 20. The unique aspect of this bridge is that there are no provisions for expansion except at the abutments. Typical details for a diaphragm at the abutment are shown in Figure 21.

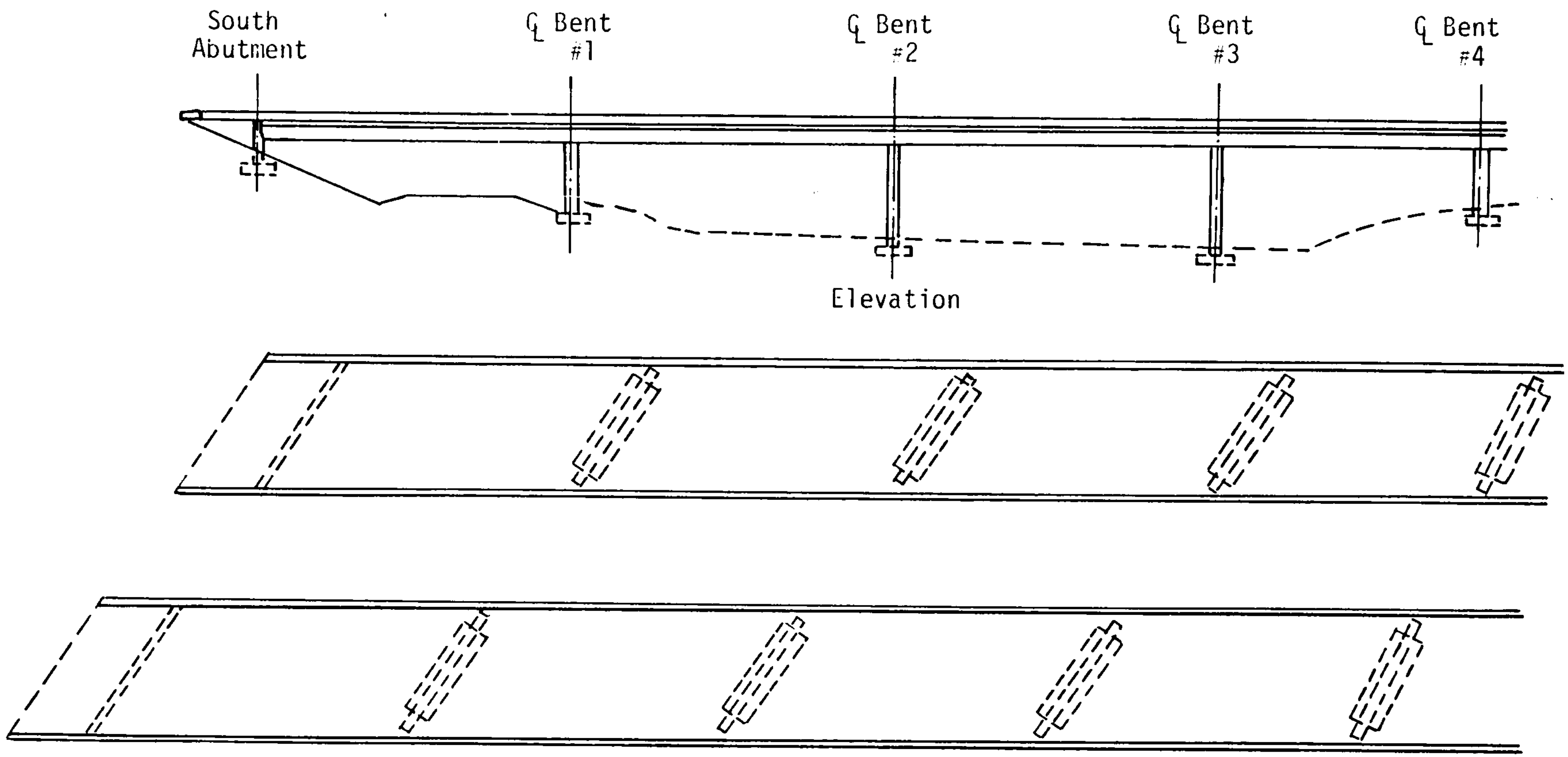

Figure 18. Elevation and plan for the bridge.

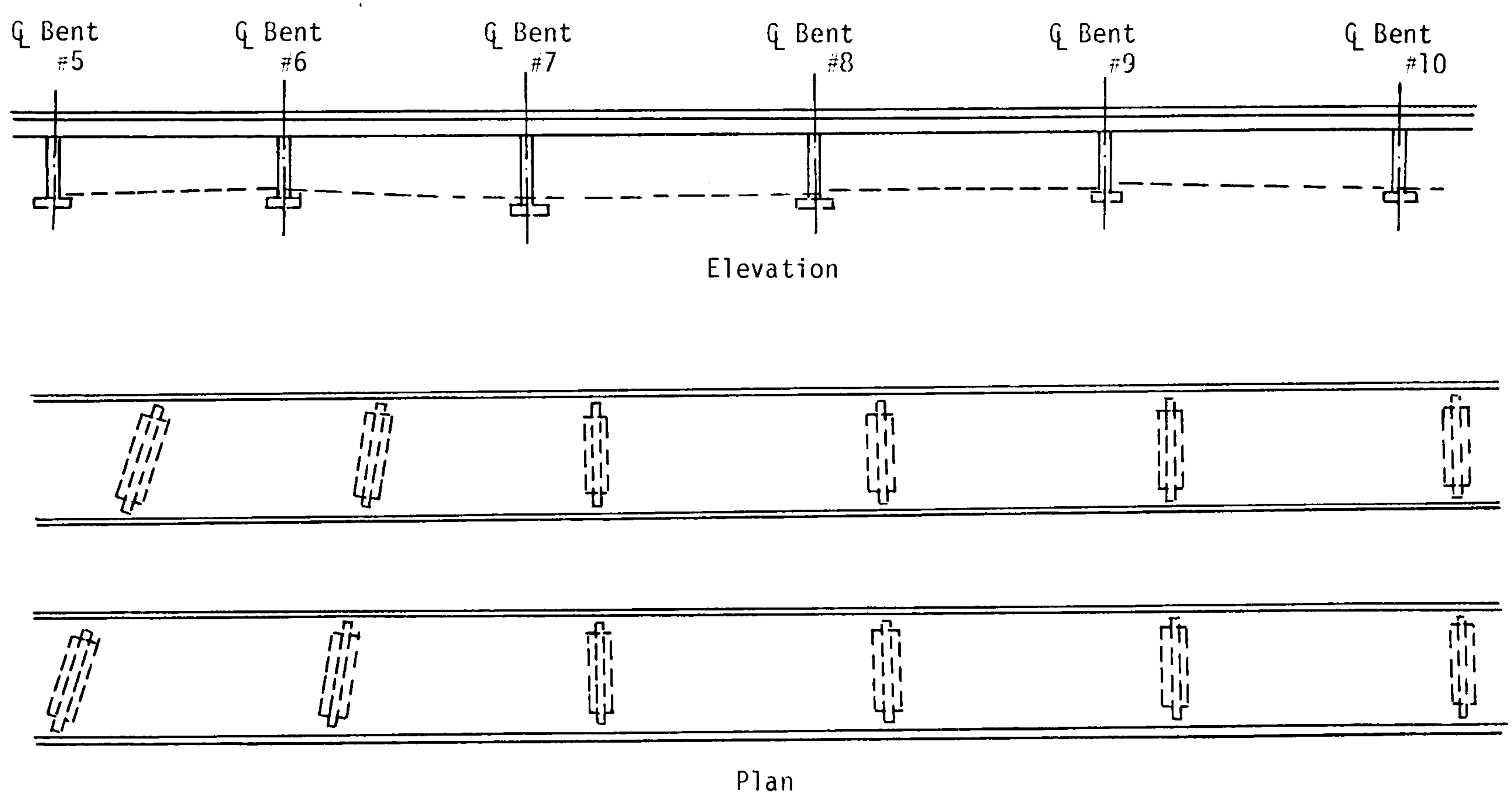

Figure 18 (continued)

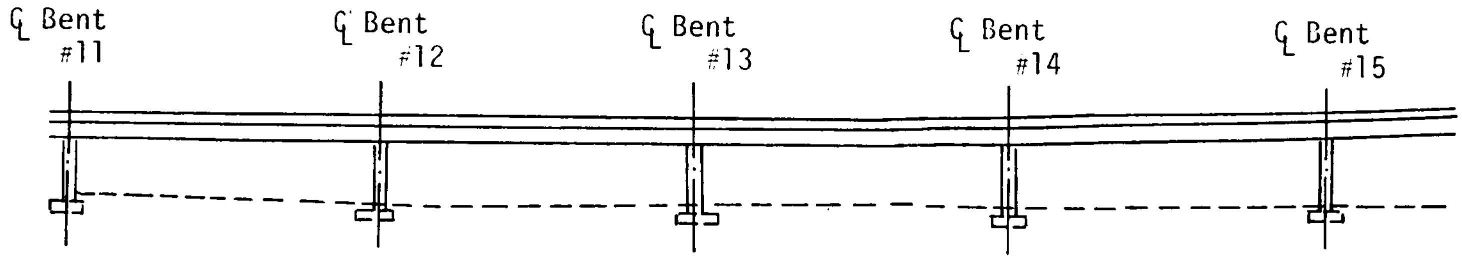

Elevation

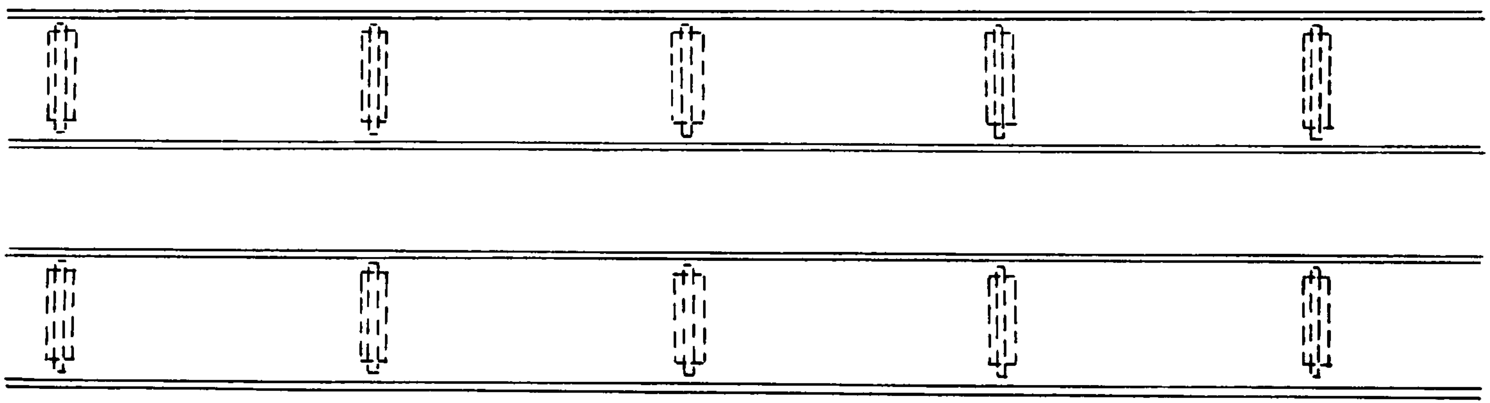

Plan

Figure 18 (continued)

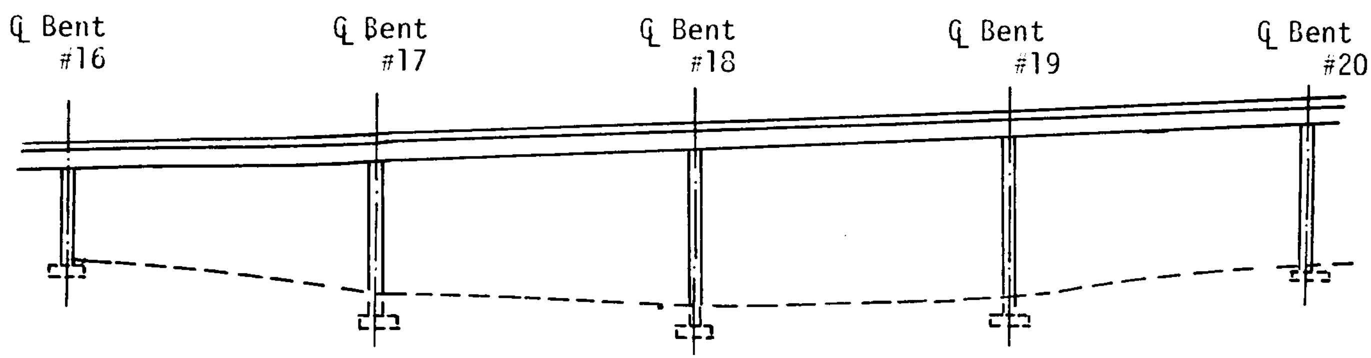

Elevation

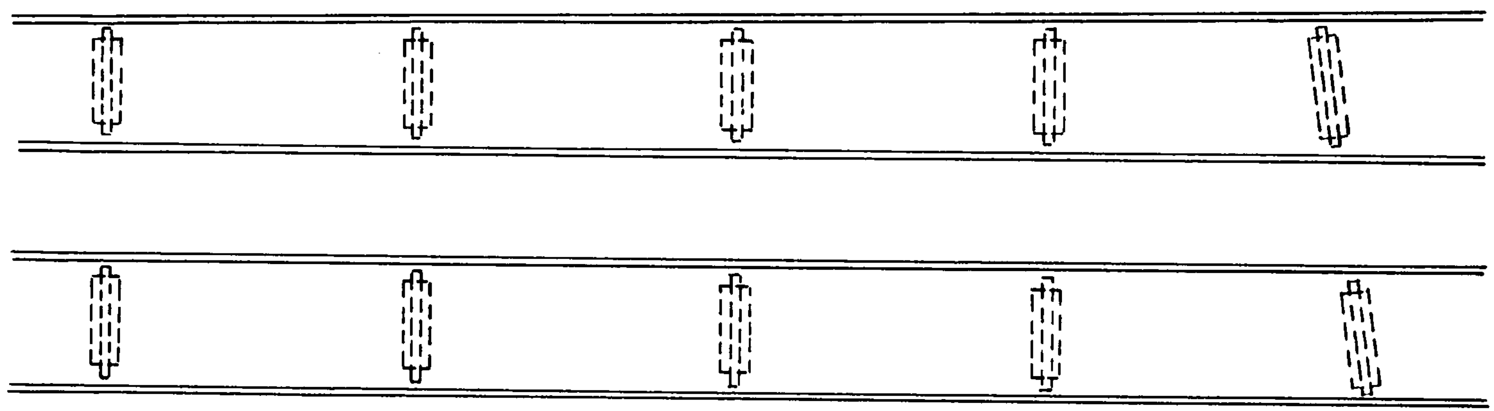

Plan

Figure 18 (continued)

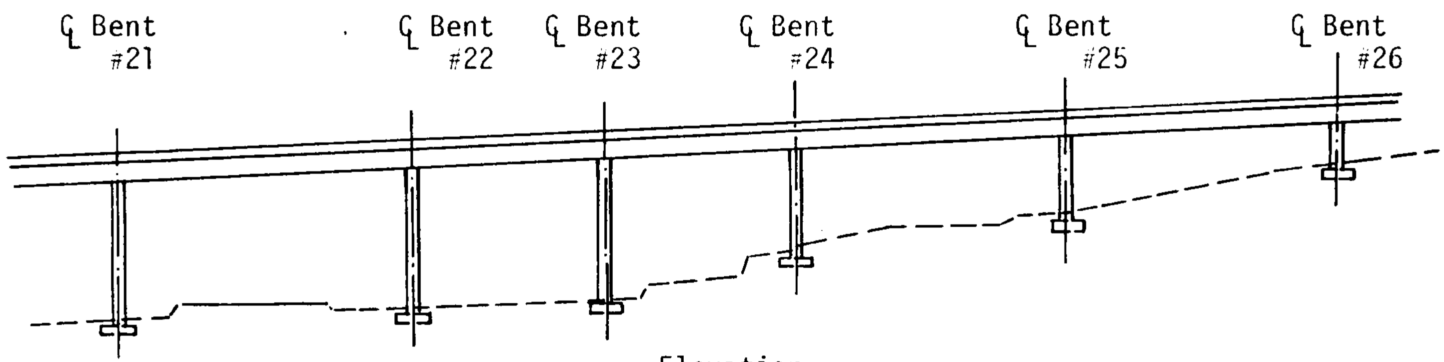

Elevation

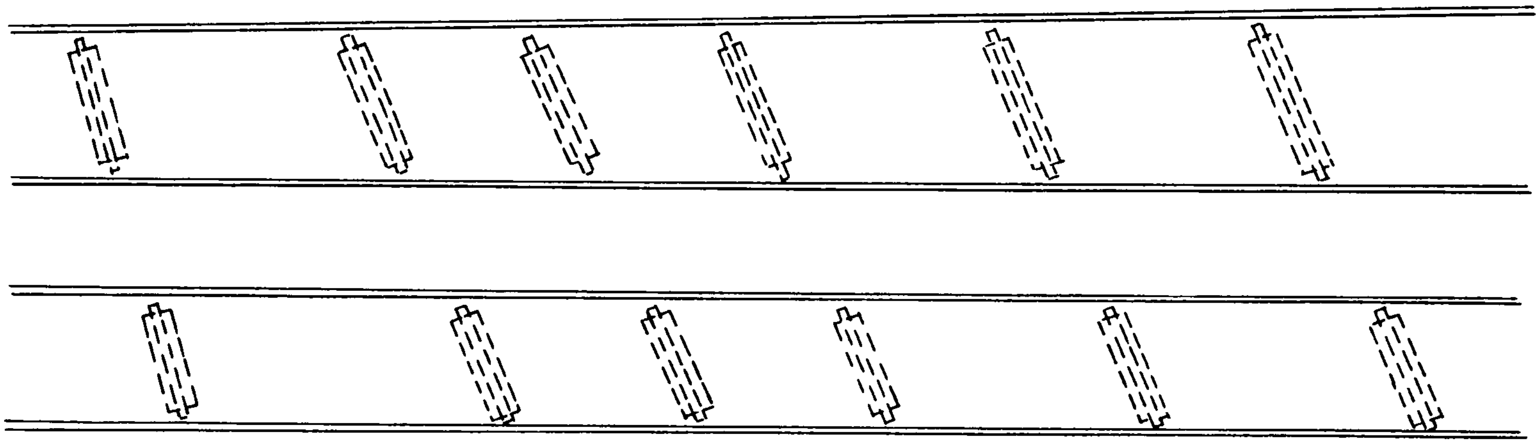

Plan

Figure 18 (continued)

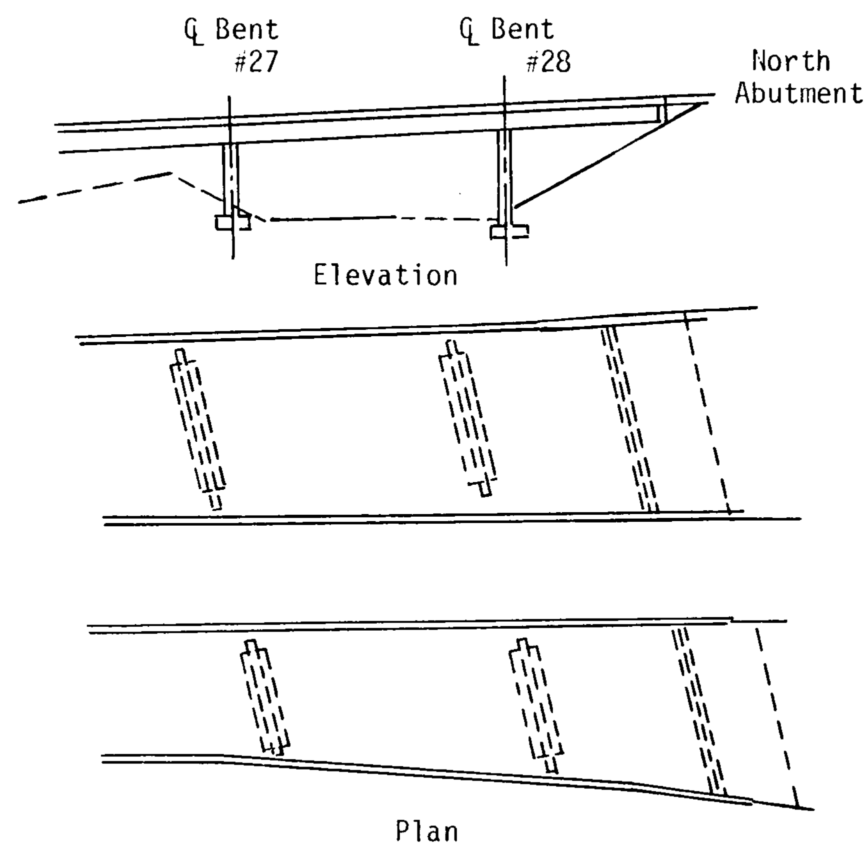

Figure 18 (continued)

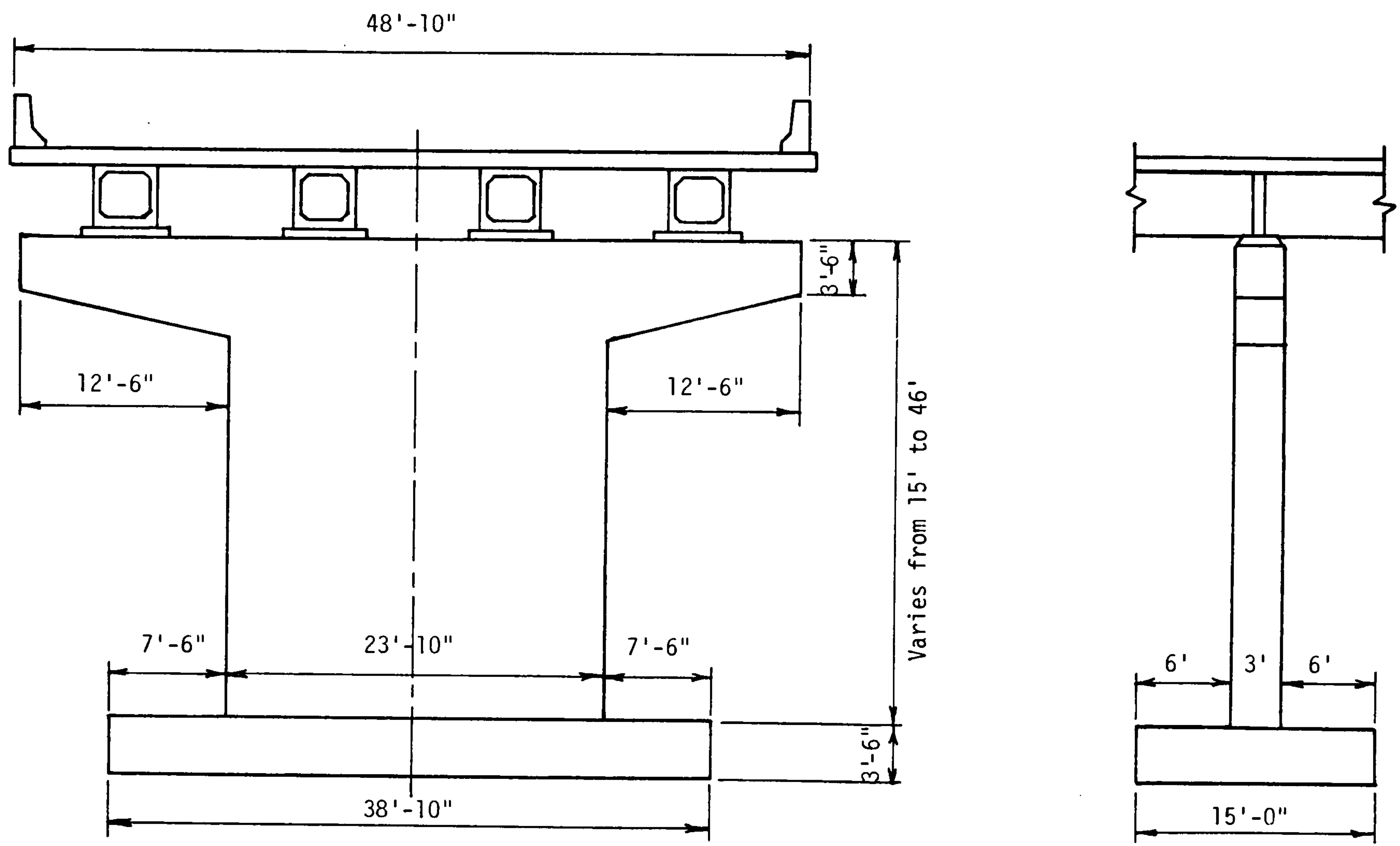

Figure 19. Elevation and side view for a typical pier.

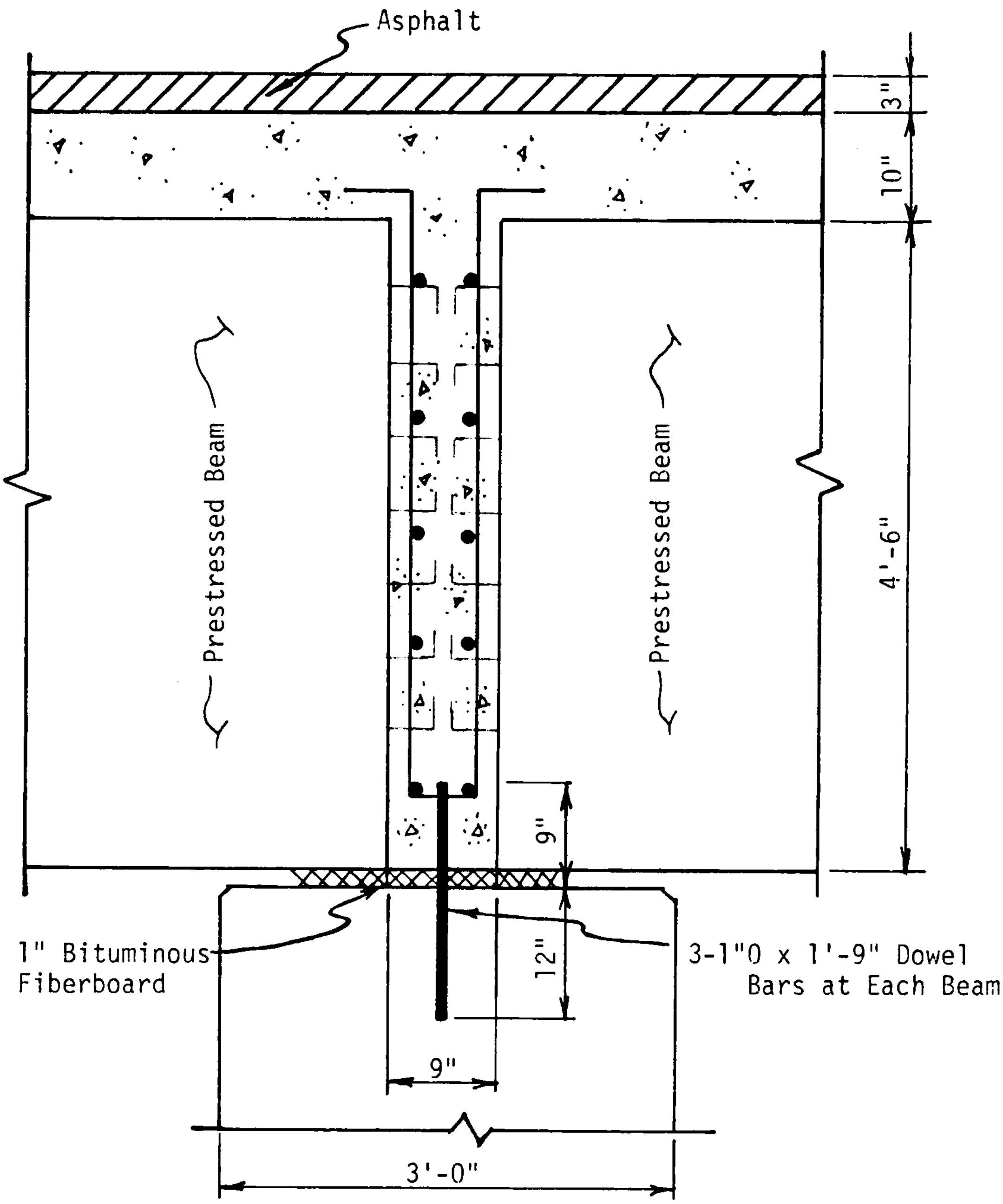

Figure 20. Support diaphragm detail.

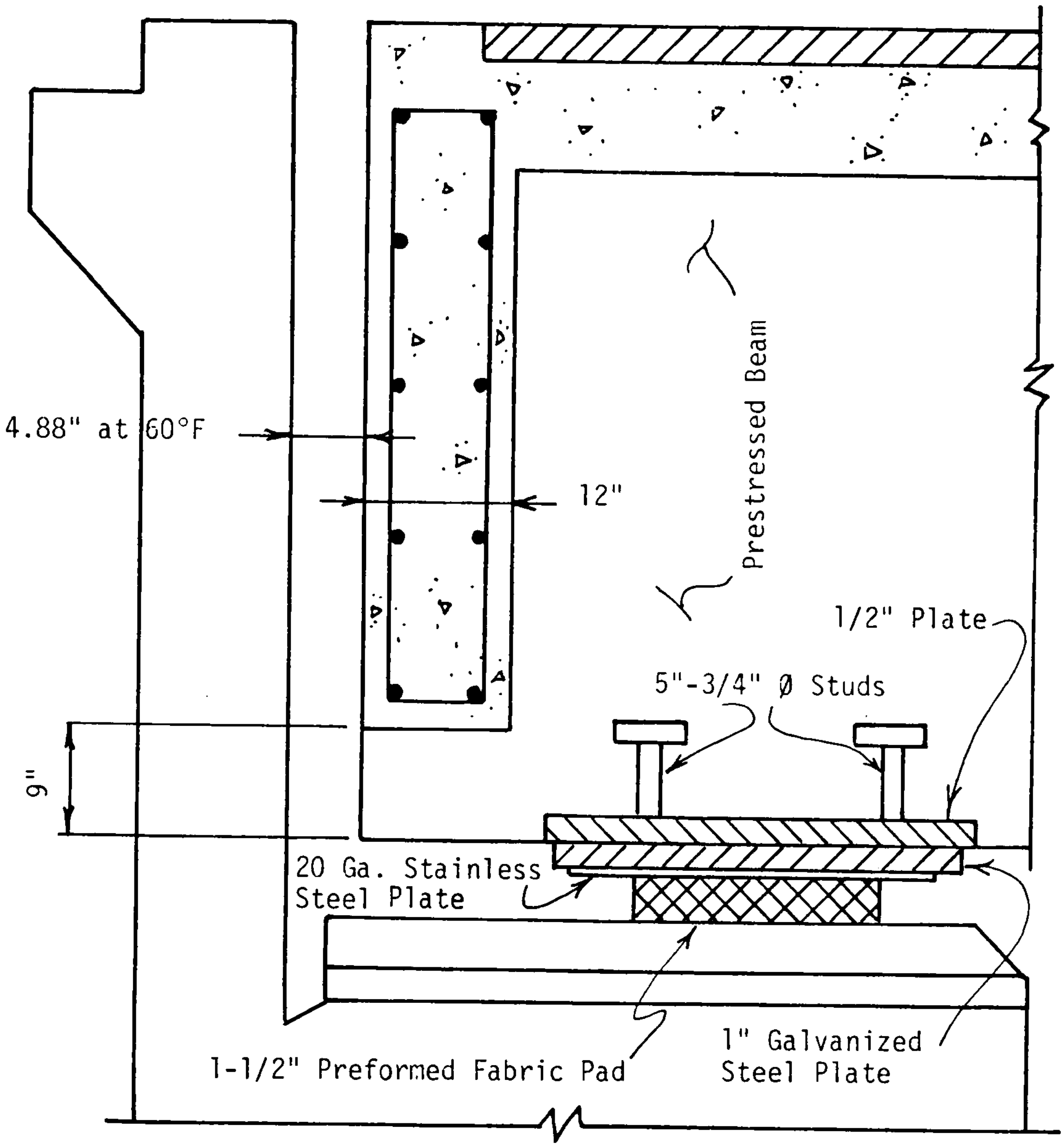

Figure 21. Typical diaphragm at abutment.

4.2. STRAIN GAGES

4.2.1. Basic Principle

Electrical-resistance strain gages have been used for the past thirty years for static and dynamic testing in many fields. It is this type of strain gage that was used in the testing of this bridge. The use of the electrical-resistance strain gage is based on three vital facts: (1) the resistance of the gage wire varies as a function of strain; (2) different materials have different sensitivities; and (3) the resistance changes due to strain can be measured by a Wheatstone bridge.

4.2.2. Strain Gage Assembly

Weldable strain gages were used because of the need for stable performance over a long period of testing, and ease of installation. The strain sensitive strand of the gage is housed within a small diameter stainless steel tube. The strand is insulated from the tube with highly compacted ceramic insulation (magnesium oxide power) as shown in Figure 22. The strain tube is provided with a thin flange. This flange is subsequently spot welded to the specimen under test to provide the bond required to transfer strain.

The strain gages were welded to the center of 5-ft long, number 6 bars in the laboratory. The development length of a number 6 bar is approximately 18 in which is less than the 30 in of bar provided on each side of the gage; thus, full stress and strain can be transmitted to the gage.

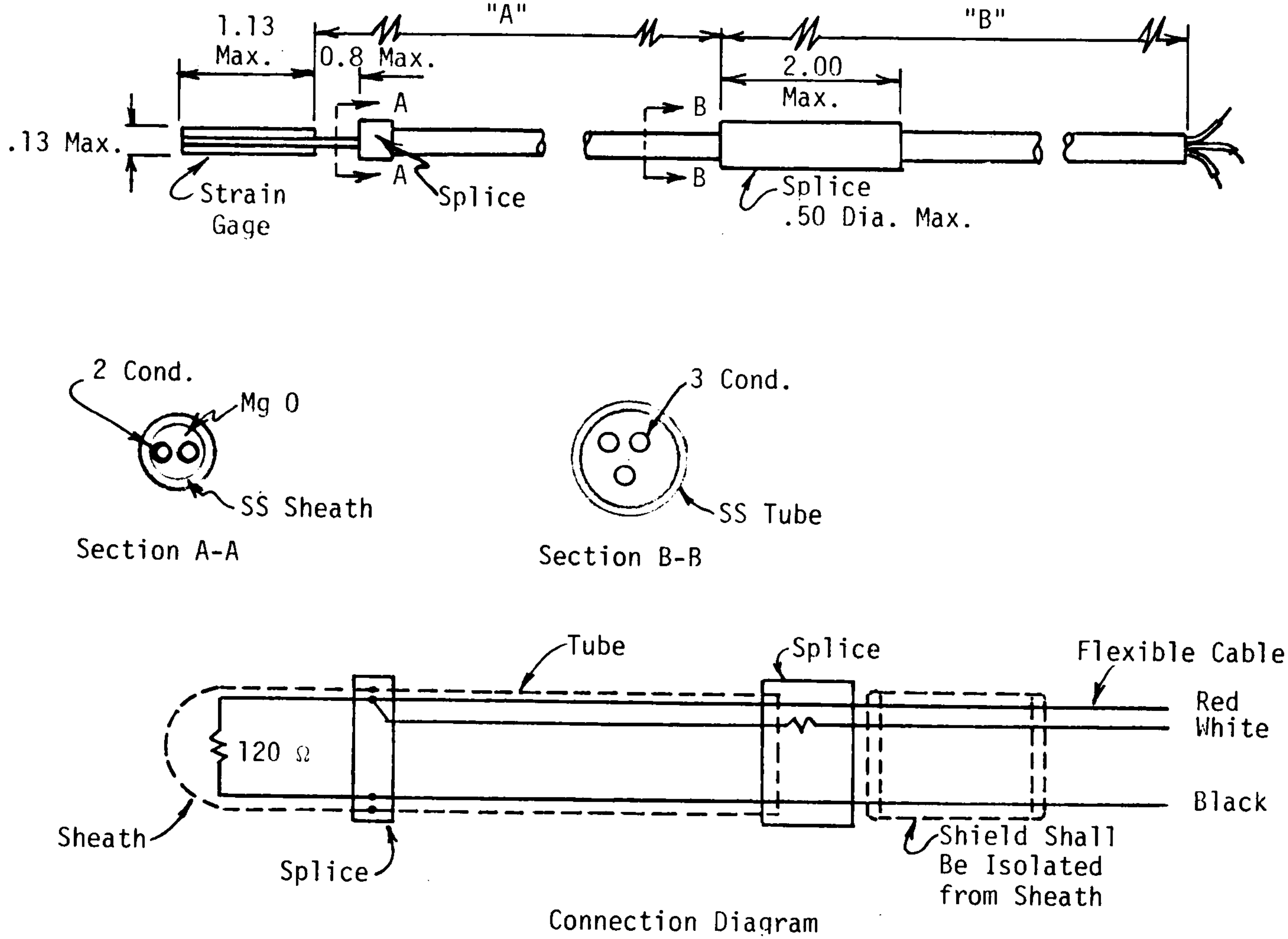

Figure 22. Strain gage assembly.

4.2.3. Theory of Operation for Weldable Strain Gages

When the specimen to which the gage is welded is subjected to tension or compression, the strain in the specimen is transferred through the welds to the mounting flange, into the strain tube, and through the magnesium oxide powder. The powder is so highly packed together that the strain in the specimen is transmitted to the sensing string all along its length with no slippage. These events can happen in a gage which measures compressive as well as tensile strains. This property of stable, reversible, strain transfer is due to the geometrical fact that in wires having small diameter the ratio of unit surface area to unit cross sectional area is a high value. So, only reasonable values of shear stress in the magnesium oxide powder are required to develop tensile stresses of large value in the sensing string.

4.2.4. Temperature Compensation of the Strain Gage

In many tests, the strain gage is subjected to changes in temperature during the test period. These temperature changes affect the gage-grid elongation, base material elongation, and resistance of the gage. The changes of the gage resistance can be expressed by the following equation:[4]

$$\left(\frac{\Delta R}{R}\right)_{\Delta t} = (\beta - \alpha_g)S_g \, \Delta t + \gamma\Delta t \tag{4.1}$$

where:

$\left(\frac{\Delta R}{R}\right)_{\Delta t}$ = change in gage resistance due to temperature change Δt,

β = coefficient of thermal expansion of base material,

α_g = coefficient of thermal expansion of gage material,

S_g = gage factor,

γ = temperature coefficient of resistivity of gage material.

From Eq. (4.1)

$$\frac{(\frac{\Delta R}{R})_{\Delta t}}{S_g} = (\beta - \alpha_g)\Delta t + \frac{\gamma}{S_g}\Delta t \; .$$

But $\varepsilon_{app.} = \frac{(\frac{\Delta R}{R})_{\Delta t}}{S_g}$

where $\varepsilon_{app.}$ = apparent strain, therefore

$$\varepsilon_{app.} = (\beta - \alpha_g)\Delta t + \frac{\gamma}{S_g}\Delta t \; . \tag{4.2}$$

The apparent strain must be calculated or compensated. There are two methods to compensate for temperature. First, compensate within the gage itself by using $\beta - \alpha_g = -\frac{\gamma}{S_g}$. The second method involves using a dummy gage in addition to the active gage. The connection of the active and dummy gages in Wheatstone bridge are shown in Figure 23. The dummy gage should be completely unrestrained and maintain the same temperature as the active gage Eq. (4.2) becomes

$$\varepsilon_{app.} = (\beta - \alpha_g)\Delta t \; . \tag{4.3}$$

So, if there is a difference between the coefficient of thermal expansion of the grid material and the base material, the gage itself will be subjected to a strain as given by Eq. (4.3) which does not occur in the specimen. Therefore, the measured strain which is read by the strain indicator should be corrected by subtracting the apparent strain.

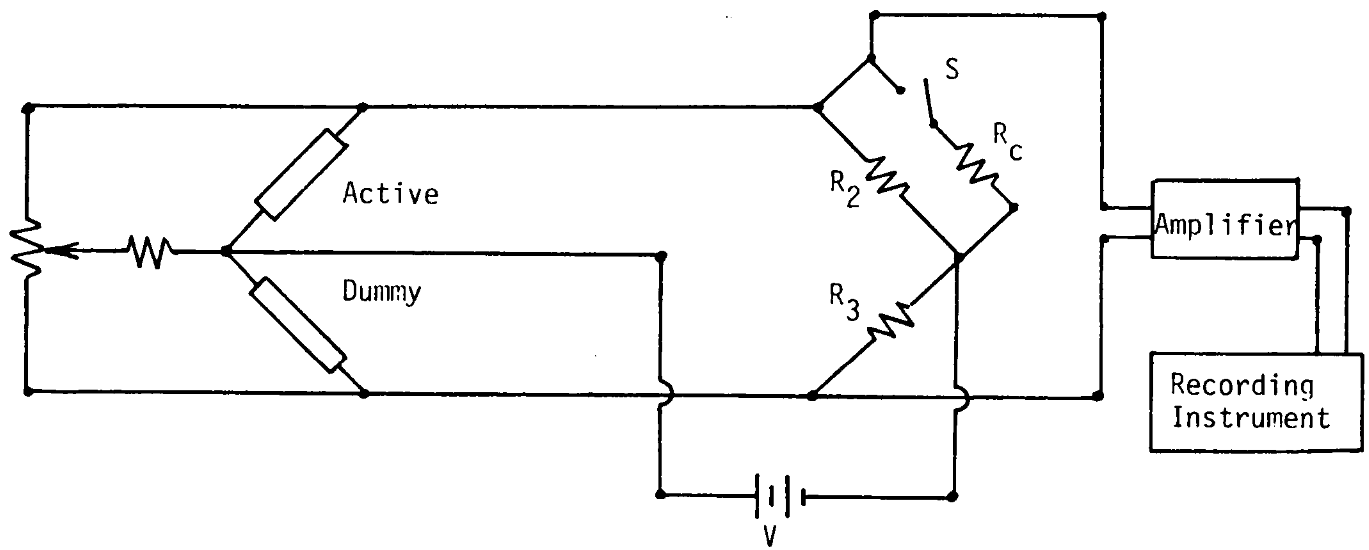

Figure 23. Strain-recording connection.

$$\varepsilon_S = \varepsilon_R - \varepsilon_{app.}$$

or:

$$\varepsilon_S = \varepsilon_R - (\beta - \alpha_g)\Delta t \tag{4.4}$$

where

ε_S = strain produced by stress,

ε_R = indicated strain.

4.2.5. Determination of the Coefficient of Thermal Expansion Coefficient of the Weldable Strain Gage

A strain gage was welded to a reinforcing bar, and a free gage which served as the dummy gage was placed beside the active gage. Both gages were maintained at the same temperature. The active and dummy gages were connected on a half bridge in the Wheatstone bridge. For temperature calibration both gages were exposed to various temperatures by inserting them into a water bath control. The temperature and the strain are recorded as shown below:

Temperature (°F)	Indicated Strain (ε_R)
50	13905
70	13880
80	13850
100	13800
110	13780
143	13715

The changes in strain readout between the different temperature increments are:

Δt (°F)	$\Delta \varepsilon R$ ($\mu \varepsilon$)
+20	-25
+10	-30
+20	-50
+10	-20
+33	-85

apply Eq. (4.4). (Since the bar to which the active gage was welded was free, the stress would be zero; that is, the strain produced by stress (ε) should be equal to zero.

$$0 = \varepsilon_R - (\beta - \alpha_g)\Delta t$$

$$-\varepsilon_R + \beta\,\Delta t = \alpha_g \Delta t$$

$$\alpha_g = \beta - \frac{\varepsilon_R}{\Delta t} .$$

But $\beta = 6.5 \times 10^{-6}$ (for reinforcing bar). Substitute the values into above equation for each $\Delta t, \Delta\varepsilon_R$ the value of α is calculated.

Δt	$\Delta \varepsilon_R$	α_g
+20	-25	7.75×10^{-6}
+10	-30	9.5×10^{-6}
+20	-50	9.0×10^{-6}
+10	-20	8.5×10^{-6}
+33	-85	9.08×10^{-6}

Average value of $\alpha = 8.766 \times 10^{-6}$ in/in/°F.

4.2.6. Strain-Gage Calibration

The strain gages are connected on a half Wheatstone bridge to Vishay units. These units are connected to a B and F Model 1C1613 Signal Conditioner recorder. The calibration system is achieved by shunting a fixed resistor (R_c) across one arm of the Wheatstone bridge (R_2) as shown in Figure 23. When the calibration resistor is on, the calibration strain (ε_c) can be calculated as:[4]

$$\varepsilon_c = \frac{1}{S_g} \frac{R_2}{R_2 + R_c} .$$

In the units which are used in the bridge testing we have the following values:

$$R_2 = 350\Omega$$

$$R_c = 175000\Omega$$

$$S_g = 2.0$$

$$\varepsilon_c = \frac{1}{2.0}\,\frac{350}{350 + 175000} = 0.001000$$

$$= 1000\ \mu\varepsilon\ .$$

4.2.7. Locations of the Strain Gages in the Bridge

The strain gages which were welded on reinforcing bars have been placed in both lanes (roadway), right and left, to provide verification of the data or back-up data in case of premature failure of the gages. Typical spans and piers were chosen for the installation of the gages. The first priority was piers No. 1 and 28 which are next to the abutment where movement due to expansion would be maximum. The next priority was a pier close to the center of the bridge, pier No. 11. The third set of piers are between the center of the bridge and the abutments, piers 7 and 22. The location of the instrumented piers is shown in Figure 24. The gaged bars were placed as vertical bars in the lower and upper stem of the bent on both faces of the bents as shown in Figure 25. Gages were also placed in the deck above bents 1, 7, 11, 22, and 28 at each girder as illustrated in Figure 26. At mid-span between bents 10, 11 and 6, 7, gages also have been placed.

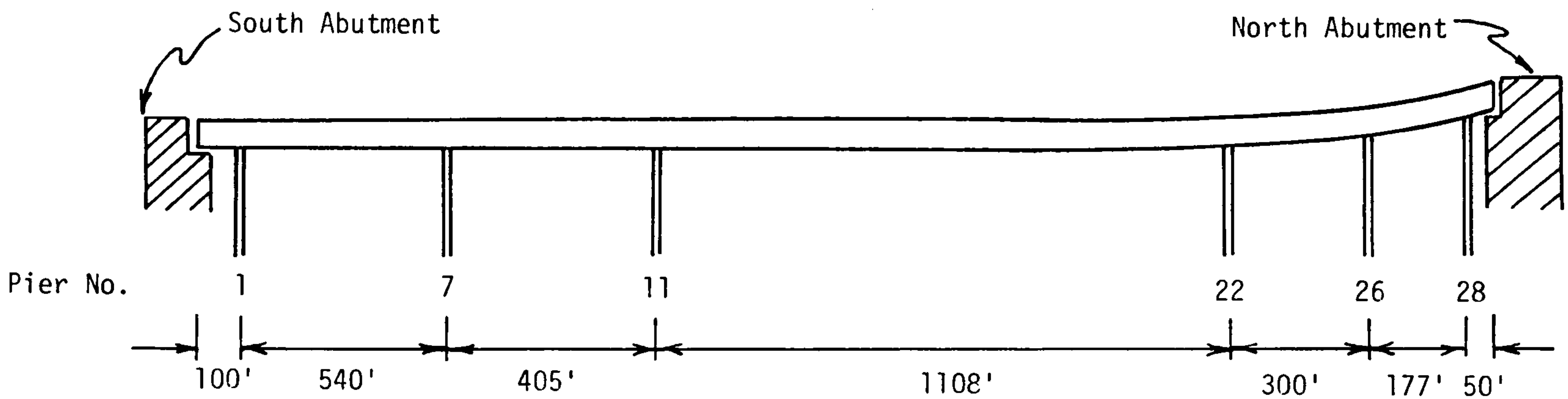

Figure 24. Location of instrumented piers.

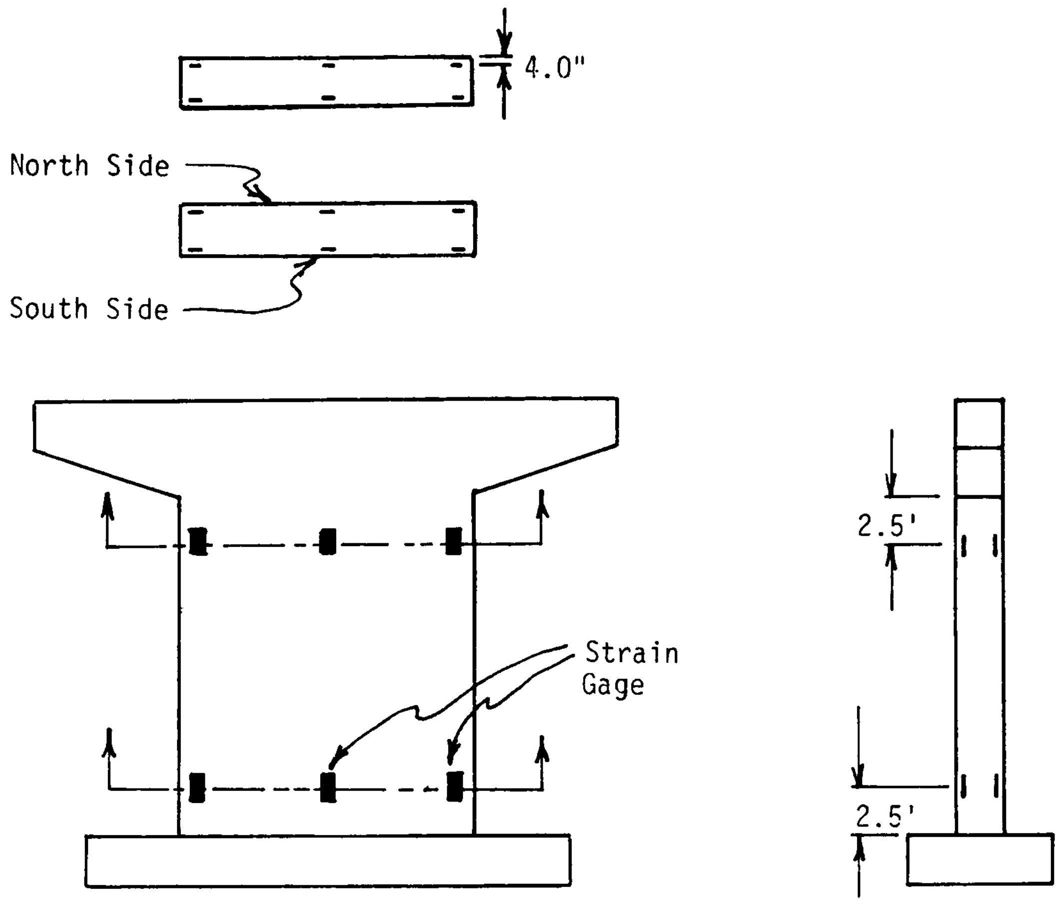

Figure 25. Strain gage locations in a typical pier.

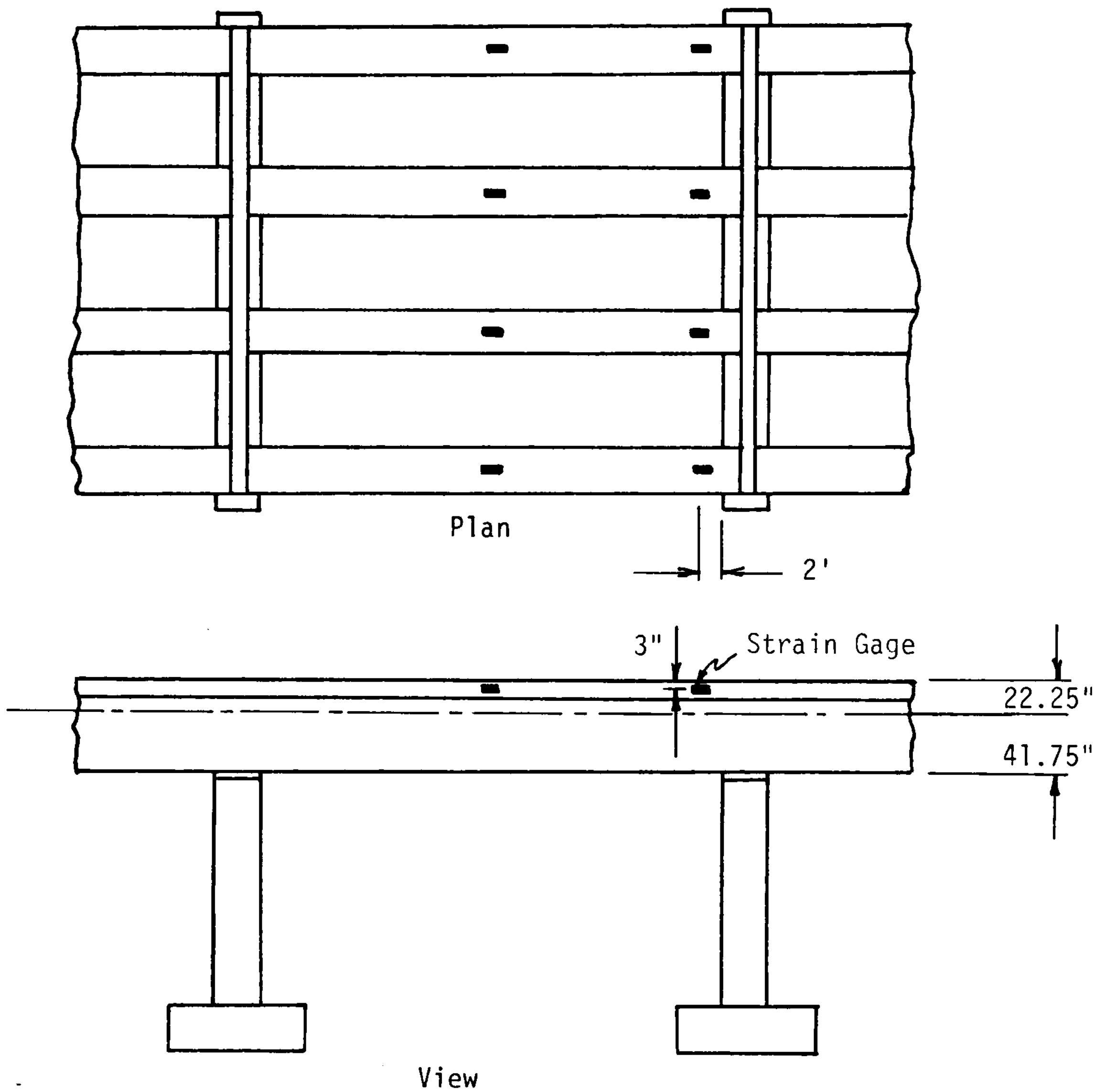

Figure 26. Location of strain gages in a typical deck.

4.3. THERMOCOUPLES

Iron-Constantan Type J thermocouples with a temperature range (0 to 150°F) were used to determine the temperatures throughout the bridge. These thermocouples were embedded in the deck of the bridge between piers 6 and 7 in both the right and left lanes as shown in Figure 27. The thermocouples were connected to a Speedomax 250 multipoint recorder (Leeds and Northrup) to obtain continuous measurements of the temperature.

4.4. CARLSON INSTRUMENTS

Two types of Carlson meters were used in the bridge:

1. The R.C. (Reinforced Concrete) Meter.
2. Carlson Stress Meter for Concrete.

The R.C. (Reinforced Concrete) Meter

This meter is a rod-like device which stimulates a bar of reinforcing steel. It has a length of 34.5 in and a diameter of 1.66 in and is threaded externally near each end. The rod is hollow to maintain the strain meter inside. The advantage of this meter is that readings will always be obtained even in the presence of fine cracks which are present in all reinforced concrete structure. The R.C. meter is also a thermometer and the correction per degree is well known. Another advantage of the R.C. meter is its ease of installation, since all the sensing elements are inside the steel rod. The gage consists of two resistances, R_1 and R_2, connected as shown below. Strain, or change in length, is observed as a change in the ratio of resistance of the two resistances.

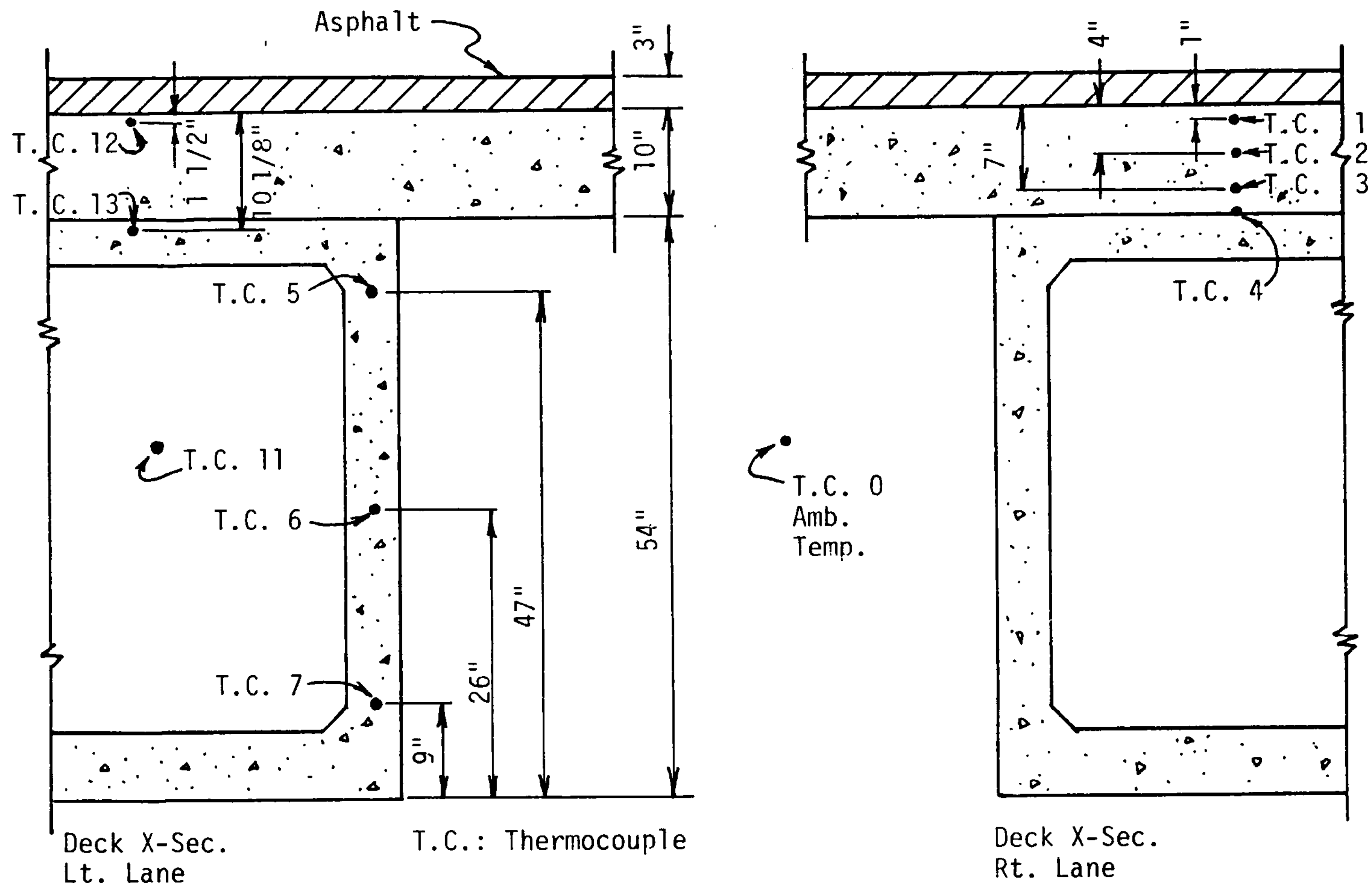

Figure 27. Location of thermocouples.

$$\text{Ratio} = \frac{R_1}{R_2}$$

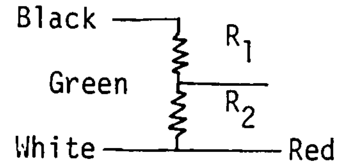

The properties of the two R.C. meters are shown below:

Meter No.	Resistance at 0(°F)	Degrees per ohm	Calibration Constant (Strain)	Calibration Constant (Stress)	Appro. Ratio When Shipped
212	48.33	10.93	3.16	96.5	0.992
214	48.29	10.93	3.19	87.8	0.997

These meters were placed in the deck, right lane, near pier 26 a distance of 3 in below the deck surface. A testing set (James G. Biddle Model 72-4010) designed especially for Carlson meters is used to measure the resistance ratios to 0.01% and resistance (for temperature) to 0.01 ohms.

Carlson Stress Meter for Concrete

This meter consists of a 7-in diameter plate with a strain-meter sensing element mounted on one face. The plate has a mercury film at its mid-thickness and a flexible rim, so that any pressure applied to the plate will be transferred to the mercury film. A thick walled steel tube is attached to the main diaphragm in such a way as to surround the sensing element without touching it. The calibration is in terms of compressive stress per 0.01% reduction in the resistance ratio of the sensing element. The properties of the stress meter are:

Meter No.	Resistance in Ohms at zero °F	Temp. Changes per Resistance Change °F/Ohms	Calibration Constant PSI per 0.01%	Approx. Ratio at Zero Stress	Mercury Thickness
C32	55.07	9.45	8.38	101.6	0.010
C33	55.58	9.36	8.82	101.4	0.012
C34	55.28	9.41	8.29	101.5	0.011

Three stress meters were placed in the diaphragm between two adjacent beams, one at pier 7 and two at pier 13 right lane. The temperature correction can be neglected because it is relatively small. Also, a strain gage bridge made by Biddle was used to get the reading for temperature and ratios.

4.5. STEVENS' WATER LEVEL RECORDERS

This recorder is an instrument designed to measure water level. Stevens' Type F recorders Model 68 were used in the bridge. It consists of a horizontal chart drum which is turned through float action proportional to changes in water levels. There is a pen which moves to the right across the width of the chart at a constant speed controlled by the clock. The combined movement of the chart drum and the pen produces a graphic record of water levels against time.

The Stevens' water level recorders were adapted to provide continuous measurements of the longitudinal movement of the bridge deck versus time. An 8-day clock was used with a gear ratio 1:1 to give a movement of 0.01 ft per division on a chart.

There are five recorders, one for each abutment and one at bent No. 1, right lane, to record the relative movement between the deck and the pier.

4.6. FIELD DATA

Continuous measurements of strains, temperatures and movements were recorded in situ. A typical plot of change in strains for December 3, 1980, is shown in Figure 28. The temperature throughout the deck and the ambient temperature are shown in Figure 29. The location of thermocouples and the strain gages were shown previously in

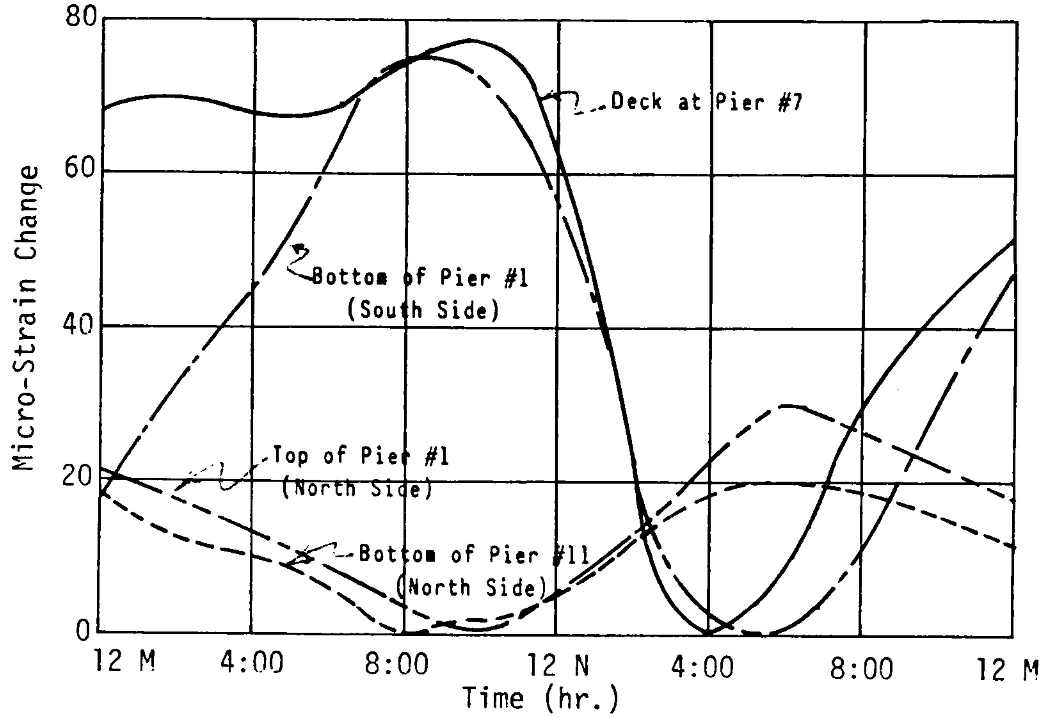

Figure 28. Change in micro-strain vs. time for December 3, 1980.

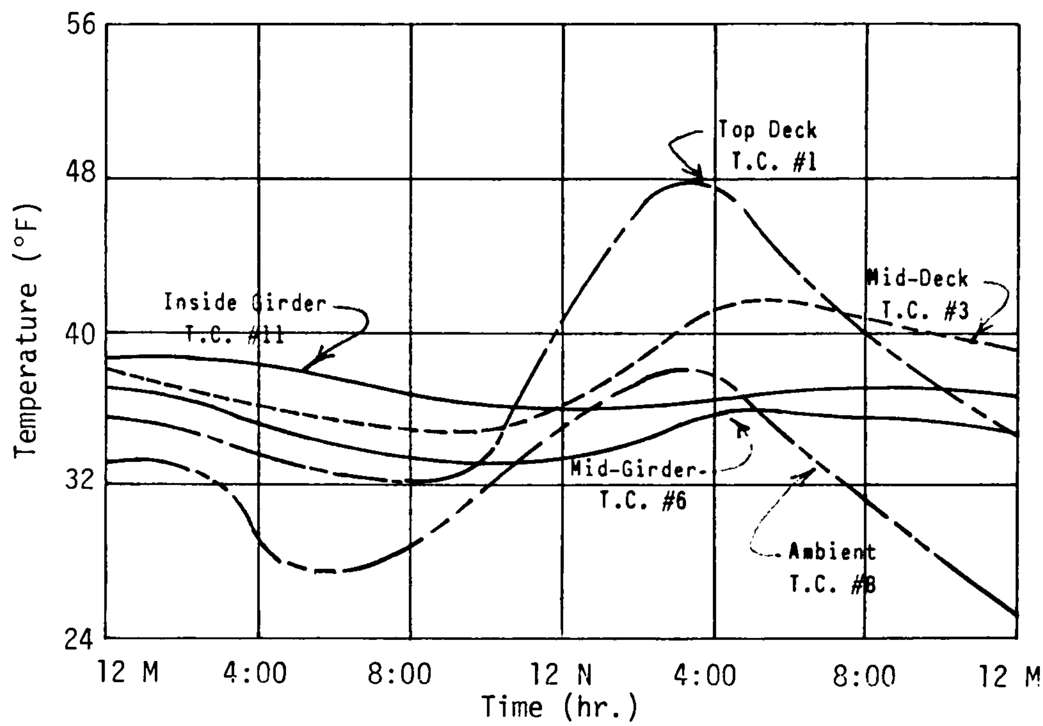

Figure 29. Temperature vs. time for December 3, 1980.

Figures 27 and 25, pp. 68 and 65. It can be seen from Figure 29 that as the ambient temperature rises the deck temperature also increases with different values than the ambient. The top deck temperature (Thermocouple 1) increases more than the mid-girder temperature (Thermocouple 6). The change in the inside-girder temperature (Thermocouple 11) is relatively small compared to the ambient since the box section tries to maintain its temperature. The peak ambient temperature occurred that day at 3:00 P.M. while the top deck temperature reached its highest value at 4:00 P.M.

As the temperature of the deck increases, the superstructure of the bridge tries to expand away from the center, thus pushing the piers. The strain at the north side of piers number 1 and 11 increases as illustrated in Figure 28. Due to the increase in deck temperature the strain in the deck decreases. The maximum change in strain for the piers is at the bottom of pier number 1, because pier 1 moves more as it is farther away from the center of the bridge.

The measurements of movement at the abutments were recorded and are shown in Figure 30. Figure 31 illustrates the inside-girder and mid-deck temperature for the same day. By looking at Figures 30 and 31, the movement and the mid-deck temperature vary in a similar manner (have same shape). The maximum movement of the right lane of the south abutment is 0.028 ft while the maximum change in mid-deck temperature is 7°F with an ambient temperature change of 10°F.

The change in strain for a cold day, February 11, 1981, is shown in Figure 32, while its temperature versus time are shown in Figure 33. The maximum change in ambient temperature is 41°F. Figures 34 and 35

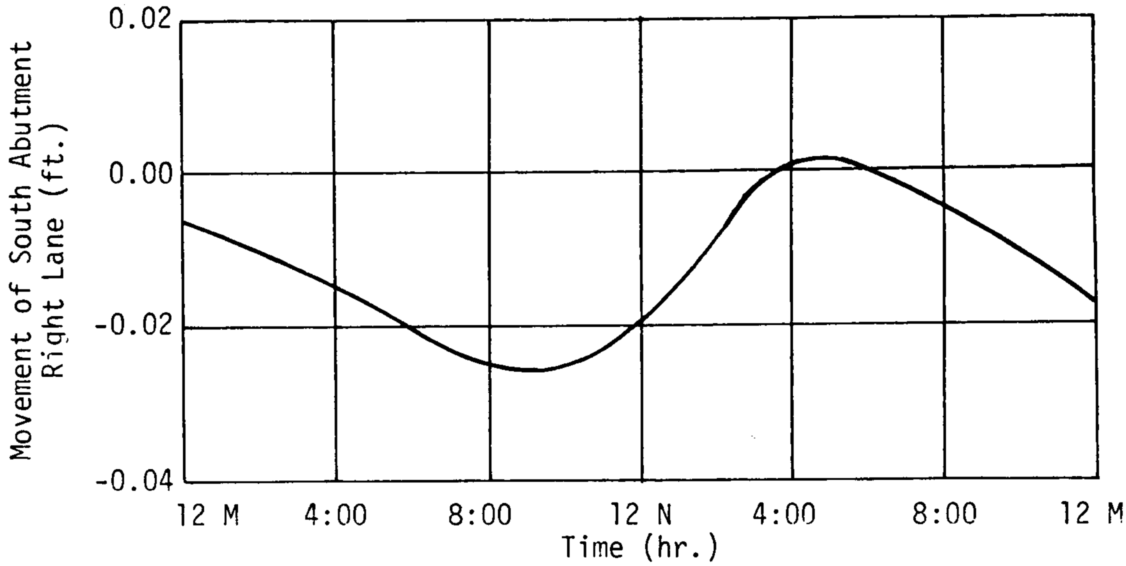

Figure 30. Movement of south abutment, right lane vs. time for December 3, 1980.

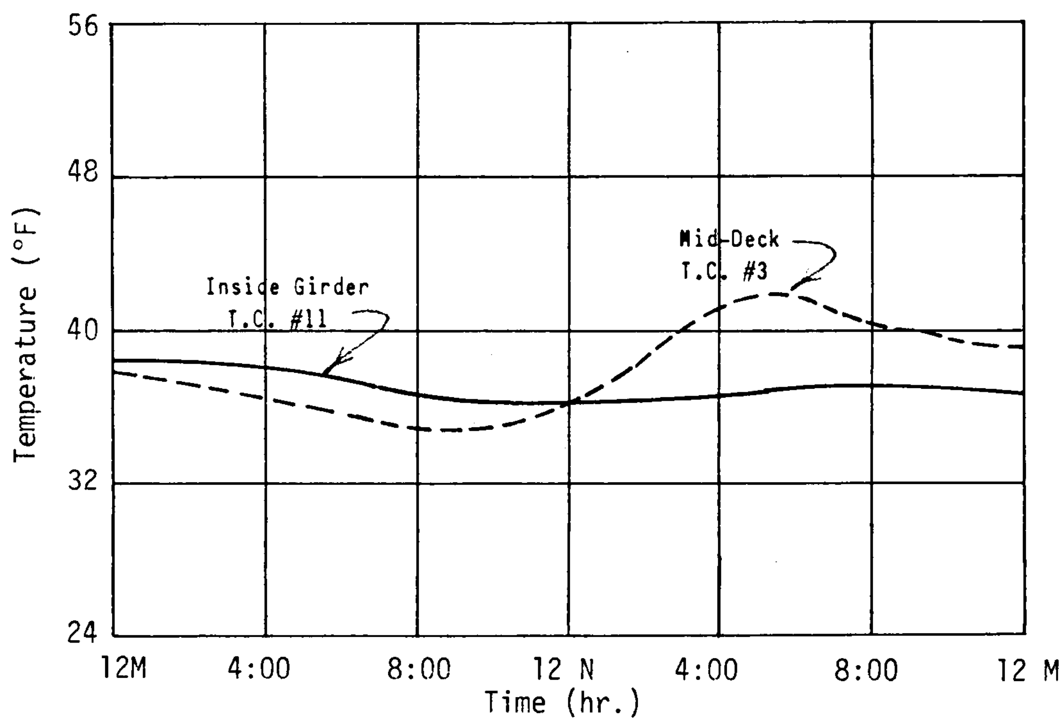

Figure 31. Inside girder and mid-deck temperature vs. time for December 3, 1980.

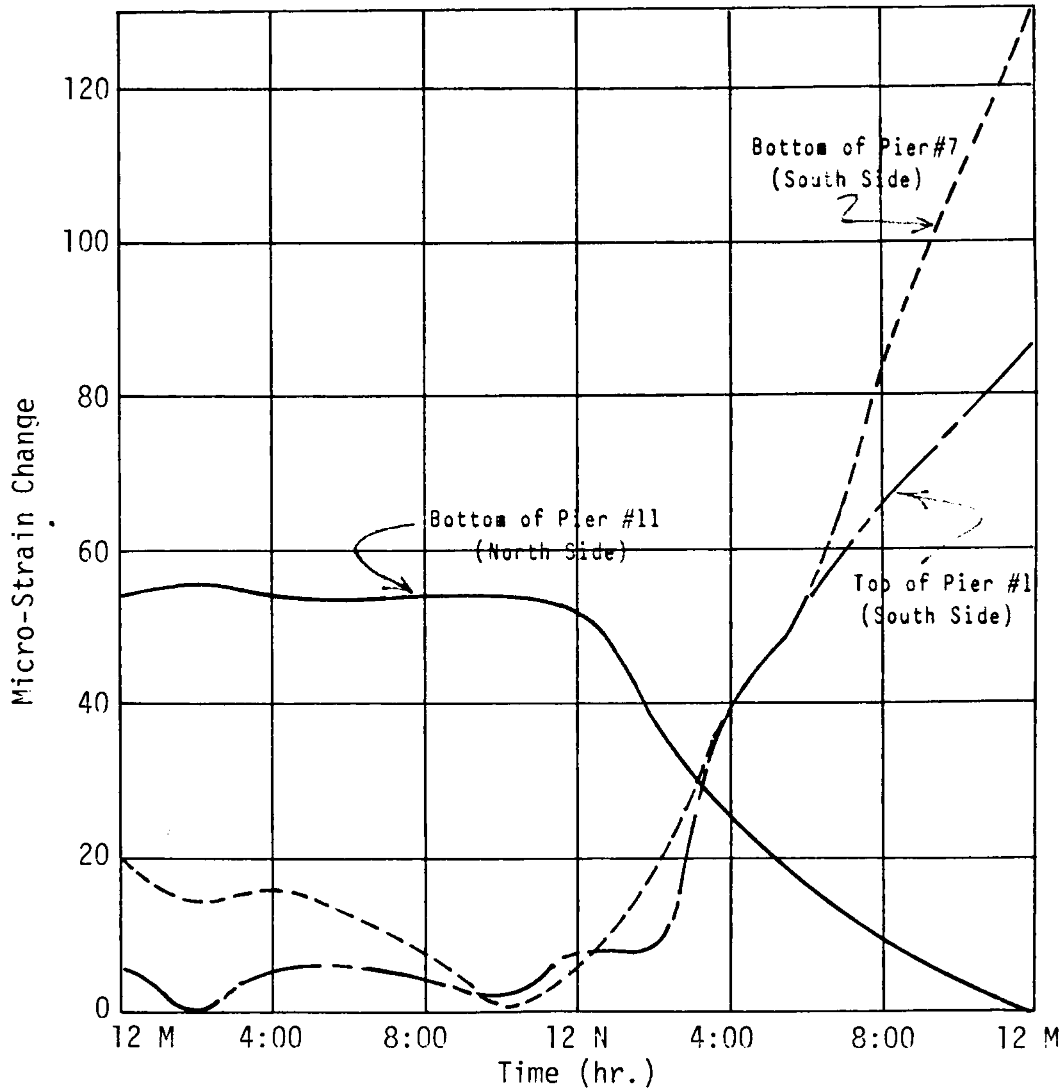

Figure 32. Change in micro-strain vs. time for February 11, 1981.

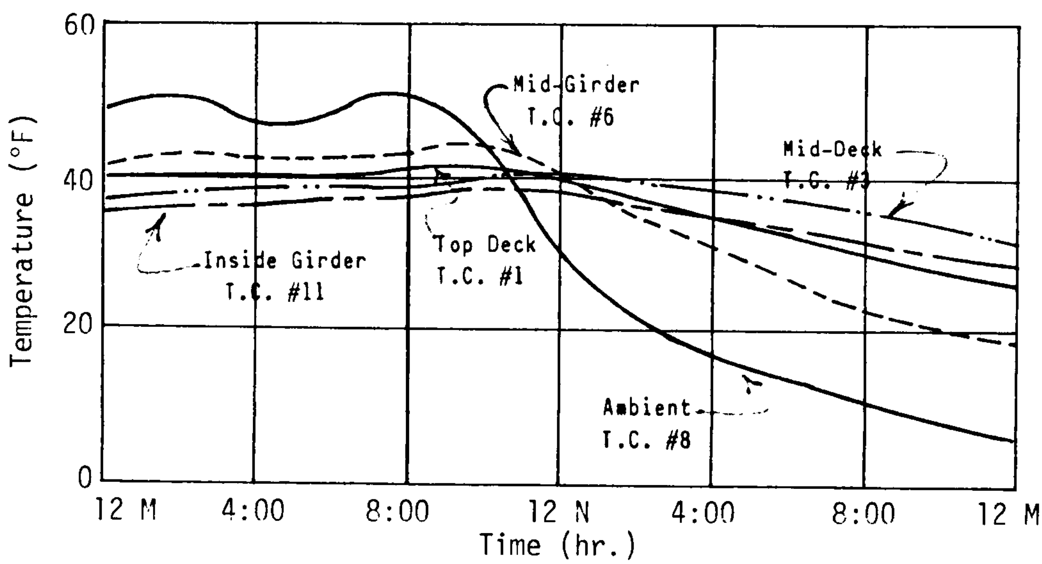

Figure 33. Temperature vs. time for February 11, 1981.

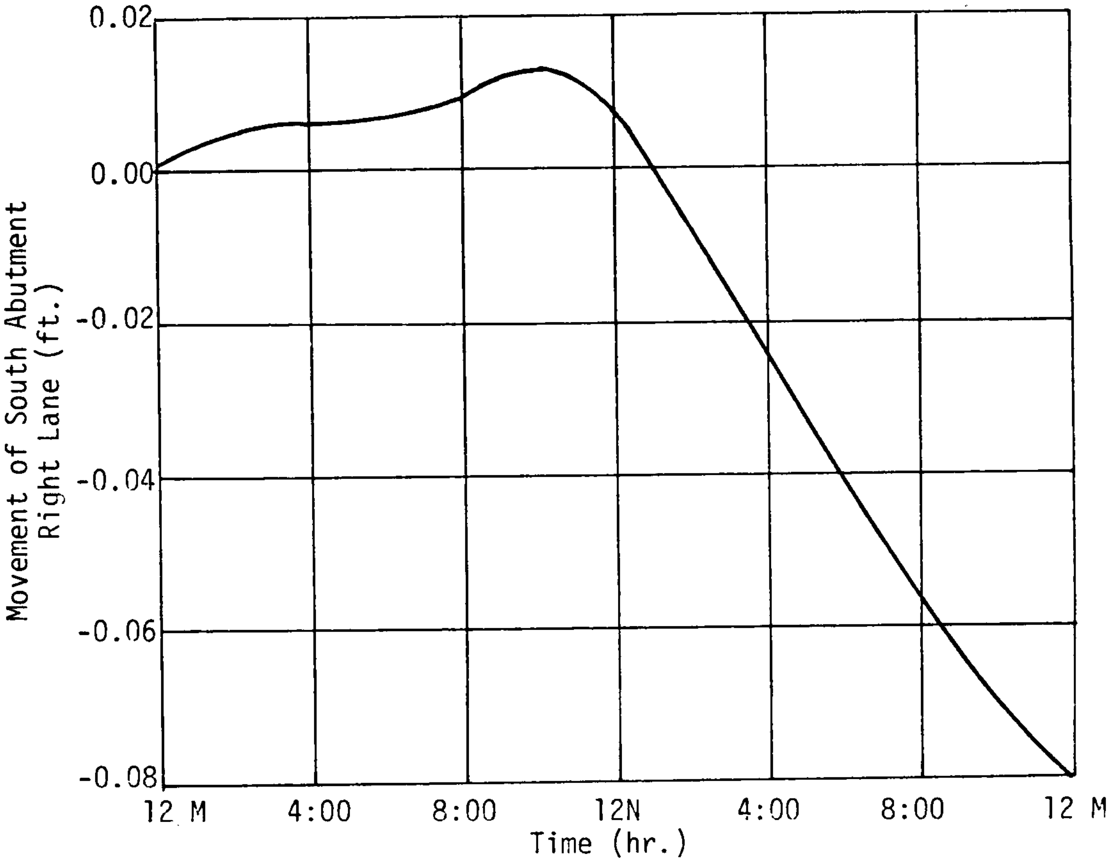

Figure 34. Movement of south abutment, right lane vs. time for February 11, 1981.

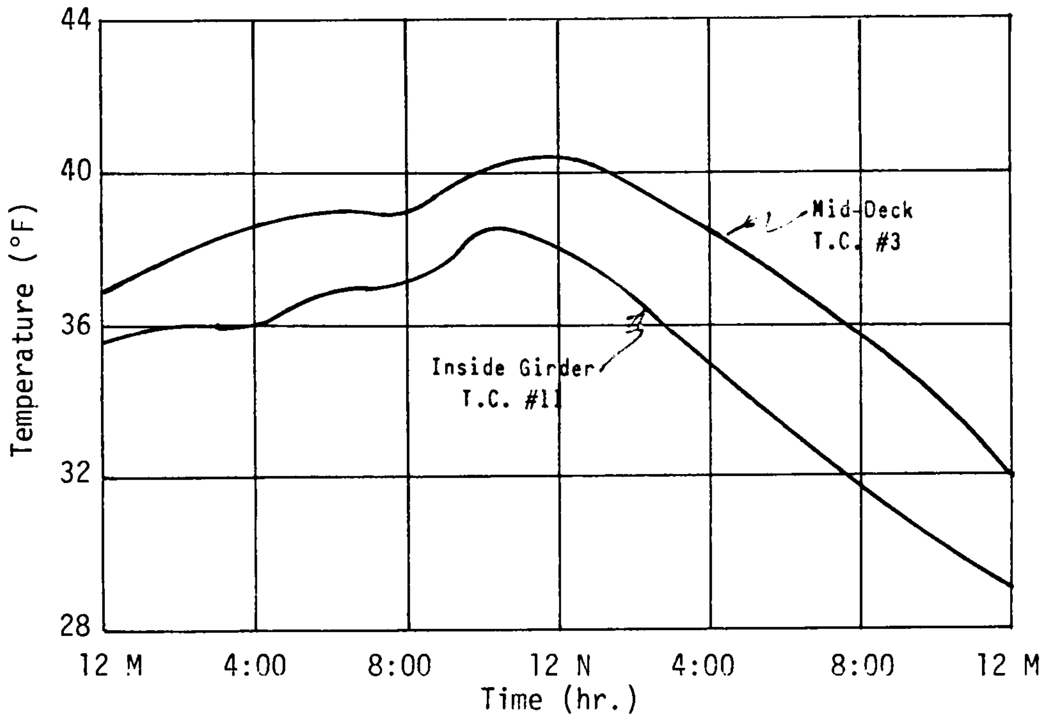

Figure 35. Inside girder and mid-deck temperature vs. time for February 11, 1981.

show the movement of the south abutment and temperature for mid-deck and its girder. The maximum movement of the south abutment, right lane, is 0.093 ft while the maximum change in mid-deck temperature is 8.4°F.

The ambient temperature continued dropping for February 12, 1981. The change in micro-strain and temperature for the same day are shown in Figures 36 and 37. Figures 38 and 39 show the change in micro-strain and inside girder and mid-deck temperature for February 12, 1981.

The analysis of vertical temperature distribution throughout a concrete section is a complex problem because the temperature is a time dependent phenomenon, and the distribution depends on the properties of concrete. A nonlinear temperature distribution throughout the deck was recorded. Figure 40 shows the temperature distribution in the deck for every hour for February 12, 1981.

As mentioned before, the temperature was recorded by installing thermocouples in the deck. The maximum temperature and its change at different locations for a typical period of time are shown in Table 1.* Also the maximum movement of the north and south abutments for both lanes are given in the same table. The maximum daily changes in micro-strain for different strain gages in the bridge are shown in Table 2 (for a period of January 16 to February 7, 1981). Also, the maximum and minimum temperature for different locations of thermocouple in the bridge are illustrated in Table 3 for a period of time between October 22, 1980, and April 9, 1981.

---

*All tables are in Appendix A.

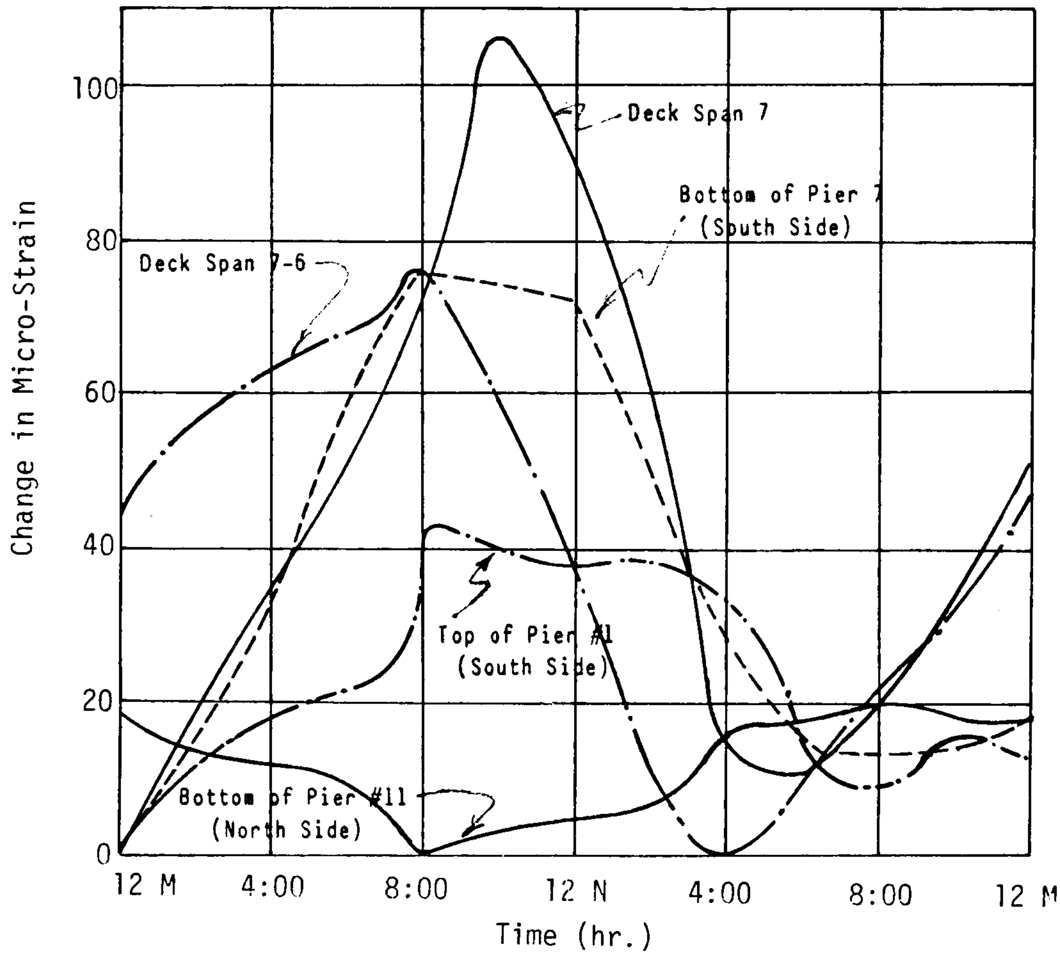

Figure 36. Change in micro-strain vs. time for February 12, 1981.

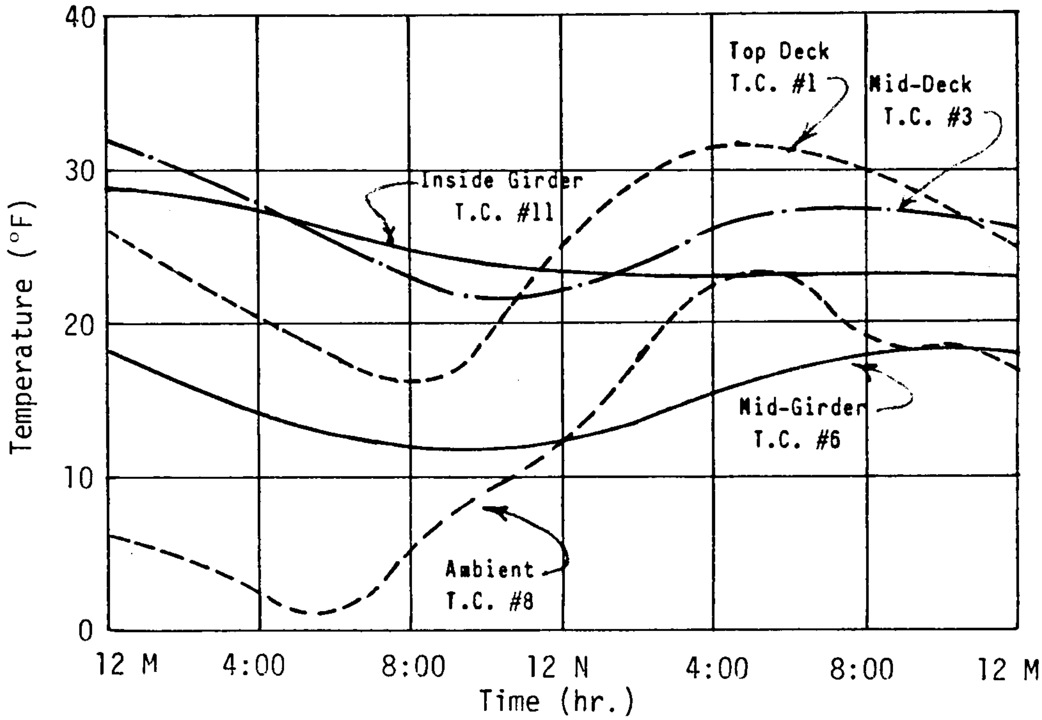

Figure 37. Temperature vs. time for February 12, 1981.

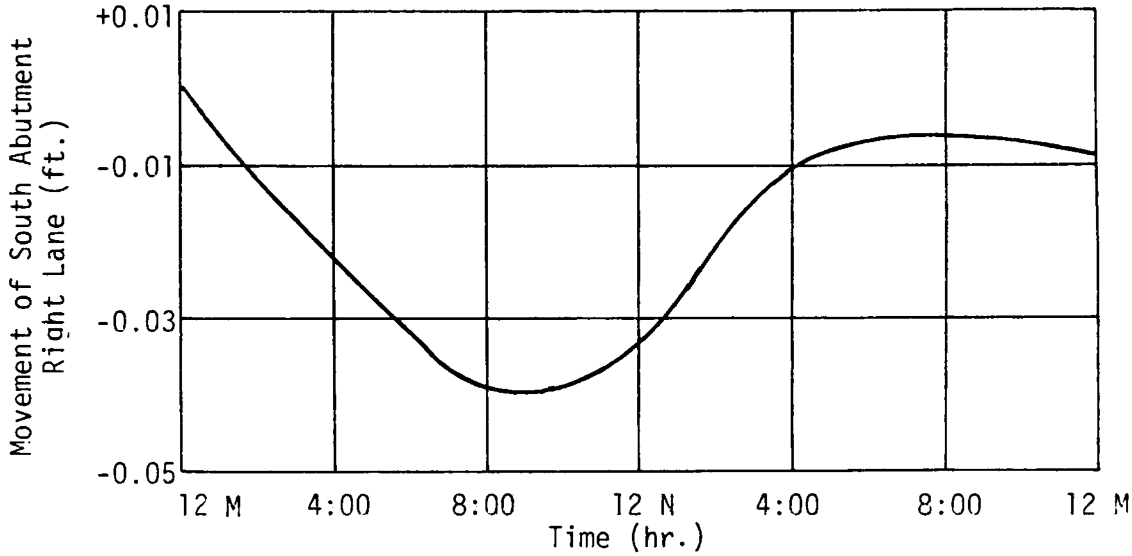

Figure 38. Movement of south abutment, right lane vs. time for February 12, 1981.

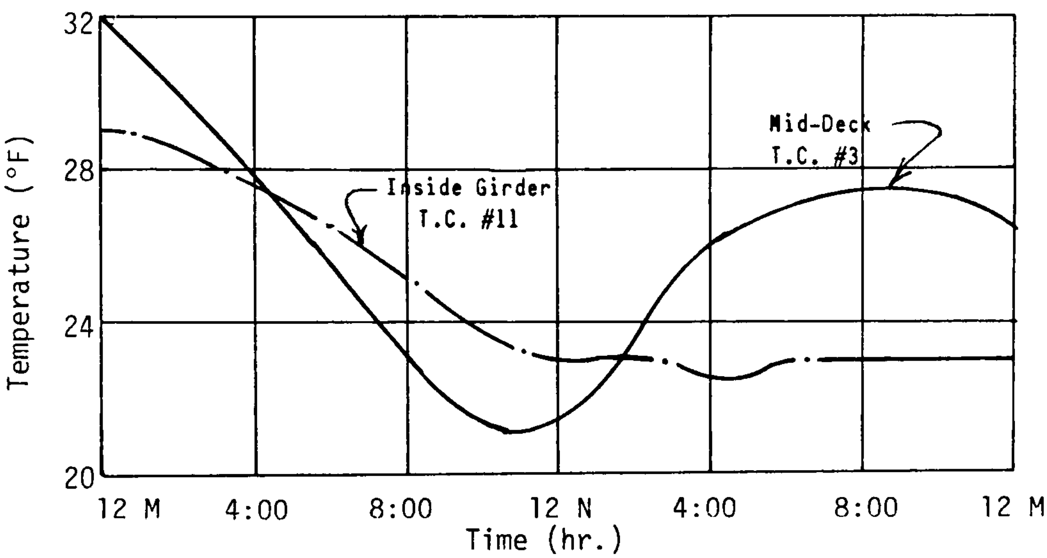

Figure 39. Inside girder and mid-deck temperature vs. time for February 12, 1981.

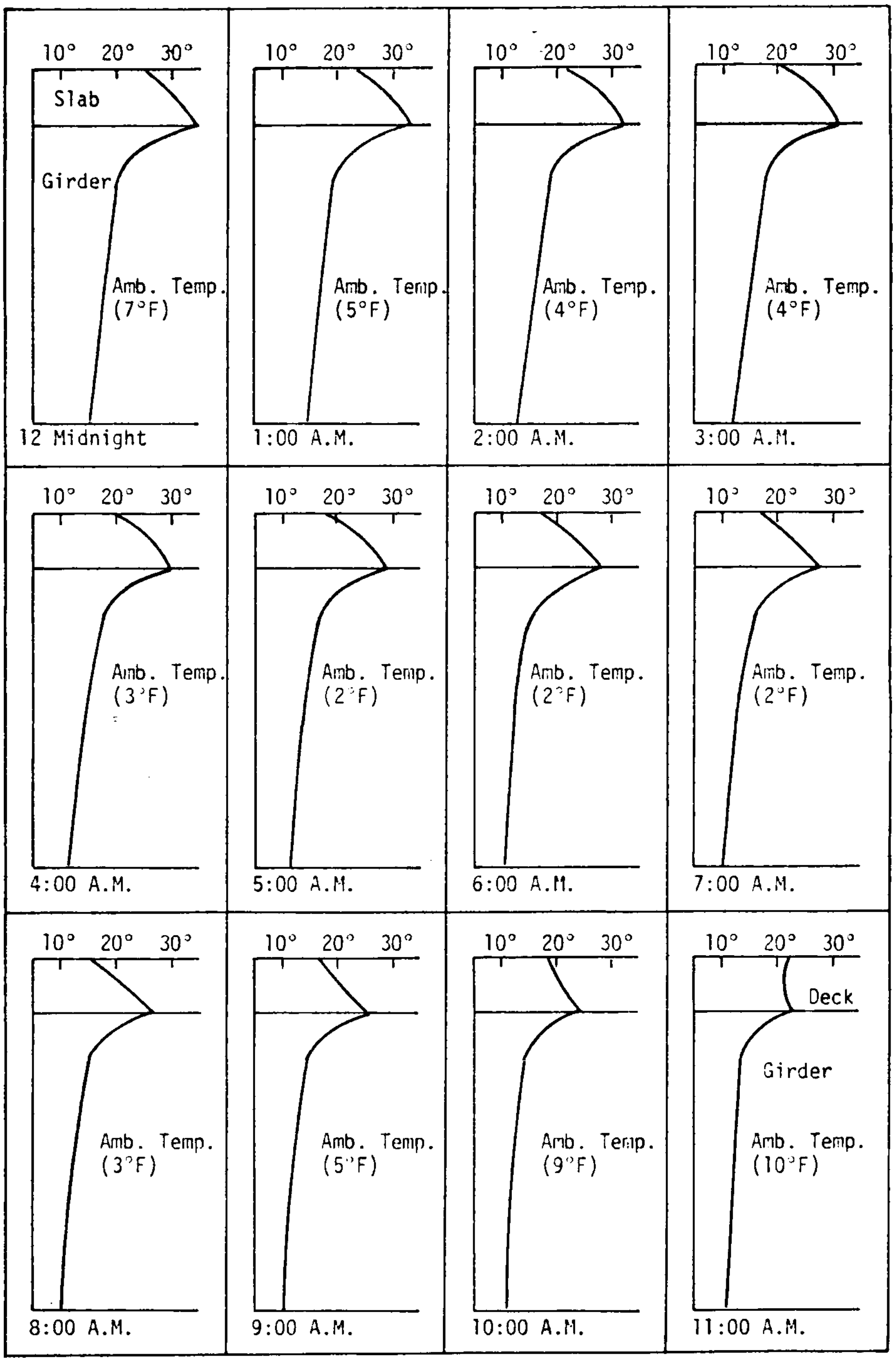

Figure 40. Temperature throughout the deck depth at different times for February 12, 1981.

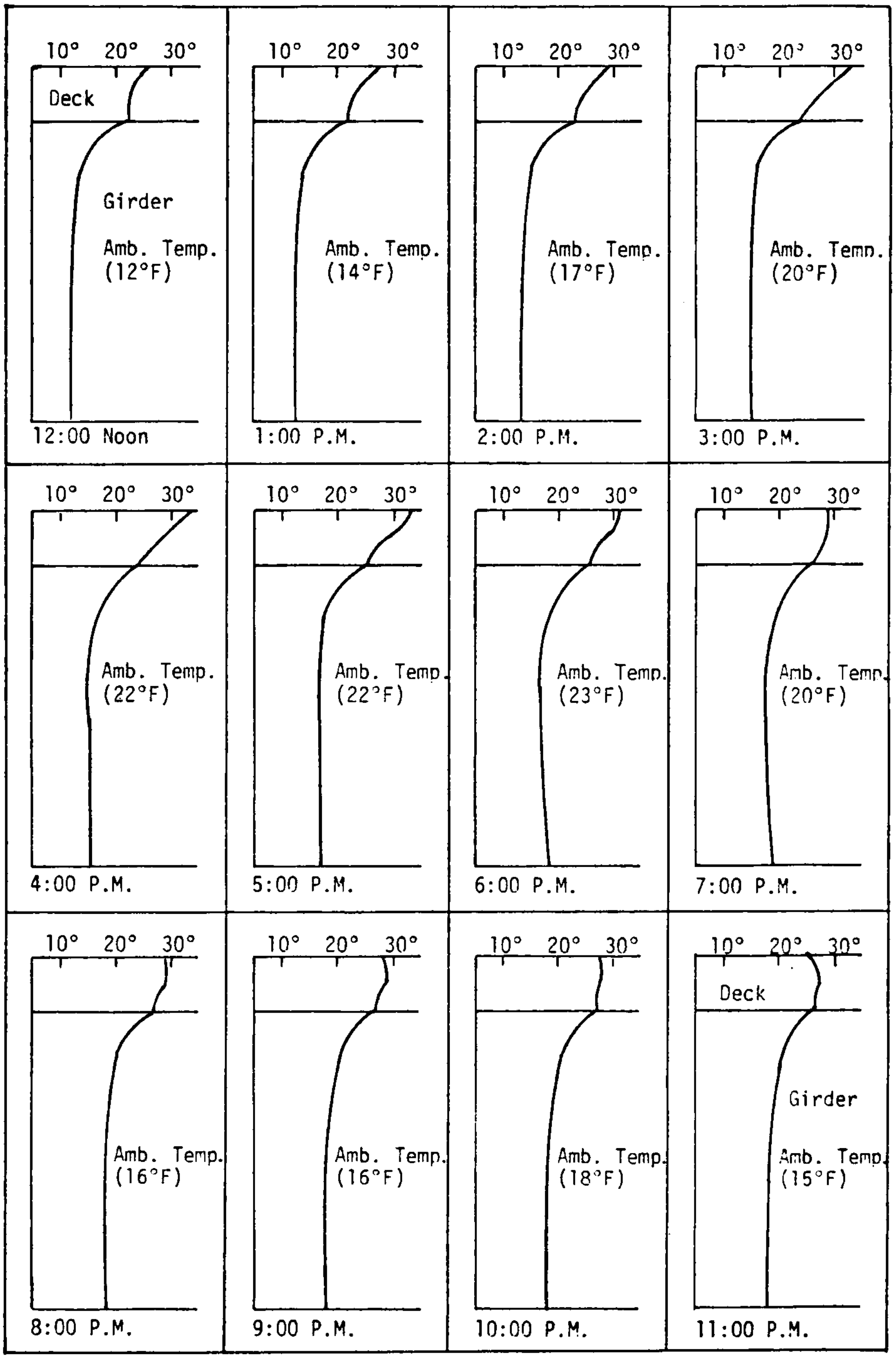

Figure 40 (continued)

4.7. FIELD OBSERVATIONS

Cracks in the diaphragm at bent 28, right lane, were observed. There are four girders coming from bent 27 to bent 28 and five girders going to the north abutment from bent 28. A thorough inspection of the bent led to the conclusion that this type of cracking was caused by an offset in the alignment of the girders at bent 28. Both lanes appeared to have slightly rotated about a vertical axis at first and last spans. The transverse sliding of the girders away from the center line of the bridge, especially at the right lane of the north abutment, produced this rotation. At the abutments only, structural angles were used on both sides of the girders. These angles were bolted to the abutments. The vertical legs of those angles only touched the girders. Due to the movement of the bridge described above, the angles located at the south abutment were bent westward and those at the north abutment eastward, with a maximum horizontal displacement of approximately 3/4-in for the outside girders at north abutment, right lane. The angles on the sides of the girders towards the centerline remained in situ, since no angle to girder connections were provided as mentioned above.

CHAPTER V

THERMAL STRESSES IN A CONCRETE BRIDGE: CALCULATIONS AND COMPARISONS

5.1. DEFINING A MODEL

The superstructure of the bridge consists of pretensioned, prestressed, concrete spreadbox beams supporting a deck slab which is continuous over the length of the bridge as shown previously in Figure 1, p. 3. In order to obtain an analytical solution, a model for the bridge is needed. Since there are dowel bars at the top surface of the girders, the girders and the slab deck are assumed to act compositely as a beam. The modeling for the bridge is shown in Figure 41. One special consideration is the connection between piers and the girders. The girder rests on the pier with three dowels of 1-in diameter, 1'-9" length, and no reinforcement that goes from the pier to the girder (see Figure 20, p. 54). Thus, very little moment will be transmitted from girder to pier. The resulting connection is considered as a hinge which will transmit shear and no moment.

Another special consideration is the fact that the girders and the deck are considered as a composite beam. The neutral axis of the cross section of the composite section is located at some distance above from the connection with the pier. This portion of the girder, which is practically rigid, is modeled as having a moment of inertia 10 to 20 times the moment of inertia of the beam. Another consideration in the modeling of the bridge is the flexibility of the support at the bottom

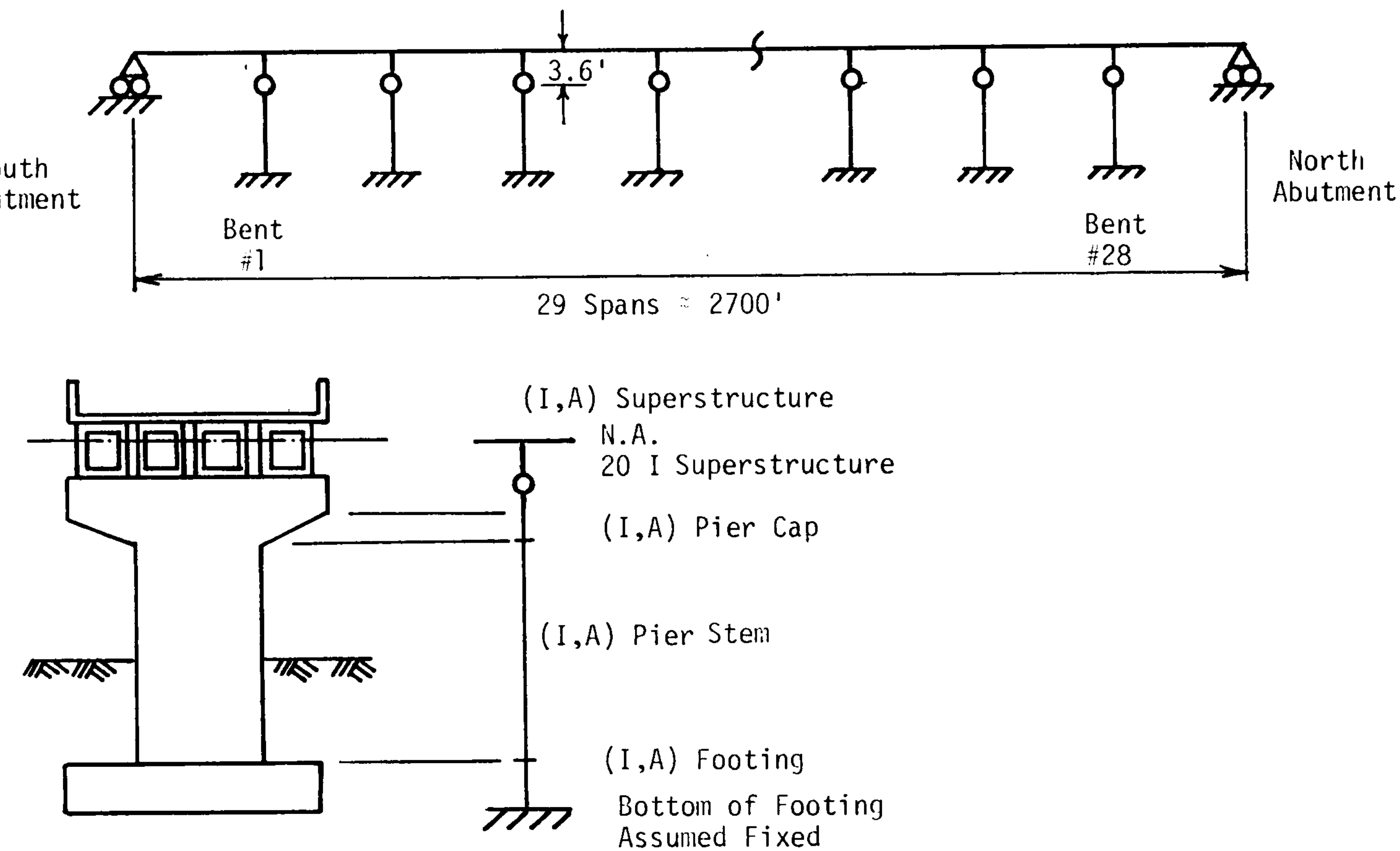

Figure 41. Model of the bridge.

of the footing. Since the footing rests on rock or on piles, the pier is essentially fixed.

The concrete compressive strength for the girder is different from that of the slab deck; thus, a reduction in the effective width of the slab deck is considered.

5.2. APPLICATION OF THE METHOD OF CALCULATING THE THERMAL STRESS IN BRIDGES

From the temperature measurements throughout the deck, it was found that a nonlinear temperature gradient exists. The procedure which was developed in Chapter III is applied for different cases of temperature on different days, and the results of stresses and movements are compared with the field data.

The following steps are followed:

STEP 1. The temperature distribution throughout the superstructure depth of the bridge is plotted for any given period of time where the change in stresses and movement are of interest.

STEP 2. The difference between the two temperature variations is considered as the thermal load on the bridge.

STEP 3. For the nonlinear thermal load found in step 2 and for the properties of the cross section of the bridge, Eq. (3.11) is applied to find the eigenstresses.

STEP 4. Equation (3.13) is applied to find the temperature required to produce eigenstresses. A computer program was developed by the author to evaluate Eqs. (3.11), (3.13) and (3.14).

STEP 5. The temperature found in step 4 is subtracted from the applied thermal load in step 2. (The same temperature can be obtained by applying Eq. (3.14).)

STEP 6. The temperature found in step 5 is the linear temperature which causes the deformation of the structure. The nonlinear part of the temperature which gives the eigenstress does not cause any deformation because the resulting forces are self-equilibrating as discussed in Chapter III.

STEP 7. The linear temperature is applied as a load on the structure by dividing into two parts: the first, which causes pure bending stresses, and the second, which results in a pure axial stress state.

STEP 8. The STRUDL program is implemented by assuming one-dimensional beam elements (see Figure 42) for the bridge and calculating the stresses and movements at the abutments.

STEP 9. The results obtained in the preceding step are compared with the measured values. The actual stress in the deck is the stress calculated or measured in step 8 plus the eigenstress.

To demonstrate the above procedure, the following three comparisons were made. A summary of the calculated and measured values is given in Table 4.

5.2.1. Comparison No. 1

The temperature and change in micro-strain for December 3, 1980, were shown previously in Figures 28 and 29, p. 71. Two different time periods were chosen to calculate the change in strain and the movement of the bridge at the abutments. Those two time periods were 7:30 A.M.

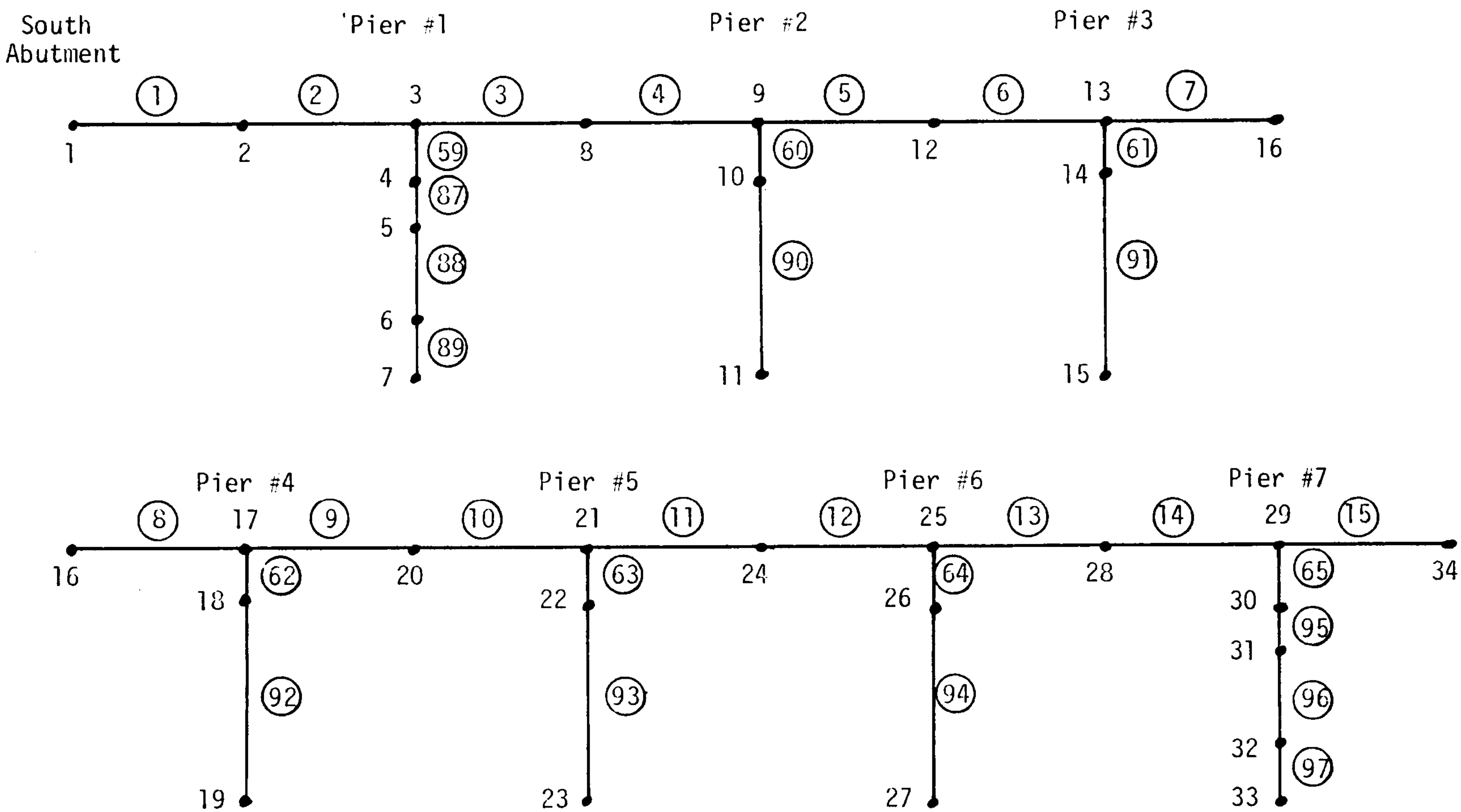

Figure 42. Beam elements of the bridge.

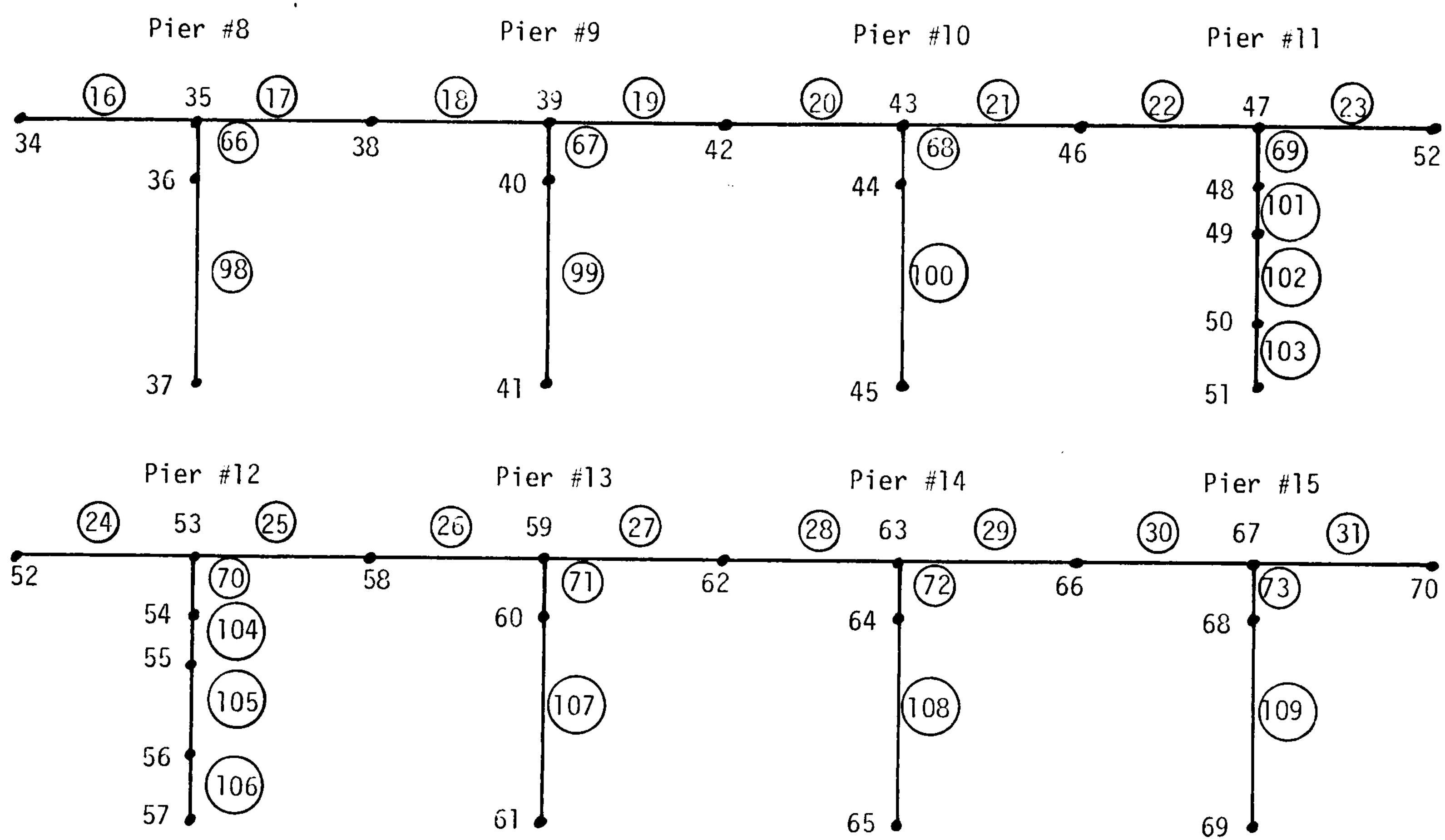

Figure 42 (continued)

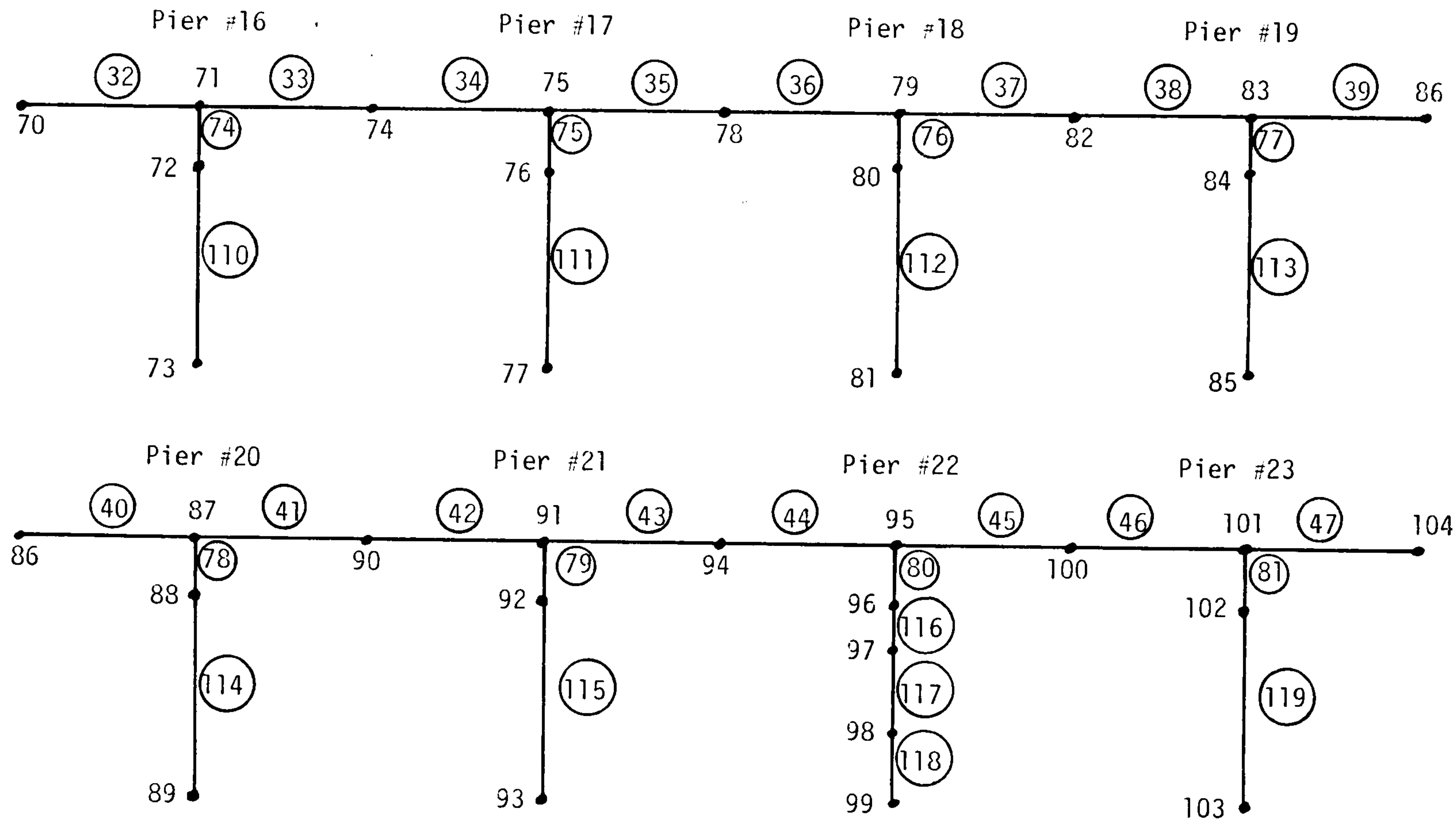

Figure 42 (continued)

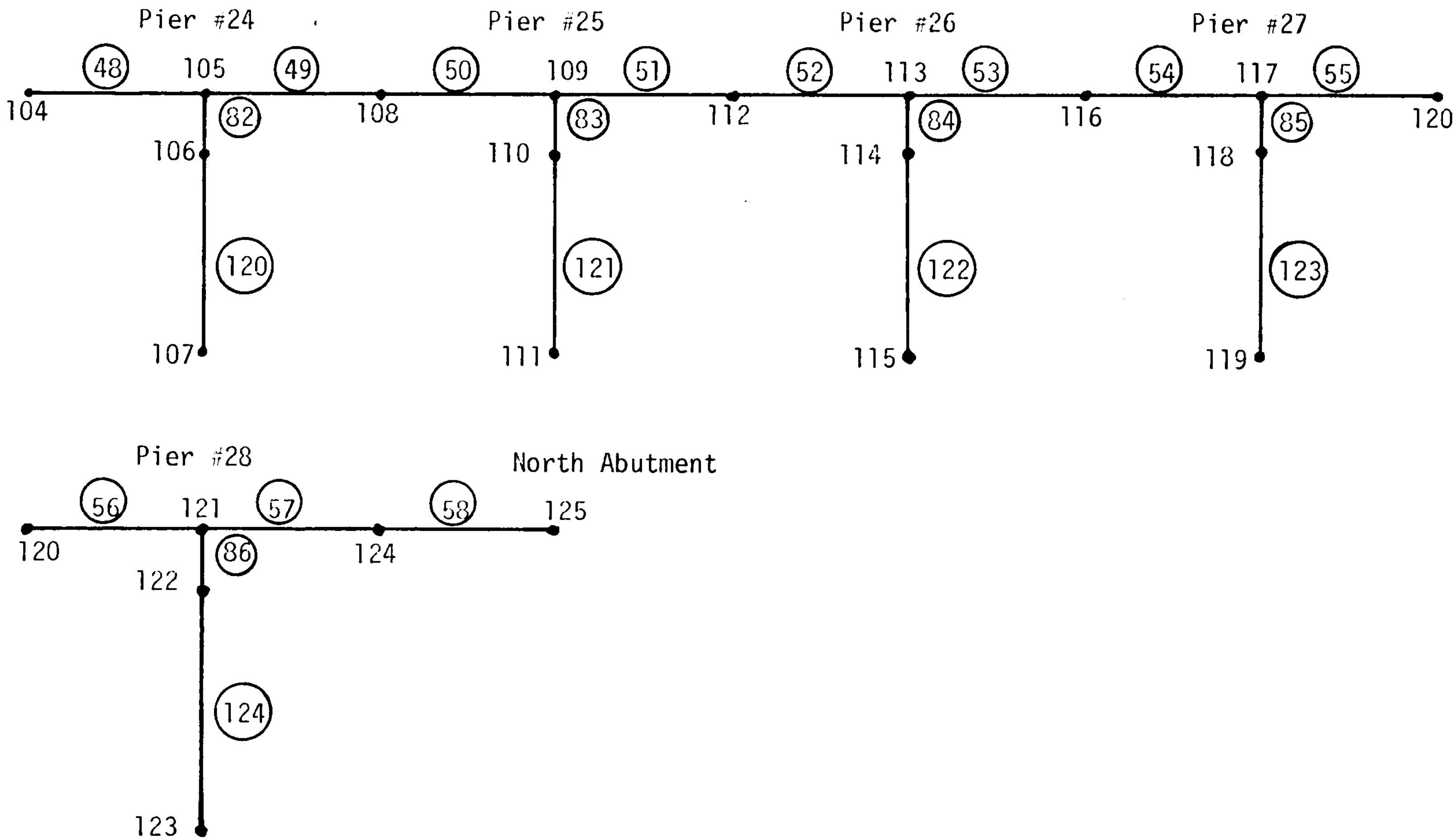

Figure 42 (continued)

and 5:30 P.M. The temperature distribution throughout the deck at those two selected times are shown in Figure 43. The change in deck temperature between those periods is shown in the same figure.

To use the program for calculating the eigenstresses, the change of temperature throughout the deck depth is divided in layers across which the change in temperature is linear. The width and the depth of the section at each layer must be given.

Since the strength of the concrete and, in turn, the modulus of elasticity of the concrete in the precast girders, are different from those in the slab, a reduction in the slab width is needed. The applied thermal load, width and depth of each layer of the section, eigenstress and linear temperature are shown in Table 5.

The following values for the constants were used:

Compressive strength of concrete for girders = 6000 psi,

Compressive strength of concrete for slab deck = 3000 psi.

The reduction factor for width of deck $= \dfrac{57000\ \sqrt{3000}}{57000\ \sqrt{6000}} = \sqrt{\dfrac{1}{2}} = 0.707.$

Coefficient of thermal expansion for concrete = 5.0×10^{-6} in/in/°F. The linear temperature across the depth of the deck was decomposed into two parts, one pure axial and the other pure bending. Both are shown in Figure 44. The resulting forces, displacements and rotation caused by linear thermal load in Figure 44 are given in STRUDL output (Appendix C). The movement and the strains at four different locations are checked as follows.

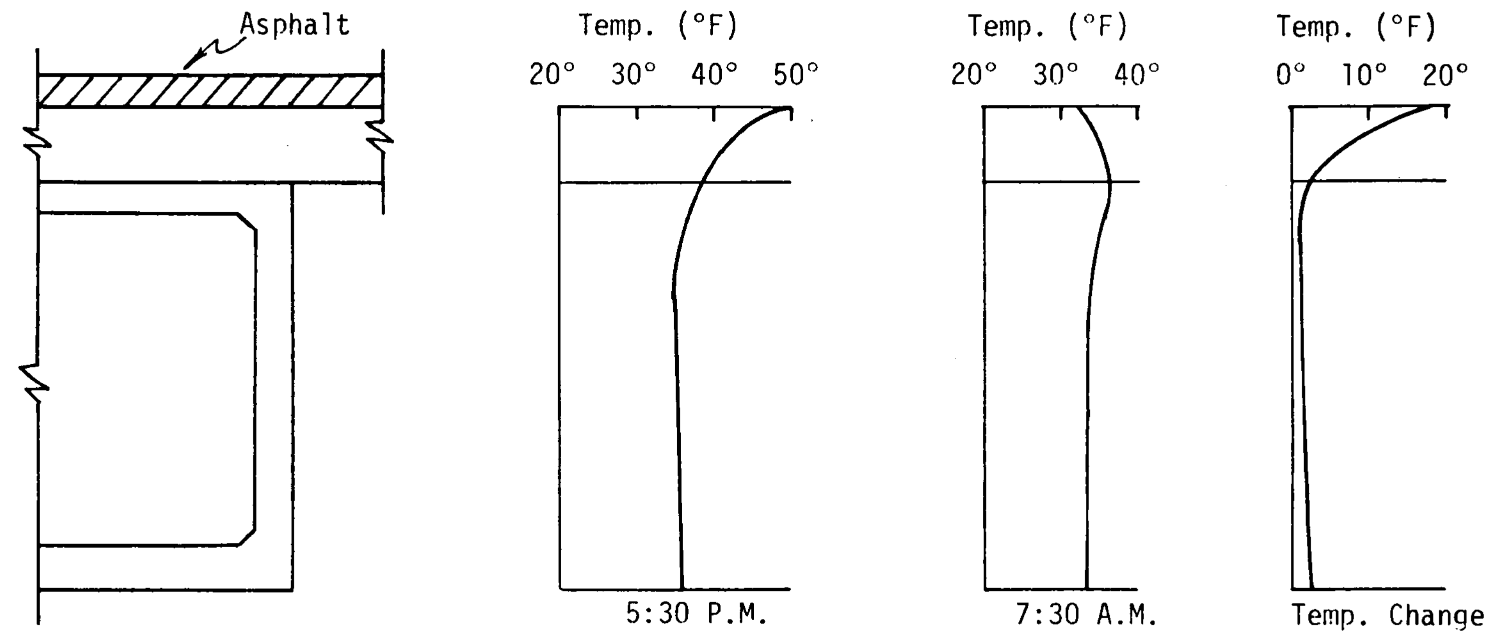

Figure 43. Temperature distribution throughout the depth for December 3, 1980.

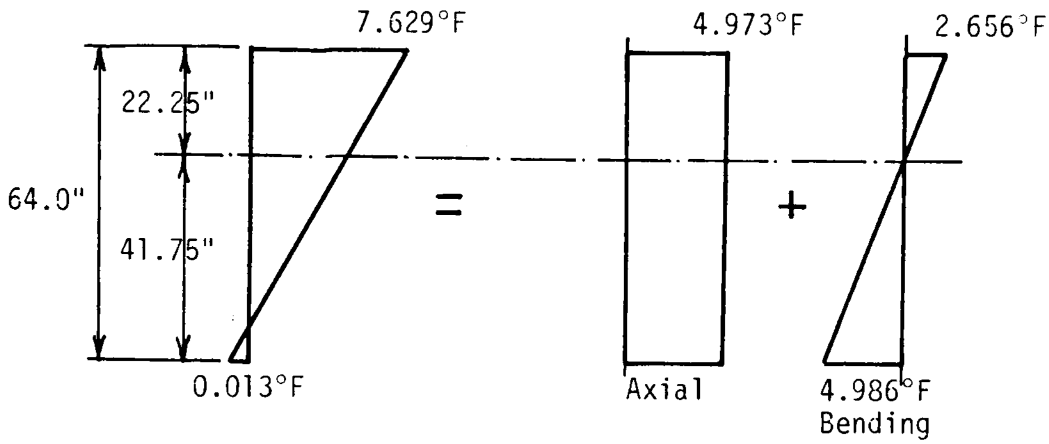

Figure 44. Linear temperature for comparison No. 1.

(1) Movement of South Abutment-Right Lane

Calculated From output results (STRDUL) 0.0265 feet

Measured From Figure 30 (p. 73) 0.0250 feet

(2) Stress at Top of Pier No. 1 (North Side)

Calculated

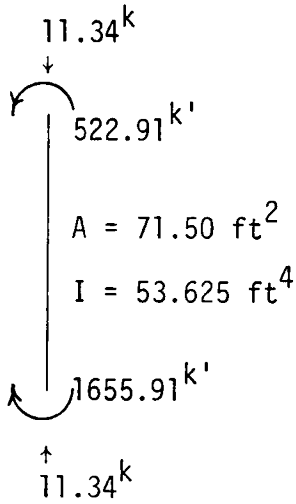

$$\text{Stress} = \left(\frac{522.91\left(1.5 - \frac{4}{12}\right)}{53.625} - \frac{11.34}{71.50}\right)\frac{1000}{144} = +\underline{\underline{77.90}}\ \text{psi}$$

Measured From Figure 28 (p. 71). Strain change = +24 $\mu\varepsilon$

$$\text{Stress} = 24 \times 10^{-6} \times 3.1 \times 10^{6} = \underline{\underline{74.40}}\ \text{psi}$$

(3) Stress at Bottom of Pier No. 1 (South Side)

Calculated $\text{Stress} = \left(-\frac{1655.91 \times 1.167}{53.625} - \frac{11.34}{71.50}\right)\frac{1000}{144} = -\underline{\underline{251.35}}\ \text{psi.}$

Measured From Figure 28. Strain change = - 74 $\mu\varepsilon$

$$\text{Stress} = -74 \times 10^{-6} \times 3.1 \times 10^{+6} = -\underline{\underline{229.4}}\ \text{psi}$$

(4) Stress at Bottom of Pier No. 11 (North Side)

Calculated

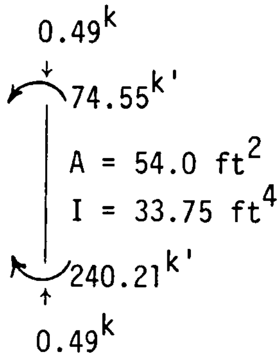

$$\text{Stress} = \left(+\frac{240.21 \times 1.167}{33.75} - \frac{0.49}{54.0}\right)\frac{1000}{144} = +\ \underline{\underline{57.62}}\ \text{psi}$$

Measured From Figure 28 (p. 71). Strain change = +18 $\mu\varepsilon$

$\text{Stress} = +18 \times 10^{-6} \times 3.1 \times 10^{-6} = \underline{\underline{55.8}}$ psi

(5) Stress in the Deck at Pier No. 7

Calculated

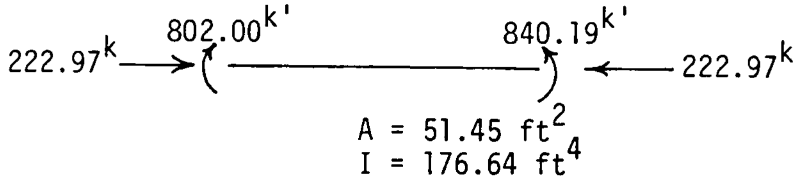

$$\text{Stress} = \left(-\frac{840.19(22.25-3)}{176.64 \times 12} - \frac{222.97}{51.45}\right)\frac{1000}{144} = -\ \underline{\underline{83.08}}\ \text{psi}$$

Measured From Figure 28. Strain change = - 68 $\mu\varepsilon$

Apply Eq. (4.4) and use $\beta = 5.0 \times 10^{-6}$ (for concrete since the gaged bar confined in the concrete).

$\text{Stress} = \varepsilon_R - (\beta - \alpha_g)\Delta t\ E$

From Figure 43. Change of temperature in the deck at 3 in from the top equal to 11°F. E for the concrete girder = 4400 ksi

$\text{Stress} = [-\ 68 - (5.0 - 8.766) \times 10^{-6} \times 11] \times 4.4 \times 10^{6} = -\ 116.93$ psi

$$\text{Stress} = \frac{-116.93}{\sqrt{2}} = -\ \underline{\underline{82.70}}\ \text{psi}$$

Note: The final actual stress in the deck is -82.70 plus the eigenstress.

5.2.2. Comparison No. 2

The method used in comparing measured strains and movements with the corresponding analytical results was checked for a second time, this time under inclement weather conditions. A cold day, February 11, 1981, was chosen to obtain field data. On this day, the ambient temperature dropped 45°F. Both the change in micro-strain and the change in temperature for this day were previously shown in Figures 32 and 33, p. 74.

The temperature change throughout the depth for February 11, 1981, at two different periods of time, 2:00 A.M. and midnight, are shown in Figure 45. Following the same approach outlined before and used in comparison 1, the following results were obtained:

(1) <u>Movement of South Abutment-Right Lane</u>

<u>Calculated</u> From STRUDL output $\underline{\underline{0.0804}}$ ft

<u>Measured</u> From Figure 34 (p. 75). $\underline{\underline{0.085}}$ ft

(2) <u>Stress at Top of Pier No. 1 (South Side)</u>

<u>Calculated</u>

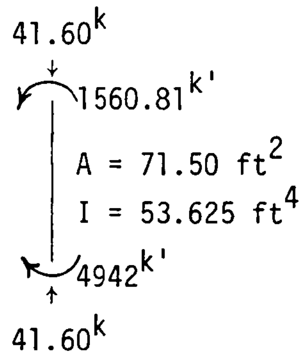

$$\text{Stress} = \left(-\frac{1560.81 \times 1.167}{53.625} - \frac{41.60}{71.50}\right)\frac{1000}{144} = -\underline{\underline{239.92}} \text{ psi}$$

<u>Measured</u> From Figure 32. Strain change = - 86 $\mu\varepsilon$

$$\text{Stress} = -86 \times 10^{-6} \times 3.1 \times 10^{6} = -\underline{\underline{266.6}} \text{ psi}$$

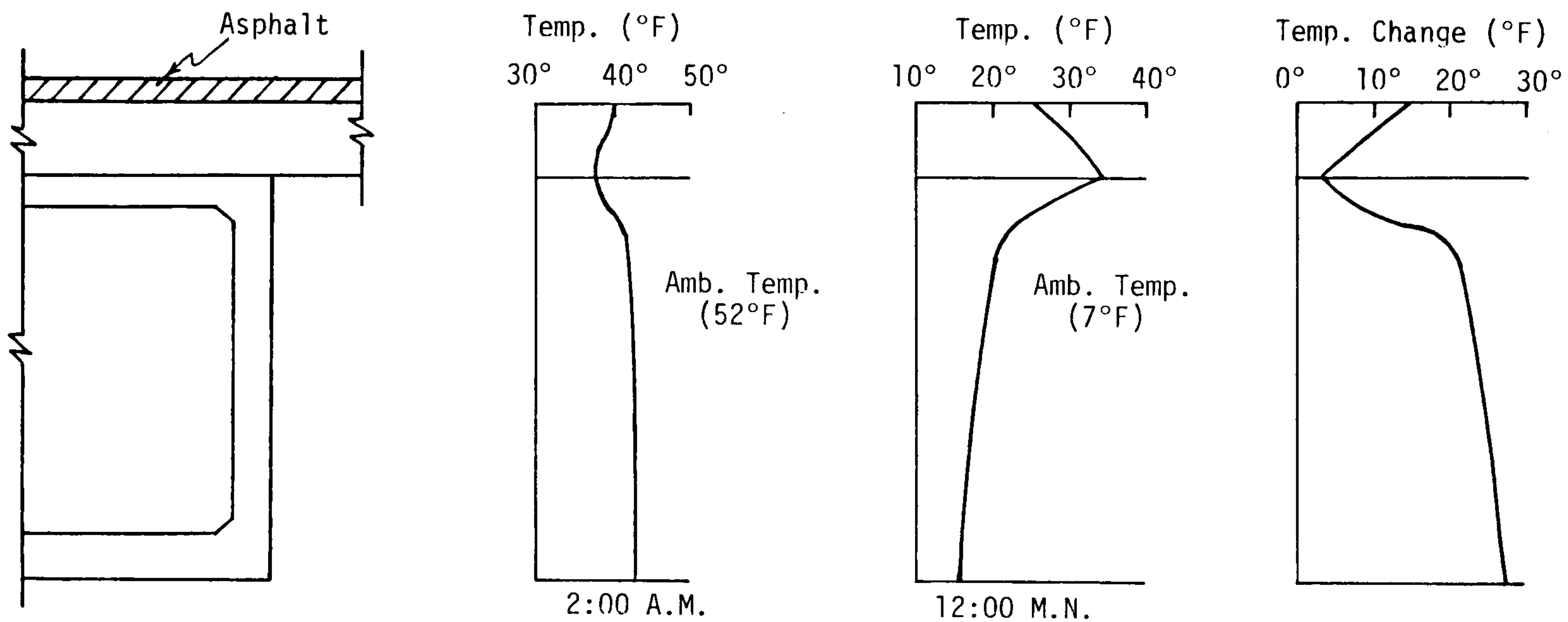

Figure 45. Temperature distribution throughout the depth for February 11, 1981.

(3) Stress at Bottom of Pier No. 11 (North Side)

Calculated

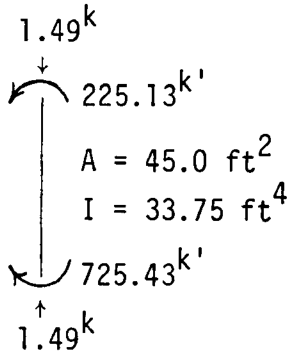

$$\text{Stress} = \left(+\frac{725.43 \times 1.167}{33.75} - \frac{1.49}{45.0}\right)\frac{1000}{144} = +\ \underline{\underline{173.96}}\ \text{psi}$$

Measured From Figure 32 (p. 74). Strain change = 56 $\mu\varepsilon$

$$\text{Stress} = 56 \times 10^{-6} \times 3.1 \times 10^{6} = \underline{\underline{173.6}}\ \text{psi}$$

(4) Stress at Bottom of Pier No. 7 (South Side)

Calculated

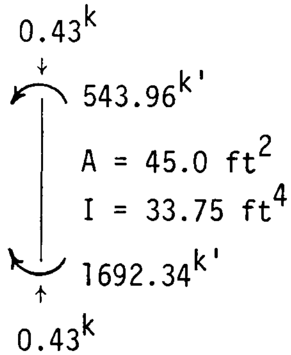

$$\text{Stress} = \left(-\frac{1692.34 \times 1.167}{33.75} + \frac{0.43}{45.0}\right)\frac{1000}{144} = -\ \underline{\underline{406.30}}\ \text{psi}$$

Measured From Figure 32. Strain change = - 116 $\mu\varepsilon$

$$\text{Stress} = -\ 116 \times 10^{-6} \times 3.1 \times 10^{6} = -\ \underline{\underline{359.60}}\ \text{psi}$$

5.2.3. Comparison No. 3

The change in micro-strain at different locations in the bridge for February 12, 1981, was shown in Figure 36, p. 77. Two different time periods, 8:00 A.M. and 8:00 P.M., were chosen to find the strain change and movement of abutments. The temperature distribution in the deck and its changes are shown in Figure 46. For this temperature change, used as a load on the bridge, the eigenstresses and linear temperature were found. Applying the linear temperature as the thermal load and using STRUDL, the following results were obtained and compared with the measured values.

(1) Movement of South Abutment-Right Lane

Calculated From STRUDL output to movement is 0.0381 ft

Measured From Figure 38 (p. 79). The movement is 0.034 ft

(2) Stress at Top of Pier No. 1 (South Side)

Calculated

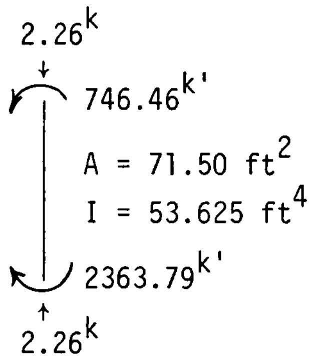

$$\text{Stress} = \left(-\ \frac{746.46 \times 1.167}{53.625} - \frac{2.25}{71.50}\right) \frac{1000}{144} = -\ 113.03 \text{ psi}$$

Measured From Figure 36 (p. 77). Strain change = - 30 $\mu\varepsilon$

$$\text{Stress} = -\ 30 \times 10^{-6} \times 3.1 \times 10^{6} = -\ 93 \text{ psi}$$

(3) Stress at Bottom of Pier No. 7 (South Side)

Calculated

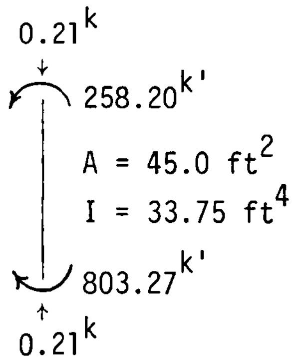

$$\text{Stress} = \left(-\ \frac{803.27 \times 1.167}{33.75} + \frac{0.21}{45.0}\right) \frac{1000}{144} = -\ 192.25 \text{ psi}$$

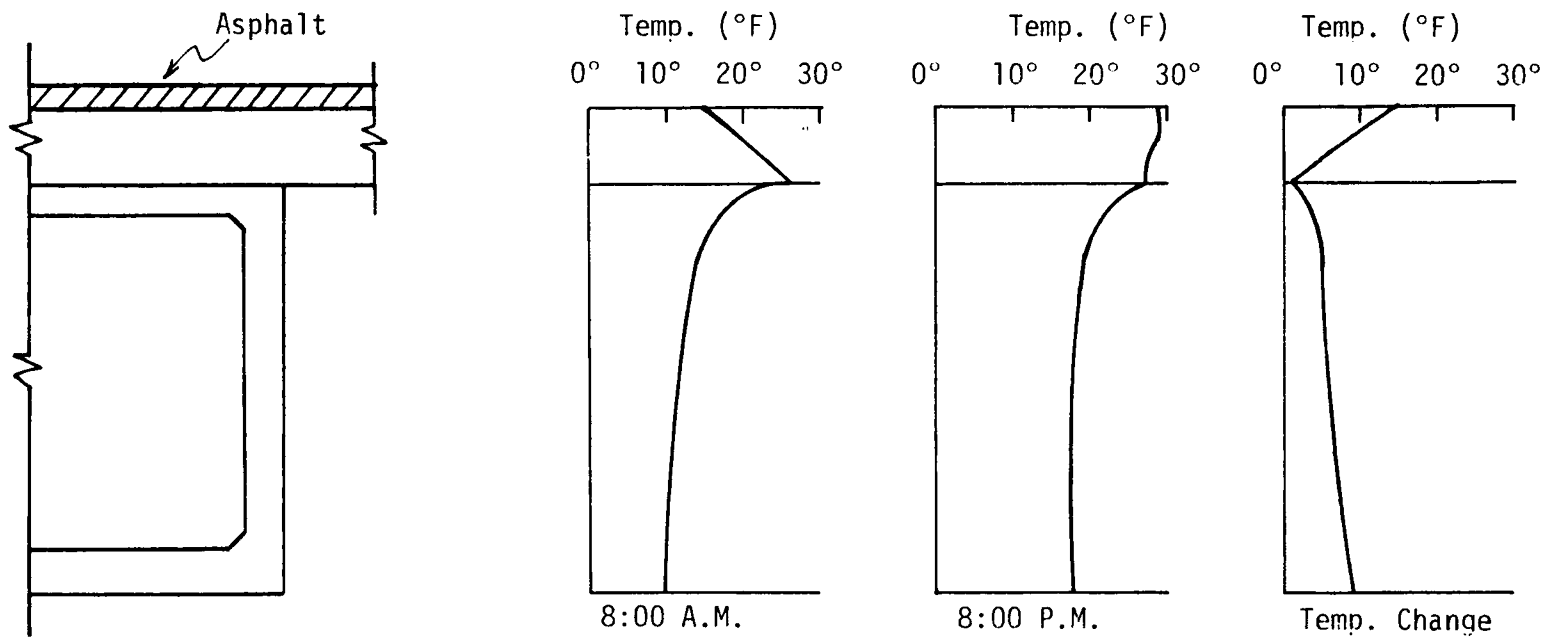

Figure 46. Temperature distribution throughout the depth for February 12, 1981.

Measured From Figure 36 (p. 77). Strain change = - 62 $\mu\varepsilon$

Stress = $-62 \times 10^{-6} \times 3.1 \times 10^{6} = -\underline{\underline{192.2}}$ psi

(4) Stress at Bottom of Pier No. 11 (North Side)

Calculated

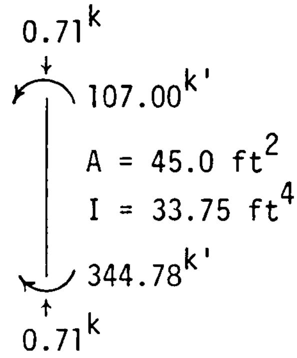

$$\text{Stress} = \left(\frac{344.78 \times 1.167}{33.75} - \frac{0.71}{45.0}\right)\frac{1000}{144} = +\underline{\underline{82.68}} \text{ psi}$$

Measured From Figure 36. Strain change = 20 $\mu\varepsilon$

Stress = $20 \times 10^{-6} \times 3.1 \times 10^{6} = \underline{\underline{63.0}}$ psi

(5) Stress in the Deck at Pier No. 7

Calculated

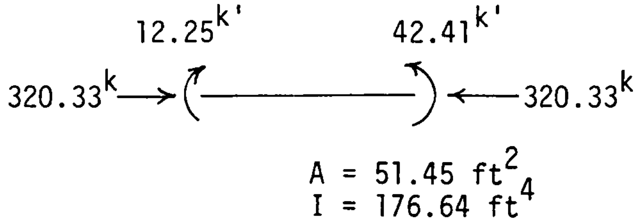

$$\text{Stress} = \left(-\frac{42.41 \times (22.25-3)}{176.64 \times 12} - \frac{320.33}{51.45}\right)\frac{1000}{144} \qquad \begin{array}{l} A = 51.45 \text{ ft}^2 \\ I = 176.64 \text{ ft}^4 \end{array}$$

$= -\underline{\underline{53.94}}$ psi

Measured From Figure 36. Strain change = - 52 $\mu\varepsilon$

From Figure 46. The change of temperature at 3 in from the deck surface is 10°F.

$$\text{Stress} = [-52 - (5-3.766)10] \times 10^{-6} \times 4.4 \times 10^{6}$$

$$= -63.10 \text{ psi}$$

$$\text{Final stress} = \frac{-63.10}{\sqrt{2}} = -\underline{\underline{44.62}} \text{ psi}$$

(6) Stress in the Span 7-6

Calculated Stress = $\left(- \dfrac{12.25\ (22.25-3)}{176.64 \times 12} - \dfrac{320.33}{51.45}\right)\dfrac{1000}{144} = -\underline{\underline{44.01}}$ psi

Measured From Figure 36, p. 77. Strain change = - 54 $\mu\varepsilon$

Stress = $[-54 - (5-8.766)10] \times 10^{-6} \times 4.4 \times 10^{6} = -71.90$ psi

Final stress = $\dfrac{-71.90}{\sqrt{2}} = -\underline{\underline{50.85}}$ psi.

5.3. COMPARISON WITH DEAD LOAD STRESSES

The dead load of the bridge deck was applied as a uniform load over the entire length of the bridge. The following stresses in the deck and piers were obtained.

5.3.1. Dead Load Stresses in the Deck

Span between Abutment and Pier 1

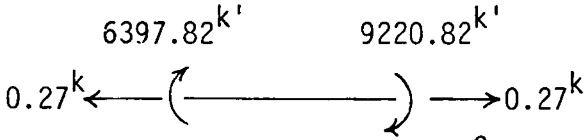

A = 51.45 ft^2
I = 176.64 ft^4

Stress at pier 1 (top fiber) = $\left(+ \dfrac{9220.82 \times 22.25}{176.64 \times 12} + \dfrac{0.271}{51.45}\right)\dfrac{1000}{144}$

$= 672.19$ psi

Note: $\dfrac{E\ \text{deck}}{E\ \text{beams}} = \sqrt{2}$

final stress = $\dfrac{672.19}{\sqrt{2}} = 475.31$ psi

Stress at the center of the span (top fiber)

$= \left(- \dfrac{6397.82 \times 22.25}{176.64 \times 12} + \dfrac{0.271}{51.45}\right)\dfrac{1000}{144}$

$= -466.33$ psi

final stress $= \dfrac{-466.33}{\sqrt{2}} = 329.79$ psi.

Span between piers 6 and 7

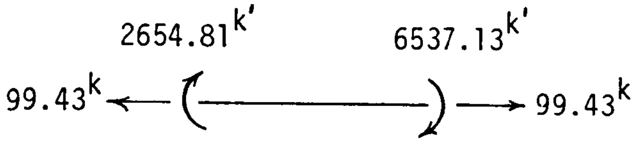

Stress at pier 7 (top fiber) $= \left(+\dfrac{6537.13 \times 22.25}{176.64 \times 12} + \dfrac{99.43}{61.45}\right)\dfrac{1000}{144}$

$= 489.94$ psi

final stress $= \dfrac{489.94}{\sqrt{2}} = 346.49$ psi

Stress at the center of the span (top fiber)

$= \left(-\dfrac{2654.81 \times 22.25}{176.64 \times 12} + \dfrac{99.43}{51.45}\right)\dfrac{1000}{144}$

$= -\ 180.10$ psi

final stress $= \dfrac{-180.10}{\sqrt{2}} = -\ 127.37$ psi

Span between piers 10 and 11

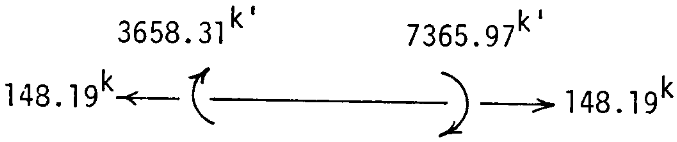

Stress at pier 11 (top fiber) $= \left(+\dfrac{7365.97 \times 22.25}{176.64 \times 12} + \dfrac{148.19}{51.45}\right)\dfrac{1000}{144}$

$= +\ 556.94$ psi

final stress $= \dfrac{556.94}{\sqrt{2}} = 393.82$ psi

Stress at the center of the span (top fiber)

$= \left(-\dfrac{3658.31 \times 22.25}{176.64 \times 12} + \dfrac{148.19}{51.45}\right)\dfrac{1000}{144}$

$= -\ 247.58$ psi

final stress $= \dfrac{-247.58}{\sqrt{2}} = -\ 175.09$ psi

Span between piers 14 and 15

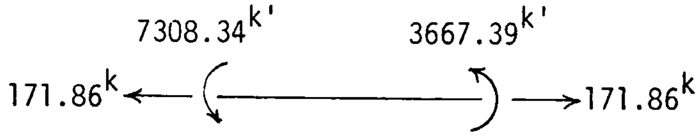

Stress at pier 14 (top fiber) $= \left(+\ \frac{7308.34 \times 22.25}{176.64 \times 12} + \frac{171.86}{51.45}\right)\frac{1000}{144}$

$= +\ 555.94$ psi

final stress $= \frac{555.94}{\sqrt{2}} = 393.16$ psi

Stress at the center of the span (top fiber)

$= \left(-\ \frac{3667.39 \times 22.25}{176.64 \times 12} + \frac{171.86}{51.45}\right)\frac{1000}{144}$

$= -\ 244.14$ psi

final stress $= \frac{-244.14}{\sqrt{2}} = 172.66$ psi.

From the above calculation for stresses, the dead load of the superstructure of the bridge creates tensile stresses in the top fiber of the deck at the span ends (or deck-pier connection). Also a compressive stress in the top fiber of the deck at the center of the span was developed by the same loads.

An increase in temperature of the bridge caused a compressive stress at the top surface of the deck over the whole length of the bridge. Thus, the dead load stresses reduce the compressive stresses in the deck at the span ends, and increase the compressive stresses in the deck at center of the span. (Of course a decrease in bridge temperature has an opposite effect.)

The actual maximum thermal stress at the top of the deck at center of the span between pier 14 and 15 was 325.58 psi in compression (206.46 psi plus the eigenstress, both of which are compressive) as can be shown earlier in the previous section (Compression No. 2). The stress due to the dead load of the bridge at the same location was 172.66 psi in compression. Therefore, the thermal stress has a comparable value to the dead load stresses.

5.3.2. Dead Load Stresses in the Piers

Pier No. 1

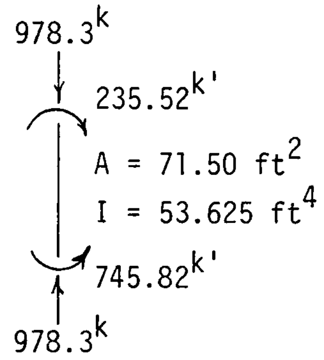

Stress at the bottom of pier No. 1 (north side)

$$= \left(- \frac{745.82 \times 1.167}{53.625} - \frac{978.3}{71.50}\right) \frac{1000}{144}$$

$$= -\ 207.70 \text{ psi}$$

Stress at the bottom of pier No. 1 (south side)

$$= \left(+ \frac{745.82 \times 1.167}{53.625} - \frac{978.3}{71.50}\right) \frac{1000}{144}$$

$$= +\ 17.73 \text{ psi}$$

Pier No. 7

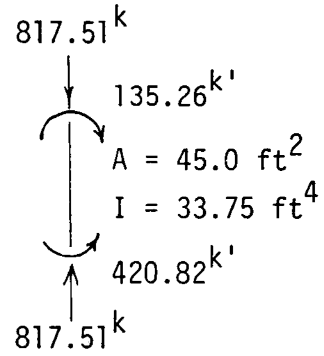

Stress at the bottom of pier No. 7 (north side)

$$= \left(- \frac{420.82 \times 1.167}{33.75} - \frac{817.51}{45.0}\right) \frac{1000}{144}$$

$$= -\ 227.2 \text{ psi.}$$

Stress at the bottom of pier No. 7 (south side)

$$= \left(\frac{420.82 \times 1.167}{33.75} - \frac{817.51}{45.0}\right) \frac{1000}{144}$$

$$= -\ 25.11 \text{ psi.}$$

Pier No. 11

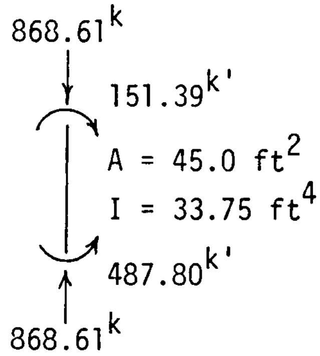

Stress at the bottom of pier No. 11 (north side)

$$= \left(- \frac{487.80 \times 1.167}{33.75} - \frac{868.61}{45.0}\right) \frac{1000}{144}$$

$$= -\ 251.18 \text{ psi}$$

Stress at the bottom of pier No. 11 (south side)

$$= \left(+ \frac{487.80 \times 1.167}{33.75} - \frac{868.61}{45.0}\right) \frac{1000}{144}$$

$$= -\ 16.91 \text{ psi.}$$

As can be seen from the preceding calculations, the dead load of the bridge superstructure caused stresses that are compressive in nature at the bottom of the north side of piers 1, 7, and 11. Those compressive stresses vary between 200 psi and 260 psi.

The stresses due to a 45 degree change in ambient temperature were most pronounced near the ends of the bridge. Tensile stresses of

740 psi, 360 psi, and 173 psi were developed by the 45 degree differential in ambient temperature at the bottom of piers 1, 7, and 11, respectively.

CHAPTER VI

SUMMARY AND CONCLUSIONS

6.1. SUMMARY

Changes in ambient temperature have definite and measurable effects on concrete structures such as bridges. Expansion bridges are used as standard practice in the design of bridges to provide for thermal effects; however, these devices can cause serious problems. In this regard, the Tennessee Department of Transportation has been motivated in the direction of minimizing or omitting expansion bearings and joints during the last few years. This Department's bridge engineers have designed longer and longer bridges with no provisions made for expansion joints over the entire bridge span except at the abutments. The bridge currently under investigation and which is the subject of this research has a 2700 foot span, the longest yet built without internal expansion devices.

Due to the continuity of the superstructure and the restraint of the superstructure against movement relative to the piers, temperature changes induce strains as well as movements. Strain measurements were obtained by installing weldable strain gages in the bridge deck and in selected piers along the bridge span. Thermocouples were placed at various depths throughout the depth of the superstructure to monitor the temperature at various locations. The ambient air temperature as well as inside girder temperature were also recorded by installing thermocouples on the outer surface of the bridge as well as the inner surface of the box girders. Continuous measurements of the movement of the superstructure at both abutments were recorded.

The purpose of this dissertation is threefold: first, to develop and present a theoretical method for calculating thermal stresses induced in continuous bridge structures; second, to collect and analyze field data obtained from strain gages and thermocouples that have been placed in the bridge; and finally, from the comparison of measured results with analytical and computer results for different models, to make recommendations for design of this type of bridge.

The procedure which was developed in this research to calculate the thermal stresses and movements in continuous bridge states is as follows:

1. From the thermocouple measurements, a nonlinear temperature distribution throughout the depth of the superstructure was applied as a thermal load on the bridge.

2. This nonlinear temperature was divided into two parts: first, a linear temperature distribution which causes deformation in the bridge (given by Eq. (3.14)); and second, a nonlinear distribution which causes no deformation in the bridge. The nonlinear part of the temperature distribution results in a nonlinear-self-equilibrating stress called the "eigenstress."

3. A mathematical model of the bridge was made as shown in Figure 42, p. 87. The linear part of the temperature distribution which was found from the previous step (using STRUDL) is applied.

4. The stresses from STRUDL output are calculated and compared with the measured values.

5. The eigenstresses due to nonlinear temperature distribution are added to the stresses found due to linear temperature.

A computer program was developed by the author to calculate the eigenstresses as well as the corresponding linear temperature distribution for any given cross section. Its listing is given in Appendix B.

Three different days were selected to compare the field data obtained from measurements with the results obtained from theoretical procedure that was developed in this work. The comparisons were made and presented in Chapter V.

The maximum change in daily temperature at various locations in the bridge and their maximum movement at abutments for a given period of time were shown in Table 1 (Appendix A). The maximum changes in strains at piers 1, 7, 11 and in the deck are presented in Table 2 (Appendix A).

6.2. CONCLUSIONS

From the comparisons made between the data collected from site measurements and the method that was developed in this dissertation, the following comparison can be made between field measurements and the corresponding theoretical results:

1. The percent difference in stress obtained from analytical considerations and those obtained from strain measurements was on the order of 5 to 15%.

2. The percent difference between the movements of the bridge deck at the abutment as measured to the movement as estimated from equations was about 7%.

The above calculations for deformation and stresses in the model were obtained from STRUDL by loading the model with a linear temperature distribution. This distribution was obtained by applying the analytical method described previously for the actual field measurement of temperature across the depth of the superstructure.

It can be concluded that the analytical model developed for the bridge predicts behavior which is in good agreement with observed behavior based on the comparisons carried out for stresses (obtained from strains) and deformations at the abutments. The analytical model used one-dimensional beam elements which greatly simplified the complexity and dimension of the problem. Also, this agreement lends support to the statement made earlier that the nonlinear part of the temperature gradient across the thickness of the bridge superstructure provided no contribution to movement as predicted in theory.

At certain locations in the bridge, the stresses due to thermal loads are greater than the dead load stresses. For example, this occurs at the bottom of pier No. 1. Maximum values for stress at pier No. 1 is 207 psi at its bottom due to dead load and 740 psi due to thermal change. In the deck, however, the stresses induced by temperature change at pier 1 were less than the dead load stresses. The temperature stresses at pier 14, on the other hand, were somewhat greater than the dead load stresses. From Figures 30, 31, 34, 35, 38 and 39 (pp. 73, 75, 79) it can be seen that the movements of the deck are proportional to mid-deck temperature (thermocouple No. 3). This movement was about 0.08 in per Fahrenheit degree. From Table 3 (Appendix A), the maximum change in ambient temperature was 76°F while the maximum change for the mid-deck temperature was 56°F. So the maximum expansion of the bridge at the south abutment was approximately 4.48 in for the given period.

6.3. DESIGN RECOMMENDATIONS

The following recommendations can be made regarding the erection of future long span bridges with no provisions made for expansion joints except at the bridge ends.

1. Thermal stresses which were most pronounced at the end piers were of significant magnitude when compared to dead load stresses. At the bottom of pier No. 1, thermal stress due to a thermal differential in ambient temperature of 45°F on one day were almost three times the stress produced by dead load. Thus, these stresses must be considered in design.

2. The change from 4 to 5 box girder beam sections near the ends for the right lane of the bridge was done by an offset in the alignment of the girders. This alignment offset appeared to be the cause of cracks in the diaphram at bent 28 and a transverse movement of the bridge deck of 3/4 in at the abutment. To avoid this situation, it is believed that if the same number of girders is used throughout the entire length of the bridge or if the offset of the girders is minimized, this potential problem can be avoided in the future.

3. It is also recommended that erection of the deck and diaphragms be carried from midspan to the ends of the bridge instead of otherwise. This allows the full maximum expansion to be achieved equally in both directions, resulting in more uniform movements at the expansion joints at the abutments.

REFERENCES

REFERENCES

1. Barber, E. S., "Calculation of Maximum Pavement Temperatures From Weather Reports," Bulletin 168, Highway Research Board, 1957, pp. 1-18.

2. Berwanger, C., "Thermal Stresses in Composite Bridges," Proceedings, ASCE Specialty Conference on Steel Structures, Engineering Extension Series.

3. Boley, V. A., and Widener, J. H., "Theory of Thermal Stresses," Chap. 10, John Wiley & Sons, Inc., NY, 1960.

4. Dally, J. W., and Riley, W. F., "Experimental Stress Analysis," McGraw-Hill Book Company, NY, 1978.

5. Dickinson, E. J., "Temperature Conditions in Vituminous Concrete Sufacings-Melbourne," Aust. Road Research, Vol. 3, No. 9, March 1969.

6. Emanuel, J. H., and Hulsey, J. L., "Temperature Distributions in Composite Bridges," Journal of the Structural Division, ASCE, Vol. 104, No. ST1, Proc. Paper 13474, January 1978, pp. 65-78.

7. Houk, I. E., Paxton, J. A., and Houghton, D. L., "Prediction of Thermal Stress and Strain Capacity of Concrete by Tests on Small Beams," Journal of American Concrete Institute, Vol. 67, No. 3, March 1970, pp. 253-261.

8. Liu, Y. N., and Zuk, W., "Thermoelastic Effects in Prestressed Flexural Members," Journal of Prestressed Concrete Institute, Vol. 8, No. 3, June 1963, pp. 64-85.

9. Maher, D. R. H., "The Effects of Differential Temperature on Continuous Prestressed Concrete Bridges," Civil Engineering Transaction, Institute of Engineers, Australia, Vol. CE12, No. 1, Paper 2793, April 1970, pp. 29-32.

10. "Precast Segmental Box Girder Bridge Manual," Prestressed Concrete Institute and Post-Tensioning Institute, 1978.

11. Priestley, M. J. N., "Model Study of a Prestressed Concrete Box-Girder Bridge Under Thermal Loading," Proceedings of the Ninth Congress of the IBASE, Amsterdam, May 1972.

12. Priestley, M. J. N., "Thermal Gradients in Bridges—Some Design Considerations," New Zealand Engineering, July 15, 1972.

13. Radolli, M., and Green, R., "Thermal Stresses in Concrete Bridge Superstructures Under Summer Conditions," Transportation Research Board 547, 1975, pp. 23-38.

14. Reynolds, J. D., and Emanuel, J. H., "Thermal Stresses and Movements in Bridges," Journal of the Structural Division, ASCE, Vol. 100, No. ST1, Proc. Paper 10275, January 1974, pp. 63-78.

15. Scholes, T. P., "Kingsport Bridge Project Instrumentation," Special Study, The University of Tennessee, Knoxville, Civil Engineering, August 1979.

16. "Standard Specifications for Highway Bridges," 12th Edition, American Association of State Highway and Transportation Officials, Washington, DC, 1977.

17. Steward, C. F., "Annual Movement Study of Bridge Deck Expansion Joints," R and D Report No. 2-69, California Division of Highways, June 1969.

18. Wroth, C. P., "The Hammersmith Flyover-Site Measurements of Prestressing Losses and Temperature Movements," Proceedings, Institute of Civil Engineers, London, England, Vol. 23, December 1962, pp. 601-624.

19. Zuk, W., "Thermal and Shrinkage Stresses in Composite Beams," Journal of American Concrete Institute, Vol. 58, No. 3, September 1961, pp. 327-340.

20. Zuk, W., "Thermal Behavior of Composite Bridges—Insulated and Uninsulated," Highway Research Record, No. 76, 1965, pp. 231-253.

21. Zuk, W., "End Movement Studies of Various Type Highway Bridges," Highway Research Record, No. 295, 1969, pp. 1-4.

22. Zuk, W., "Simplified Design Check of Thermal Stress in Composite Highway Bridges," Highway Research Record, No. 103, 1965, pp. 10-13.

APPENDICES

APPENDIX A

TABLES

Table 1. Maximum Daily Temperature and Movements for Period January 16, 1981, to February 7, 1981

Date	Maximum Temperature and Δ Temperature (°F)									Abutment Movements in Feet			
	Ambient		Mid-Deck		Inside Girders		Top of Deck		ΔT Top-Btm.	Right North	Right South	Left North	Left South
	T	ΔT	T	ΔT	T	ΔT	T	ΔT					
2- 7-81	45	26	34	8	28	3	38	15	7	0.0575	0.043	0.0375	0.045
2- 6-81	40	26	29	6	25	3	35	13	4	0.053	0.040	0.0375	0.040
2- 5-81	33	27	26	8	22	1	34	20	11	0.0625	0.040	0.043	0.045
2- 4-81	28	22	25	8	23	3	30	17	6	0.070	0.045	0.045	0.045
2- 3-81	21	11	30	8	23	2	28	8	9	0.0575	0.040	0.040	0.425
2- 2-81	40	25	33	3	32	4	35	7	7	0.060	0.045	0.045	0.0525
2- 1-81	50	31	30	4	32	3	33	8	7	0.065	0.045	0.045	0.045
1-31-81	39	31	31	4	34	5	33	10	4	0.040	0.030	0.0275	0.030
1-30-81	30	17	37	7	37	3	35	7	2	0.045	0.030	0.0325	0.0325
1-29-81	41	20	39	4	39	2	42	10	5	0.0325	0.0275	0.020	0.0275
1-28-81	45	22	43	6	40	2	48	14	9	0.0325	0.025	0.0225	0.025
1-27-81	50	16	44	2	40	1	47	7	3	--	--	--	--
1-26-81	56	28	44	7	39	4	50	15	7	--	--	--	--
1-25-81	55	32	43	10	35	3	51	21	14	-	--	--	--
1-24-81	48	26	40	8	34	1	48	17	12	--	--	--	--
1-23-81	40	22	38	4	34	1	42	9	6	--	--	--	--
1-22-81	38	4	36	2	34	2	38	4	2	--	--	--	--
1-21-81	38	6	35	3	33	3	37	4	4	--	--	--	--
1-20-81	39	14	32	4	30	3	34	6	2	--	--	--	--
1-19-81	43	28	31	8	27	3	37	17	7	--	--	--	--
1-18-81	35	27	28	8	25	2	34	17	7	0.060	0.040	0.040	0.0425
1-17-81	27	10	29	5	28	2	31	9	6	0.035	0.020	0.0225	0.0225
1-16-81	33	13	30	2	29	1	33	7	4	0.025	0.020	0.020	0.0225

Table 2. Maximum Daily Change in Micro-Strain at Selected Strain Gages in the Bridge for a Time Period of January 16, 1981, to February 7, 1981

Date	Maximum Δ Temperature in °F			Maximum Change in Micro-Strain					
				Pier No. 1		Pier No. 7	Pier No. 11	Deck at	
	Amb.	Mid-Deck	Inside Grd.	Top	Btm.	Btm.	Btm.	Pier No. 7	Pier No. 6-7
2- 7-81	26	8	3	48	148	58	12	92	66
2- 6-81	26	6	3	44	138	68	26	62	46
2- 5-81	27	8	1	58	166	66	22	132	66
2- 4-81	22	8	3	40	150	76	20	90	66
2- 3-81	11	8	2	22	74	56	10	70	44
2- 2-81	25	3	4	64	181	80	32	98	84
2- 1-81	31	4	3	66	168	72	32	46	14
1-31-81	31	4	5	38	84	38	22	48	20
1-31-81	17	7	3	32	108	48	14	70	22
1-29-81	20	4	2	22	80	38	18	64	32
1-28-81	22	6	2	20	66	32	10	102	66
1-27-81	16	2	1	16	8	20	8	20	8
1-26-81	28	7	4	36	84	34	26	70	50
1-25-81	32	10	3	40	144	70	40	140	80
1-24-81	26	8	1	26	130	60	30	120	70
1-23-81	22	4	1	20	60	30	20	60	40
1-22-81	4	2	2	10	20	20	10	40	20
1-21-81	6	3	3	20	32	12	6	26	10
1-20-81	14	4	3	26	74	28	18	26	22
1-19-81	28	8	3	46	150	62	22	116	62
1-18-81	27	8	2	36	146	72	28	100	60
1-17-81	10	5	3	14	76	46	16	56	42
1-16-81	13	2	1	26	90	34	26	52	46

Table 3. Temperature Extremes During Collection Time Period between October 22, 1980, and April 9, 1981

Location	Minimum Temperature (°F)	Date	Time	Maximum Temperature (°F)	Date	Time
Ambient	2	2-12-81	6:00 A.M.	78	4-4-81	5:30 P.M.
Top-Deck	16	2-12-81	8:00 A.M.	86	4-4-81	5:30 P.M.
Mid-Deck	21	2-12-81	11:00 A.M.	77	4-4-81	7:00 P.M.
Mid-Girder	12	2-12-81	10:00 A.M.	71	4-4-81	6:30 P.M.
Inside Girder	22.5	2-12-81	4:00 A.M.	65.5	4-5-81	2:30 A.M.
Differential Top to Bottom	--	--	--	25	4-7-81	4:00 P.M.

Table 4. The Calculated and Measured Values for the Three Comparisons

		Calculated	Measured
Comparison No. 1	Movement of south abutment	0.0265 ft	0.0250 ft
	Stress at top of pier No. 1	77.90 psi	74.40 psi
	Stress at bottom of pier No. 1	-251.35 psi	-229.4 psi
	Stress at bottom of pier No. 11	57.62 psi	55.8 psi
	Stress in the deck at pier No. 7	-83.08 psi	-82.70 psi
Comparison No. 2	Movement of south abutment	0.080 ft	0.085 ft
	Stress at top of pier No. 1	-239.92 psi	-266.60 psi
	Stress at bottom of pier No. 11	173.96 psi	173.60 psi
	Stress at bottom of pier No. 7	-406.30 psi	-359.60 psi
Comparison No. 3	Movement of south abutment	0.0331 ft	0.034 ft
	Stress at top of pier No. 1	-113.03 psi	-93.0 psi
	Stress at bottom of pier No. 7	-192.25 psi	-192.20 psi
	Stress at bottom of pier No. 11	82.68 psi	63.0 psi
	Stress in the deck at pier No. 7	-53.94 psi	-44.62 psi
	Stress in the span 7-6	-44.01 psi	-50.85 psi

Table 5. Eigenstresses for Comparison No. 1

X(I) (in)	Y(I) (in)	Temp.(I) (°F)	Eigenstress (ksi)	Linear Temp. (°F)
192.0	0.0	2.5	-0.0553	-0.013
192.0	6.5	2.0	-0.0272	0.763
40.0	6.5	2.0	-0.0272	0.763
40.0	50.5	1.0	0.1104	6.017
192.0	50.5	1.0	0.1104	6.016
192.0	54.0	1.0	0.1196	6.435
373.0	54.0	1.0	0.1196	6.435
373.0	57.0	4.5	0.0504	6.793
373.0	57.0	4.5	0.0504	6.793
373.0	62.5	14.0	-0.1441	7.450
373.0	62.5	14.0	-0.1441	7.450
373.0	64.0	17.0	-0.2062	7.629

APPENDIX B

EIGENSTRESS PROGRAM

```
$JOB

CCCCCCCCCCCCCCCCCCCCCCCCCCCCCCCCCCCCCCCCCCCCCCCCCCCCCCCCCCCCCCCCCCCCCCCCCCCCC
CCCCCCCCCCCCCCCCCCCC                                     CCCCCCCCCCCCCCCCCCCCCC
CCCCCCCCCCCCCCCCCCCC                                     CCCCCCCCCCCCCCCCCCCCCC
CCCCCCCCCCCCCCCCCCCC             NOTATION                CCCCCCCCCCCCCCCCCCCCCC
CCCCCCCCCCCCCCCCCCCC                                     CCCCCCCCCCCCCCCCCCCCCC
CCCCCCCCCCCCCCCCCCCC                                     CCCCCCCCCCCCCCCCCCCCCC
CCCCCCCCCCCCCCCCCCCCCCCCCCCCCCCCCCCCCCCCCCCCCCCCCCCCCCCCCCCCCCCCCCCCCCCCCCCCC
C                                                                           C
C                                                                           C
C                                                                           C
C                                                                           C
CCCCC             AT: TOTAL AREA OF CROSS SECTION                      CCCCCC
CCCCC             MA: MOMENT OF AREAS ABOUT NEUTRAL AXIS               CCCCCC
CCCCC             CGY: Y-COORDINATE OF CENTER OF GRAVITY OF X-SECTION  CCCCCC
CCCCC             ROT: MOMENT OF INERTIA OF TOTAL AREA ABOUT NA        CCCCCC
CCCCC             DD: SQUARE OF HEIGHT OF RECTANGLE                    CCCCCC
CCCCC             RO:MOMENT OF INERTIA OF AREA ABOUT ITS OWN N.A.      CCCCCC
CCCCC             ARM:MOMENT ARM OF AN AREA ABOUT C.G.                 CCCCCC
CCCCC             ARM2: TWICE ARM                                      CCCCCC
CCCCC             RTO: ADDITIONAL MOM OF INERTIA BY PARALLEL AXIS      CCCCCC
CCCCC             ROM: REPRESENTS CURRENT VALUE OF ROT IN DO LOOP      CCCCCC
C                                                                           C
C                                                                           C
C                                                                           C
C                                                                           C
C                                                                           C
CCCCCCCCCCCCCCCCCCCCCCCCCCCCCCCCCCCCCCCCCCCCCCCCCCCCCCCCCCCCCCCCCCCCCCCCCCCCC
C
C
C
      DIMENSION A(9),X(20),Y(20),M(20) ,ROM(20),CCG(20)
      DIMENSION DD(20),RO(20),ARM2(20),ARM(20),RTO(20)
      DIMENSION TT(20),PTX(20),T(20),TARA(20),SIGMAZ(20),ELT(20)
      DIMENSION YY(20),DYFB(20),DDYFB(20),DDYTAR(20),TTDDYT(20)
      READ(5,5)NCL,E,ALPHA
    5 FORMAT(I10,F10.2,F10.7)
      WRITE(6,50)NCL,E,ALPHA
      K=0
    1 K=K+1
      READ(5,50,END=2) X(K),Y(K),T(K)
      GO TO 1
    2 CONTINUE
      AT=0
      MA=0.
      DO 10 I=1,NOL
      J=2*I
C
C- CALCULATION FOR THE AREA
C
      A(I)=(X(J-1)+X(J))*(Y(J)-Y(J-1))*.50000
      M(I)=A(I)*(Y(J)+Y(J-1))*0.5000
      AT=AT+A(I)
      MA=MA+M(I)
   10 CONTINUE
      WRITE(6,100)AT
C
C- CALCULATION FOR THE CENTER OF GRAVITY


 C
      CGY=MA/AT
      WRITE(6,200)CGY
      ROT=0.
      DO 20 II=1,NCL
      JJ=2*II
      A(II)=(X(JJ-1)+X(JJ))*(Y(JJ)-Y(JJ-1))*0.500
C
C- CALCULATION FOR THE MOMENT OF INERTIA
C
      DD(II)=(Y(JJ)-Y(JJ-1))*(Y(JJ)-Y(JJ-1))
      RO(II)=A(II)*DD(II)/12.
      ARM2(II)=2.*CGY-Y(JJ)-Y(JJ-1)
      ARM(II)=ARM2(II)*0.500
```

```
      RTC(II)=A(II)*ARM(II)*ARM(II)
      RCM(II)=RC(II)+RTC(II)
      RCT=RCT+RCM(II)
   20 CONTINUE
      WRITE(6,300)RCT
C-
C-
C-  N=NUMBER OF SUBDIVISIONS WITHIN A BLOCK OF CONSTANT X
C-  M=4 NUMBER OF LAYERS
C-  CALCULATION FOR TEMPERATURE AREA
      N=5
      ARTOT=0.
      PTXTOT=0.
      TTTDDY=0.
      DO 70 MI=1,NCL
      TAREA=0.
      TDDYTA=0.
      MM=2*MI
      TBOT=T(MM-1)
      TTOP=T(MM)
      YBOT=Y(MM-1)
      YTOP=Y(MM)
      DELTAT=TTOP-TBOT
      DELTAY=YTOP-YBOT
      DY=DELTAY/N
      DT=DELTAT/N
      TT(1)=TBOT
      YY(1)=YBOT
      DO 30 L=1,N
      TT(L+1)=TBOT+DT*L
      TARA(L)=ABS((TT(L)+TT(L+1))*DY*0.5)
C
C
      YY(L+1)=YBOT+DY*L
      DYFB(L)=(YY(L)+YY(L+1))/2.
      DDYFB(L)=DYFB(L)-CGY
      DDYTAR(L)=DDYFB(L)*TARA(L)
      TDDYTA=TDDYTA+DDYTAR(L)
      TAREA=TAREA+TARA(L)
   30 CONTINUE
      ARTOT=TAREA+ARTOT
      XBAR=(X(MM-1)+X(MM))/2.
      PTX(MI)=XBAR*TAREA
      PTXTOT=PTXTOT+PTX(MI)
C
      TTDDYT(MI)=XBAR*TDDYTA
      TTTDDY=TTTDDY+TTDDYT(MI)
   70 CONTINUE
C
C CALCULATION FOR EIGEN STRESSES
C
      NNCL=2*NCL
      D=E*ALPHA
      B=PTXTOT/AT
      C=TTTDDY/RCT
      DO 80 LL=1,NNCL
      DCG(LL)=Y(LL)-CGY
      SIGMAZ(LL)=D*(-1.*T(LL)+DCG(LL)*C+B)
C-
C- CALCULATION FOR LINEAR TEMPERATURE
C-
      ELT(LL)=DCG(LL)*C+B
   80 CONTINUE
      WRITE(6,400)ARTOT
      WRITE(6,500)PTXTOT
      WRITE(6,600)TTTDDY
      WRITE(6,650)
      WRITE(6,700)(X(I),Y(I),T(I),SIGMAZ(I),I=1,NNCL)
      WRITE(6,750)
      WRITE(6,800)(X(I),Y(I),ELT(I),I=1,NNCL)
   50 FORMAT(3F10.5)
   90 FORMAT('1',30X,'NUMBER OF LAYER= ',I2,10X,'E= ',F15.2,10X,'ALPHA
     *= ',F10.7)
  100 FORMAT(30X,'THE TOTAL AREA IS = ',F10.5)
  200 FORMAT(30X,'THE LOCATION OF CG IS = ',F10.5)
  300 FORMAT(30X,'THE TOTAL MOMENT OF INERTIA ABOUT N.A. IS =',F20.5)
  400 FORMAT(30X,'THE TOTAL AREA OF TEMP = ',F14.5)
  500 FORMAT(30X,'THE PRODUCT OF TEMP AND XBAR = ',F20.5)
```

```
  600   FORMAT(30X,'THE MOMENT OF TEMP. AREA ABOUT N.A. IS = ',F20.5)
  650   FORMAT(//,9X,'X(I)',17X,'Y(I)',15X,'TEMP(I)',12X,'EIGEN STRESS',/)
  700   FORMAT(5X,F10.5,10X,F10.5,10X,F10.5,10X,F12.6)
  750   FORMAT(////,8X,'X(I)',15X,'Y(I)',15X,'LINEAR TEMP',/)
  800   FORMAT(5X,F10.5,10X,F10.5,5X,F10.5)
        STOP
        END
```

$ENTRY

```
NUMBER OF LAYER=  6   E= 4400.00   ALPHA  =  0.0000050
THE TOTAL AREA IS = 8830.00000
THE LOCATION OF CG IS =     44.52728
THE TOTAL MOMENT OF INERTIA ABOUT N.A. IS =        4029193.00000
THE TOTAL AREA OF TEMP =        166.49970
THE PRODUCT OF TEMP AND XBAR =          48543.04000
THE MOMENT OF TEMP. AREA ABOUT N.A. IS =          523511.80000
```

X(I)	Y(I)	TEMP(I)	EIGEN STRESS
192.00000	0.00000	2.50000	-0.061334
192.00000	6.50000	2.00000	-0.031754
40.00000	6.50000	2.00000	-0.031754
40.00000	50.50000	1.00000	0.116018
192.00000	50.50000	1.00000	0.116018
192.00000	54.00000	1.00000	0.126023
515.00000	54.00000	1.00000	0.126023
515.00000	57.00000	4.50000	0.057598
515.00000	57.00000	4.50000	0.057598
515.00000	62.50000	14.00000	-0.135680
515.00000	62.50000	14.00000	-0.135680
515.00000	64.00000	17.00000	-0.197393

X(I)	Y(I)	LINEAR TEMP
192.00000	0.00000	-0.29790
192.00000	6.50000	0.55664
40.00000	6.50000	0.55664
40.00000	50.50000	6.27355
192.00000	50.50000	6.27355
192.00000	54.00000	6.72830
515.00000	54.00000	6.72830
515.00000	57.00000	7.11809
515.00000	57.00000	7.11809
515.00000	62.50000	7.83270
515.00000	62.50000	7.83270
515.00000	64.00000	8.02760

APPENDIX C

STRUDL OUTPUT FOR COMPARISON NO. 1

```
STRUDL 'CE5930' 'KINGSFCRT BRIDGE'

*************************************************
*                                               *
*              ICES STRUDL-II                   *
*        THE STRUCTURAL DESIGN LANGUAGE         *
*                                               *
*     CIVIL ENGINEERING SYSTEMS LABORATORY      *
*     MASSACHUSETTS INSTITUTE CF TECHNOLOGY     *
*         CAMBRIDGE, MASSACHUSETTS              *
*          V2 M2          JUNE, 1972            *
*          15:30:40         4/15/81             *
*                                               *
*************************************************

TYPE PLANE FRAME XY
UNITS FEET KIPS FAHR
JOINT COORDINATES
1 112.19 97.74 S
2 162.845 97.70
3 213.50 97.66
4 213.50 94.06
5 213.50 85.06
6 213.50 65.56
7 213.50 59.56 S
8 263.575 97.80
9 313.65 97.94
10 313.65 94.34
11 313.65 57.34 S
12 363.725 98.09
13 413.80 98.24
14 413.80 94.64
15 413.80 60.64 S
16 459.05 98.38
17 504.30 98.52
18 504.30 94.92
19 504.30 54.92 S
20 549.545 98.66
21 594.79 98.80
22 594.79 95.20
23 594.79 61.20 S
24 640.54 98.94
25 686.29 99.08
26 686.29 95.48
27 686.29 61.48 S
28 731.535 99.22
29 776.78 99.36
30 776.78 95.76
31 776.78 86.76
32 776.78 67.76
33 776.78 61.76 S
34 826.905 99.51
35 877.03 99.66
36 877.03 96.06
37 877.03 61.56 S
38 927.655 99.815
39 978.28 99.97
40 978.28 96.37
41 978.28 59.87 S
42 1028.905 100.12
43 1079.53 100.27
44 1079.53 96.67
45 1079.53 60.67 S
46 1130.155 100.425
47 1180.78 100.58
48 1180.78 96.98
49 1180.78 87.98
```

50 1180.78 67.98
51 1180.78 61.98 S
52 1231.42 100.835
53 1282.06 101.09
54 1282.06 97.48
55 1282.06 88.48
56 1282.06 65.98
57 1282.06 59.48 S
58 1332.67 101.615
59 1383.28 102.14
60 1383.28 98.54
61 1383.28 61.54 S
62 1433.905 102.94
63 1484.53 103.74
64 1484.53 100.14
65 1484.53 61.64 S
66 1535.155 104.815
67 1585.78 105.89
68 1585.78 102.29
69 1585.78 62.04 S
70 1636.43 107.245
71 1687.08 108.60
72 1687.08 105.00
73 1687.08 61.00 S
74 1737.68 110.225
75 1788.28 111.85

76 1788.28 108.25
77 1788.28 32.25 S
78 1838.905 113.755
79 1889.53 115.66
80 1889.53 112.06
81 1889.53 47.06 S
82 1940.155 117.835
83 1990.78 120.01
84 1990.78 116.41
85 1990.78 49.91 S
86 2040.64 122.35
87 2090.50 124.69
88 2090.50 121.09
89 2090.50 61.59 S
90 2140.42 127.035
91 2190.34 129.38
92 2190.34 125.78
93 2190.34 69.53 S
94 2240.40 131.73
95 2290.46 134.08
96 2290.46 130.48
97 2290.46 121.48
98 2290.46 80.43
99 2290.46 72.68 S
100 2320.96 135.485

101 2351.46 136.89
102 2351.46 133.29
103 2351.46 76.54 S
104 2381.96 138.295
105 2412.46 139.70
106 2412.46 136.10
107 2412.46 85.60 S
108 2455.96 141.70
109 2499.46 143.70
110 2499.46 140.10
111 2499.46 99.60 S
112 2541.655 145.60
113 2583.85 147.50
114 2583.85 143.90
115 2583.85 121.65 S
116 2626.05 149.13
117 2668.25 150.76
118 2668.25 147.16
119 2668.25 114.16 S
120 2711.75 152.805
121 2755.25 154.85
122 2755.25 151.27
123 2755.25 114.14 S
124 2781.425 156.22
125 2807.60 157.59 S

MEMBER INCIDENCES

1 1 2

2 2 3

3 3 8

4 8 9

5 9 12

6 12 13

7 13 16

8 16 17

9 17 20

10 20 21

11 21 24

12 24 25

13 25 28

14 28 29

15 29 34

16 34 35

17 35 38

18 38 39

19 39 42

20 42 43

21 43 46

22 46 47

23 47 52

24 52 53

25 53 58

26 58 59

27 59 62

28 62 63

29 63 66

30 66 67

31 67 70

32 70 71

33 71 74

34 74 75

35 75 78

36 78 79

37 79 82

38 82 83

39 83 86

40 86 87

41 87 90

42 90 91

43 91 94

44 94 95

45 95 100

46 100 101

47 101 104

48 104 105

49 105 108

50 108 109

51 109 112

52 112 113

53 113 116

54 116 117

55 117 120

56 120 121

57 121 124

58 124 125

59 3 4

60 9 10

61 13 14

62 17 18

63 21 22

64 25 26

65 29 30

66 35 36

67 39 40

68 43 44

69 47 48

70 53 54

71 59 60

72 63 64

73 67 68

74 71 72

75 75 76

76 79 80

77 83 84

```
78 87 88
79 91 92
80 95 96
81 101 102
82 105 106
83 109 110
84 113 114
85 117 118
86 121 122
87 4 5
88 5 6
89 6 7
90 10 11
91 14 15
92 18 19
93 22 23
94 26 27
95 30 31
96 31 32
97 32 33
98 36 37
99 40 41
100 44 45
101 48 49
102 49 50
103 50 51
104 54 55
105 55 56
106 56 57
107 60 61
108 64 65
109 68 69
110 72 73
111 76 77
112 80 81
113 84 85
114 88 89
115 92 93
116 96 97
117 97 98
118 98 99
119 102 103
120 106 107
121 110 111
122 114 115
123 118 119
124 122 123
PLOT PLANE
```

```
MEMBER PROPERTIES
1 TO 54 AX 51.45 IZ 176.64 YD 5.333 YC 1.854
55 VAR
SEG 1 AX 53.433 IZ 178.27 YC 2.039 YD 5.333 XC 21.75
SEG 2 AX 54.327 IZ 180.65 YC 2.012 YD 5.333 XC 21.75
56 VAR
SEG 1 AX 55.223 IZ 189.95 YC 1.986 YD 5.333 XC 21.75
SEG 2 AX 56.12 IZ 185.73 YC 1.961 YD 5.333 XC 21.75
57 VAR
SEG 1 AX 61.658 IZ 197.95 YC 1.82 YD 5.333 XC 13.0875
SEG 2 AX 62.403 IZ 199.05 YC 1.805 YD 5.333 XC 13.0875
58 VAR
SEG 1 AX 62.943 IZ 200.12 YC 1.793 YD 5.333 XC 13.0875
SEG 2 AX 63.478 IZ 201.16 YC 1.781 YD 5.333 XC 13.0875
59 TO 86 PRI AX 400.0 IZ 300000.0
87 VAR
SEG 1 AX 146.50 IZ 109.875 L  3.5
SEG 2 AX 127.75 IZ 95.81 L  1.5
SEG 3 AX 90.25 IZ 68.69 L  1.5
SEG 4 AX 71.50 IZ 53.625 L  2.5
88 PRI AX 71.50 IZ 53.625
89 VAR
SEG 1 AX 71.50 IZ 53.625 L 2.5
SEG 2 AX 582.5 IZ 10921. L 3.5
90 VAR
SEG 1 AX 146.50 IZ 109.875 L  3.5
SEG 2 AX 127.75 IZ 95.81 L  1.5
SEG 3 AX 90.25 IZ 68.69 L  1.5
SEG 4 AX 71.50 IZ 53.625 L  27.0
SEG 5 AX 582.5 IZ 10921. L 3.5
91 VAR
SEG 1 AX 146.50 IZ 109.875 L  3.5
SEG 2 AX 127.75 IZ 95.81 L  1.5
SEG 3 AX 90.25 IZ 68.69 L  1.5
SEG 4 AX 71.50 IZ 53.625 L  24.0
SEG 5 AX 582.5 IZ 10921. L 3.5
92 VAR
SEG 1 AX 135.25 IZ 101.44 L  3.5
SEG 2 AX 116.5 IZ 87.375 L  1.5
SEG 3 AX 79.0 IZ 59.25 L  1.5
SEG 4 AX 60.25 IZ 45.19 L  30.0
SEG 5 AX 526.25 IZ 9867. L 3.5
93 VAR
SEG 1 AX 126.75 IZ 95.06 L  3.5
SEG 2 AX 108.0 IZ 81.0 L  1.5
SEG 3 AX 70.5 IZ 52.875 L  1.5
SEG 4 AX 51.75 IZ 38.81 L  24.0
SEG 5 AX 483.75 IZ 9070. L 3.5
94 VAR
```

```
SEG 1 AX 121.75 IZ 91.31 L  3.5
SEG 2 AX 103.0 IZ 77.25 L  1.5
SEG 3 AX 65.5 IZ 49.125 L  1.5
SEG 4 AX 46.75 IZ 35.06 L  24.0
SEG 5 AX 458.75 IZ 8601.0 L 3.5
95 VAR
SEG 1 AX 120.0 IZ 90.0 L  3.5
SEG 2 AX 101.25 IZ 75.94 L  1.5
SEG 3 AX 63.75 IZ 47.81 L  1.5
SEG 4 AX 45.0 IZ 33.75 L  2.5
96 PRI AX 45.0 IZ 33.75
97 VAR
SEG 1 AX 45.0 IZ 33.75 L 2.5
SEG 2 AX 45.0 IZ 8438. L 3.5
98 VAR
SEG 1 AX 120.0 IZ 90.0 L  3.5
SEG 2 AX 101.25 IZ 75.94 L  1.5
SEG 3 AX 63.75 IZ 47.81 L  1.5
SEG 4 AX 45.0 IZ 33.75 L  24.5
SEG 5 AX 450. IZ 8438. L 3.5
99 VAR
SEG 1 AX 120.0 IZ 90.0 L  3.5
SEG 2 AX 101.25 IZ 75.94 L  1.5
SEG 3 AX 63.75 IZ 47.81 L  1.5
SEG 4 AX 45.0 IZ 33.75 L  26.5
SEG 5 AX 450. IZ 8438. L 3.5
100 VAR
SEG 1 AX 120.0 IZ 90.0 L  3.5
SEG 2 AX 101.25 IZ 75.94 L  1.5
SEG 3 AX 63.75 IZ 47.81 L  1.5
SEG 4 AX 45.0 IZ 33.75 L  26.0
SEG 5 AX 450. IZ 8438. L 3.5
101 VAR
SEG 1 AX 120.0 IZ 90.0 L  3.5
SEG 2 AX 101.25 IZ 75.94 L  1.5
SEG 3 AX 63.75 IZ 47.81 L  1.5
SEG 4 AX 45.0 IZ 33.75 L  2.5
103 VAR
SEG 1 AX 45. IZ 33.75 L 2.5
SEG 2 AX 450. IZ 8438. L 3.5
104 VAR
SEG 1 AX 120.0 IZ 90.0 L  3.5
SEG 2 AX 101.25 IZ 75.94 L  1.5
SEG 3 AX 63.75 IZ 47.81 L  1.5
SEG 4 AX 45.0 IZ 33.75 L  2.5
102,105 PRI AX 45.0 IZ 33.75
106 VAR
SEG 1 AX 45. IZ 33.75 L 2.5
SEG 2 AX 864. IZ 41472. L 4.0
107 VAR
```

```
SEG 1 AX 120.0 IZ 90.0 L  3.5
SEG 2 AX 101.25 IZ 75.94 L  1.5
SEG 3 AX 63.75 IZ 47.81 L  1.5
SEG 4 AX 45.0 IZ 33.75 L  26.5
SEG 5 AX 864. IZ 41472.  L 4.0
108 VAR
SEG 1 AX 120.0 IZ 90.0 L  3.5
SEG 2 AX 101.25 IZ 75.94 L  1.5
SEG 3 AX 63.75 IZ 47.81 L  1.5
SEG 4 AX 45.0 IZ 33.75 L  28.0
SEG 5 AX 864. IZ 41472.  L 4.0
109 VAR
SEG 1 AX 120.0 IZ 90.0 L  3.5
SEG 2 AX 101.25 IZ 75.94 L  1.5
SEG 3 AX 63.75 IZ 47.81 L  1.5
SEG 4 AX 45.0 IZ 33.75 L  29.75
SEG 5 AX 864. IZ 41472.  L 4.0
110 VAR
SEG 1 AX 120.0 IZ 90.0 L  3.5
SEG 2 AX 101.25 IZ 75.94 L  1.5
SEG 3 AX 63.75 IZ 47.81 L  1.5
SEG 4 AX 45.0 IZ 33.75 L  33.50
SEG 5 AX 864. IZ 41472.  L 4.0
111 VAR
SEG 1 AX 120.0 IZ 90.0 L  3.5
SEG 2 AX 101.25 IZ 75.94 L  1.5
SEG 3 AX 63.75 IZ 47.81 L  1.5
SEG 4 AX 45.0 IZ 33.75 L  65.50
SEG 5 AX 864. IZ 41472.  L 4.0
112 VAR
SEG 1 AX 120.0 IZ 90.0 L  3.5
SEG 2 AX 101.25 IZ 75.94 L  1.5
SEG 3 AX 63.75 IZ 47.81 L  1.5
SEG 4 AX 45.0 IZ 33.75 L  54.50
SEG 5 AX 864. IZ 41472.  L 4.0
113 VAR
SEG 1 AX 120.0 IZ 90.0 L  3.5
SEG 2 AX 101.25 IZ 75.94 L  1.5
SEG 3 AX 63.75 IZ 47.81 L  1.5
SEG 4 AX 45.0 IZ 33.75 L  56.0
SEG 5 AX 864. IZ 41472.  L 4.0
114 VAR
SEG 1 AX 121.11 IZ 90.83 L  3.5
SEG 2 AX 102.36 IZ 76.76 L  1.5
SEG 3 AX 64.86 IZ 48.645 L  1.5
SEG 4 AX 46.11 IZ 34.58 L  49.0
SEG 5 AX 872. IZ 41858. L 4.0
115 VAR
SEG 1 AX 124.75 IZ 93.56 L  3.5
SEG 2 AX 106.0 IZ 79.5 L  1.5
```

```
SEG 3 AX 68.5 IZ 51.375 L  1.5
SEG 4 AX 49.75 IZ 37.31 L  44.50
SEG 5 AX 307. IZ 3684. L 5.25
116 VAR
SEG 1 AX 131.5 IZ 98.625 L  3.5
SEG 2 AX 112.75 IZ 84.56 L  1.5
SEG 3 AX 75.25 IZ 56.44 L  1.5
SEG 4 AX 56.5 IZ 42.375 L  2.5
117 PRI AX 56.5 IZ 42.375
118 VAR
SEG 1 AX 56.5 IZ 42.375 L 2.5
SEG 2 AX 332. IZ 3984. L 5.25
119 VAR
SEG 1 AX 131.5 IZ 98.625 L  3.5
SEG 2 AX 112.75 IZ 84.56 L  1.5
SEG 3 AX 75.25 IZ 56.44 L  1.5
SEG 4 AX 56.5 IZ 42.375 L  45.0
SEG 5 AX 332. IZ 3984. L 5.25
120 VAR
SEG 1 AX 131.5 IZ 98.625 L  3.5
SEG 2 AX 112.75 IZ 84.56 L  1.5
SEG 3 AX 75.25 IZ 56.44 L  1.5
SEG 4 AX 56.5 IZ 42.375 L  38.75
SEG 5 AX 332. IZ 3984. L 5.25
121 VAR
SEG 1 AX 131.5 IZ 98.625 L  3.5
SEG 2 AX 112.75 IZ 84.56 L  1.5
SEG 3 AX 75.25 IZ 56.44 L  1.5
SEG 4 AX 56.5 IZ 42.375 L  28.75
SEG 5 AX 332. IZ 3984. L 5.25
122 VAR
SEG 1 AX 126.375 IZ 94.78 L  3.5
SEG 2 AX 107.625 IZ 80.72 L  1.5
SEG 3 AX 70.125 IZ 52.59 L  1.5
SEG 4 AX 51.375 IZ 38.53 L 10.50
SEG 5 AX 313. IZ 3756. L 5.25
123 VAR
SEG 1 AX 122.875 IZ 92.16 L  3.5
SEG 2 AX 104.125 IZ 78.09 L  1.25
SEG 3 AX 66.625 IZ 49.97 L  1.25
SEG 4 AX 47.875 IZ 35.91 L  21.75
SEG 5 AX 299.5 IZ 35.44 L 5.25
124 VAR
SEG 1 AX 142.5 IZ 106.875 L  3.5
SEG 2 AX 123.75 IZ 92.81 L  1.375
SEG 3 AX 86.25 IZ 64.69 L  1.375
SEG 4 AX 67.5 IZ 50.625 L  25.63
SEG 5 AX 378. IZ 4536. L 5.25
JOINT RELEASES
1,125 FORCE X
```

```
1,125 MOM Z
MEMBER 59 TO 86 RELEASES END MOMENT Z
UNITS INCHES
CONSTANTS E 4400. 1 TO 86 3100. 87 TO 124
POISSON 0.15 ALL
CTE 0.000005 ALL
UNITS FEET
LOADING 'FIVE'
MEMBER TEMPERATURE LOADS
1 TO 54 AXI 4.973
55 TO 58 AXI 5.504
1 TO 54 BEND Z -7.642
55 TO 58 BEND Z -8.318
LOADING 'SIX'
MEMBER 1 TO 54 LOADS FORCE Y UNI W -8.58
MEMBER 55 LOADS FORCE Y UNI W -9.0
MEMBER 56 LOADS FORCE Y UNI W -9.3
MEMBER 57 LOADS FORCE Y UNI W -10.5
MEMBER 58 LOADS FORCE Y UNI W -10.65
```

```
***************************
*RESULTS OF LATEST ANALYSES*
***************************
```

PROBLEM - CE5930   TITLE - KINGSPORT BRIDGE

ACTIVE UNITS FEET KIP RAD DEGF SEC

ACTIVE STRUCTURE TYPE PLANE FRAME

ACTIVE COORDINATE AXES X Y

LOADING - FIVE

MEMBER FORCES

MEMBER	JOINT	FORCE AXIAL	FORCE SHEAR Y	FORCE SHEAR Z	MOMENT TORSIONAL	MOMENT BENDING Y	MOMENT BENDING Z
1	1	-0.0085778	10.8631907				-0.0001236
1	2	0.0085778	-10.8631907				550.2749023
2	2	-0.0085822	10.8631907				-550.2749023
2	3	0.0085822	-10.8631907				1100.5502930
3	3	58.1004639	-0.6365578				-891.3842773
3	8	-58.1004639	0.6365578				859.5087891
4	8	58.1004639	-0.6365341				-859.5085449
4	9	-58.1004639	0.6365341				827.6240332
5	9	99.3539276	2.2796545				-679.1533203
5	12	-99.3539276	-2.2796545				793.3068848
6	12	99.3539276	2.2796574				-793.3068848
6	13	-99.3539276	-2.2796574				907.4616699
7	13	148.5677948	1.2887526				-730.2827148
7	16	-148.5677948	-1.2887526				788.5991211
8	16	148.5677948	1.2887526				-788.5991211
8	17	-148.5677948	-1.2887526				846.9155273
9	17	170.5082245	0.9213212				-767.9265137
9	20	-170.5082245	-0.9213212				809.6118164
10	20	170.5082245	0.9212409				-809.6118164
10	21	-170.5082245	-0.9212409				851.2934570
11	21	199.5522919	1.1081419				-746.7370605
11	24	-199.5522919	-1.1081419				797.4348145
12	24	199.5522919	1.1081419				-797.4348145
12	25	-199.5522919	-1.1081419				848.1325684

13	25	222.9733582	0.8440617	-763.8146973
13	28	-222.9733582	-0.8440617	802.0046387
14	28	222.9733582	0.8439565	-802.0046387
14	29	-222.9733582	-0.8439565	840.1894531
15	29	242.9159088	0.6550922	-768.3935547
15	34	-242.9159088	-0.6550922	801.2302246
16	34	242.9159088	0.6551908	-801.2302246
16	35	-242.9159088	-0.6551908	834.0717773
17	35	259.2543945	0.4869426	-775.2519531
17	38	-259.2543945	-0.4869426	799.9035645
18	38	259.2543945	0.4870465	-799.9035645
18	39	-259.2543945	-0.4870465	824.5605469
19	39	270.6413574	0.3576218	-783.5661621
19	42	-270.6413574	-0.3576218	801.6706543
20	42	270.6413574	0.3578393	-801.6708984
20	43	-270.6413574	-0.3578393	819.7863770
21	43	280.3525391	0.3321838	-784.8261719
21	46	-280.3525391	-0.3321838	801.6430664
22	46	280.3525391	0.3322966	-801.6430664
22	47	-280.3525391	-0.3322966	818.4658203
23	47	288.6384277	0.2302889	-788.6467285
23	52	-288.6384277	-0.2302889	800.3088379
24	52	288.6384277	0.2302695	-800.3085938
24	53	-288.6384277	-0.2302695	811.9694824
25	53	293.3764648	0.1333998	-794.9094238
25	58	-293.3764648	-0.1333998	801.6611328
26	58	293.3764648	0.1333604	-801.6608887
26	59	-293.3764648	-0.1333604	808.4106445
27	59	296.5424805	0.0762622	-797.0886230
27	62	-296.5424805	-0.0762622	800.9497070
28	62	296.5424805	0.0761429	-800.9499512
28	63	-296.5424805	-0.0761429	804.8051758
29	63	297.5639648	0.0030891	-801.2321777
29	66	-297.5639648	-0.0030891	801.3884277
30	66	297.5639648	0.0029694	-801.3884277
30	67	-297.5639648	-0.0029694	801.5388184
31	67	296.9426270	-0.0528702	-803.9108887
31	70	-296.9426270	0.0528702	801.2319336
32	70	296.9426270	-0.0527507	-801.2316895
32	71	-296.9426270	0.0527507	798.5590820
33	71	295.3706055	-0.0358305	-804.3850058
33	74	-295.3706055	0.0358305	802.5710449
34	74	295.3706055	-0.0358305	-802.5708008
34	75	-295.3706055	0.0358305	800.7563359
35	75	294.9558105	-0.0227643	-802.4536133
35	78	-294.9558105	0.0227643	801.3002930
36	78	294.9558105	-0.0226457	-801.3002930
36	79	-294.9558105	0.0226457	800.1530762

37	79	293.9228516	-0.0427219	-804.0922852
37	82	-293.9228516	0.0427219	801.9274902
38	82	293.9228516	-0.0427219	-801.9277344
38	83	-293.9228516	0.0427219	799.7626953
39	83	292.6579590	-0.0607628	-804.4965820
39	86	-292.6579590	0.0607628	801.4633789
40	86	292.6579590	-0.0607922	-801.4631348
40	87	-292.6579590	0.0607922	798.4284668
41	87	290.2988281	-0.1105762	-806.9042969
41	90	-290.2988281	0.1105762	801.3784180
42	90	290.2988281	-0.1106939	-801.3779297
42	91	-290.2988281	0.1106939	795.8459473
43	91	286.4287109	-0.1658556	-809.7521973
43	94	-286.4287109	0.1658556	801.4404297
44	94	286.4287109	-0.1657683	-801.4399414
44	95	-286.4287109	0.1657683	793.1323242
45	95	281.7753906	-0.1264045	-809.8305664
45	100	-281.7753906	0.1264045	805.9709473
46	100	281.7753906	-0.1264045	-805.9709473
46	101	-281.7753906	0.1264045	802.1115723
47	101	276.3823242	-1.1172438	-821.3422852
47	104	-276.3823242	1.1172438	787.2302246
48	104	276.3823242	-1.1174278	-787.2299805
48	105	-276.3823242	1.1174278	753.1123047
49	105	268.0148926	1.2833738	-783.5969238
49	108	-268.0148926	-1.2833738	839.4826660
50	108	268.0148926	1.2833738	-839.4826660
50	109	-268.0148926	-1.2833738	895.3684082
51	109	247.6464081	-7.9647331	-967.0781250
51	112	-247.6464081	7.9647331	630.6684570
52	112	247.6464081	-7.9648857	-630.6677246
52	113	-247.6464081	7.9648857	294.2490234
53	113	73.9751129	5.8649521	-920.8886523
53	116	-73.9751129	-5.8649521	1168.5551758
54	116	73.9751129	5.8649168	-1168.5546875
54	117	-73.9751129	-5.8649168	1416.2395020
55	117	47.8730621	-1.8480997	-1509.0742187
55	120	-47.8730621	1.8480997	1428.5530176
56	120	47.8730621	-1.8480778	-1428.5557031
56	121	-47.8730621	1.8480778	1348.1154785
57	121	-1.5172825	-28.5888306	-1519.6250000
57	124	1.5172825	28.5888306	755.8107910
58	124	-1.5173054	-28.5888153	-759.8149414
58	125	1.5173054	28.5888153	-0.0000000
59	3	-11.3372955	-58.1020050	-209.1657104
59	4	11.3372955	58.1020050	0.0
60	9	3.0513697	-41.2446136	-148.4803772
60	10	-3.0513697	41.2446136	0.0

61	13	-0.8288851	-45.2164307	-177.1789788
61	14	0.8288851	45.2164307	0.0
62	17	-0.2994946	-21.9414062	-78.9889832
62	18	0.2994946	21.9414062	0.0
63	21	0.2698720	-29.0433960	-104.5560608
63	22	-0.2698720	29.0433960	0.0
64	25	-0.1847981	-23.4216156	-84.3176880
64	26	0.1847981	23.4216156	0.0
65	29	-0.1519266	-19.9432831	-71.7957001
65	30	0.1519266	19.9432831	0.0
66	35	-0.1012869	-16.3390808	-58.8202667
66	36	0.1012869	16.3390808	0.0
67	39	-0.1211014	-11.3874006	-40.9943542
67	40	0.1211014	11.3874006	0.0
68	43	0.0309439	-9.7111788	-34.9601898
68	44	-0.0309439	9.7111788	0.0
69	47	0.4931457	-8.2830925	-29.8190765
69	48	-0.4931457	8.2830925	0.0
70	53	1.4928188	-4.7258196	-17.0602112
70	54	-1.4928188	4.7258196	0.0
71	59	1.5851440	-3.1450472	-11.3222160
71	60	-1.5851440	3.1450472	0.0
72	63	1.5585594	-0.9925265	-3.5730896
72	64	-1.5585594	0.9925265	0.0
73	67	1.5679226	0.6589718	2.3723078
73	68	-1.5679226	-0.6589718	0.0
74	71	1.5568476	1.6184292	5.8263006
74	72	-1.5568476	-1.6184292	0.0
75	75	1.6235056	0.4713156	1.6967239
75	76	-1.6235056	-0.4713156	0.0
76	79	1.5049934	1.0942364	3.5392252
76	80	-1.5049934	-1.0942364	0.0
77	83	1.0854349	1.3149033	4.7236740
77	84	-1.0854349	-1.3149033	0.0
78	87	-0.1476253	2.3546591	8.4767580
78	88	0.1476253	-2.3546591	0.0
79	91	-0.2457814	3.8629923	13.9067469
79	92	0.2457814	-3.8629923	0.0
80	95	-0.4253373	4.6383743	16.6981201
80	96	0.4253373	-4.6383743	0.0
81	101	-1.2381506	5.3418312	19.2306824
81	102	1.2381506	-5.3418312	0.0
82	105	1.9894800	8.4678345	30.4843140
82	106	-1.9894800	-8.4678345	0.0
83	109	-10.4082336	19.9194183	71.7102051
83	110	10.4082336	-19.9194183	0.0
84	113	5.5324287	174.0602264	626.6191406
84	114	-5.5324287	-174.0602264	0.0
95	117	-8.3137016	25.7865906	92.8320618

85	118	8.3137016	-25.7865906	
86	121	-29.4305420	47.9070435	0.0
86	122	29.4305420	-47.9070435	171.5069580
87	4	-11.3372955	-58.1020050	0.0
87	5	11.3372955	58.1020050	-0.0000000
88	5	-11.3372955	-58.1020050	-522.9179688
88	6	11.3372955	58.1020050	522.9179688
89	6	-11.3372955	-58.1020050	-1655.9062500
89	7	11.3372955	58.1020050	1655.9062500
90	10	3.0513697	-41.2445221	-2004.5180664
90	11	-3.0513697	41.2445221	-0.0000000
91	14	-0.8288851	-49.2164307	-1526.0461426
91	15	0.8288851	49.2164307	0.0000000
92	18	-0.2994946	-21.9414062	-1673.3581543
92	19	0.2994946	21.9414062	-0.0000000
93	22	0.2698720	-29.0434723	-877.6567383
93	23	-0.2698720	29.0434723	0.0000000
94	26	-0.1847981	-23.4215088	-987.4780273
94	27	0.1847981	23.4215088	0.0000000
95	30	-0.1519266	-19.9432831	-796.3312988
95	31	0.1519266	19.9432831	0.0000000
96	31	-0.1519266	-19.9432831	-179.4894562
96	32	0.1519266	19.9432831	179.4894562
97	32	-0.1519266	-19.9432831	-558.4118652
97	33	0.1519266	19.9432831	558.4118652
98	36	-0.1012869	-16.3388672	-678.0715332
98	37	0.1012869	16.3388672	0.0000000
99	40	-0.1211014	-11.3874006	-563.6911621
99	41	0.1211014	11.3874006	-0.0000000
100	44	0.0309439	-9.7111788	-415.6401367
100	45	-0.0309439	9.7111788	0.0000000
101	48	0.4931457	-8.2830925	-249.6022949
101	49	-0.4931457	8.2830925	0.0000000
102	49	0.4931457	-8.2830925	-74.5478210
102	50	-0.4931457	8.2830925	74.5478210
103	50	0.4931457	-8.2830925	-240.2096100
103	51	-0.4931457	8.2830925	240.2096100
104	54	1.4928188	-4.7258196	-289.9079590
104	55	-1.4928188	4.7258196	0.0000000
105	55	1.4928188	-4.7258196	-42.5323639
105	56	-1.4928188	4.7258196	42.5323639
106	56	1.4928188	-4.7258196	-148.8632965
106	57	-1.4928188	4.7258196	148.8632965
107	60	1.5851440	-3.1450472	-179.5811310
107	61	-1.5851440	3.1450472	-0.0000000
108	64	1.5585594	-0.9925265	-116.3667145
108	65	-1.5585594	0.9925265	-0.0000000
109	68	1.5679226	0.6589692	-38.2122650
				0.0000000

109	69	-1.5679226	-0.6589692	26.5235138
110	72	1.5568476	1.6184282	-0.0000000
110	73	-1.5568476	-1.6184282	71.2138459
111	76	1.6235056	0.4713156	0.0000000
111	77	-1.6235056	-0.4713156	35.8199768
112	80	1.5049934	1.0942364	-0.0000000
112	81	-1.5049934	-1.0942364	71.1253567
113	84	1.0854349	1.3150291	0.0000000
113	85	-1.0854349	-1.3150291	87.4494781
114	88	-0.1476253	2.3544292	0.0
114	89	0.1476253	-2.3544292	140.0884705
115	92	-0.2457814	3.8629923	0.0000000
115	93	0.2457814	-3.8629923	217.2932892
116	96	-0.4253373	4.6383743	0.0000000
116	97	0.4253373	-4.6383743	41.7453766
117	97	-0.4253373	4.6383743	-41.7454681
117	98	0.4253373	-4.6383743	232.1505195
118	98	-0.4253373	4.6383743	-232.1506195
118	99	0.4253373	-4.6383743	268.0979004
119	102	-1.2381506	5.3418312	0.0000000
119	103	1.2381506	-5.3418312	303.1489258
120	106	1.9894800	8.4678345	-0.0000000
120	107	-1.9894800	-8.4678345	427.6254883
121	110	-10.4082336	19.9194031	-0.0000000
121	111	10.4082336	-19.9194031	806.7360840
122	114	5.5324287	174.0600433	-0.0000000
122	115	-5.5324287	-174.0600433	3872.8352051
123	118	-8.3137016	25.7865906	0.0000000
123	119	8.3137016	-25.7865906	850.9572754
124	122	-29.4305420	47.9070435	-0.0009649
124	123	29.4305420	-47.9070435	1778.7875977

RESULTANT JOINT LOADS - SUPPORTS

JOINT		/----- FORCE	-----	-----//	----- MOMENT	-----	-----/
		X FORCE	Y FORCE	Z FORCE	X MOMENT	Y MOMENT	Z MOMENT
1	GLOBAL	0.0000000	10.8631945				-0.0001236
7	GLOBAL	58.1020050	-11.3372955				-2004.5135547
11	GLOBAL	41.2445221	3.0513697				-1526.0466309
15	GLOBAL	49.2164307	-0.8288851				-1673.3586426
19	GLOBAL	21.9414062	-0.2994946				-877.6567383
23	GLOBAL	29.0434723	0.2698720				-987.4780273
27	GLOBAL	23.4215088	-0.1847981				-796.3315430
33	GLOBAL	19.9432831	-0.1519266				-678.0715332
37	GLOBAL	16.3388672	-0.1012869				-563.6911621
41	GLOBAL	11.3874006	-0.1211014				-415.6401367
45	GLOBAL	9.7111788	0.0309439				-345.6025391

51	GLOBAL	8.2830925	0.4931457	-289.9082031
57	GLOBAL	4.7258196	1.4928188	-179.5811615
61	GLOBAL	3.1450472	1.5851440	-116.3667450
65	GLOBAL	0.9925265	1.5585594	-38.2122650
69	GLOBAL	-0.6589692	1.5679226	26.5235138
73	GLOBAL	-1.6184282	1.5568476	71.2108612
77	GLOBAL	-0.4713156	1.6235056	35.8199921
81	GLOBAL	-1.0942364	1.5049934	71.1254120
85	GLOBAL	-1.3150291	1.0854349	87.4494934
89	GLOBAL	-2.3544292	-0.1476253	140.0884857
93	GLOBAL	-3.8629923	-0.2457814	217.2933197
99	GLOBAL	-4.6383743	-0.4253373	268.0979004
103	GLOBAL	-5.3418312	-1.2381506	303.1489258
107	GLOBAL	-8.4678345	1.9894800	427.6254883
111	GLOBAL	-19.9194031	-10.4082336	806.7360840
115	GLOBAL	-174.0600433	5.5324287	3872.8359375
119	GLOBAL	-25.7865906	-8.3137016	850.9575195
123	GLOBAL	-47.9070435	-29.4305420	1778.7878418
125	GLOBAL	0.0000000	29.0285034	-0.0000000

RESULTANT JOINT DISPLACEMENTS - SUPPORTS

JOINT		DISPLACEMENT			ROTATION		
		X DISP.	Y DISP.	Z DISP.	X ROT.	Y ROT.	Z ROT.
1	GLOBAL	-0.0264823	0.0				0.0001970
7	GLOBAL	0.0	0.0				0.0
11	GLOBAL	0.0	0.0				0.0
15	GLOBAL	0.0	0.0				0.0
19	GLOBAL	0.0	0.0				0.0
23	GLOBAL	0.0	0.0				0.0
27	GLOBAL	0.0	0.0				0.0
33	GLOBAL	0.0	0.0				0.0
37	GLOBAL	0.0	0.0				0.0
41	GLOBAL	0.0	0.0				0.0
45	GLOBAL	0.0	0.0				0.0
51	GLOBAL	0.0	0.0				0.0
57	GLOBAL	0.0	0.0				0.0
61	GLOBAL	0.0	0.0				0.0
65	GLOBAL	0.0	0.0				0.0
69	GLOBAL	0.0	0.0				0.0
73	GLOBAL	0.0	0.0				0.0
77	GLOBAL	0.0	0.0				0.0
81	GLOBAL	0.0	0.0				0.0
85	GLOBAL	0.0	0.0				0.0
89	GLOBAL	0.0	0.0				0.0

93	GLOBAL	0.0	0.0				0.0
99	GLOBAL	0.0	0.0				0.0
103	GLOBAL	0.0	0.0				0.0
107	GLOBAL	0.0	0.0				0.0
111	GLOBAL	0.0	0.0				0.0
115	GLOBAL	0.0	0.0				0.0
119	GLOBAL	0.0	0.0				0.0
123	GLOBAL	0.0	0.0				0.0
125	GLOBAL	0.0243651	0.0				-0.0000766

RESULTANT JOINT DISPLACEMENTS - FREE JOINTS

JOINT		/----------------DISPLACEMENT	----------------//		----------------ROTATION	----------------/	
		X DISP.	Y DISP.	Z DISP.	X ROT.	Y ROT.	Z ROT.
2	GLOBAL	-0.0252204	0.0028894				-0.0000414
3	GLOBAL	-0.0239631	0.0000103				-0.0000307
4	GLOBAL	-0.0240738	0.0000102				0.0011486
5	GLOBAL	-0.0139337	0.0000080				0.0010693
6	GLOBAL	-0.0002347	0.0000010				0.0001819
8	GLOBAL	-0.0228054	-0.0006419				0.0000022
9	GLOBAL	-0.0216514	-0.0000030				0.0000208
10	GLOBAL	-0.0215764	-0.0000030				0.0009543
12	GLOBAL	-0.0205592	0.0000949				-0.0000085
13	GLOBAL	-0.0194664	0.0000007				0.0000132
14	GLOBAL	-0.0194190	0.0000007				0.0009413
16	GLOBAL	-0.0185478	0.0001220				-0.0000040
17	GLOBAL	-0.0176285	0.0000004				0.0000024
18	GLOBAL	-0.0176198	0.0000004				0.0007159
20	GLOBAL	-0.0167399	-0.0000707				-0.0000029
21	GLOBAL	-0.0158518	-0.0000003				0.0000087
22	GLOBAL	-0.0158205	-0.0000003				0.0007651
24	GLOBAL	-0.0149944	0.0000415				-0.0000035
25	GLOBAL	-0.0141367	0.0000002				0.0000050
26	GLOBAL	-0.0141186	0.0000002				0.0004822
28	GLOBAL	-0.0133212	-0.0000009				-0.0000026
29	GLOBAL	-0.0125056	0.0000002				0.0000051
30	GLOBAL	-0.0124871	0.0000002				0.0006032
31	GLOBAL	-0.0071527	0.0000002				0.0005627
32	GLOBAL	-0.0001253	0.0000000				0.0003974
34	GLOBAL	-0.0116328	0.0000075				-0.0000025
35	GLOBAL	-0.0107599	0.0000001				0.0000046
36	GLOBAL	-0.0107435	0.0000001				0.0005108
38	GLOBAL	-0.0099038	0.0000228				-0.0000019
39	GLOBAL	-0.0090476	0.0000002				0.0000028
40	GLOBAL	-0.0090376	0.0000002				0.0004044
42	GLOBAL	-0.0082091	0.0000024				-0.0000014
43	GLOBAL	-0.0073706	-0.0000000				0.0000026

44	GLOBAL	-0.0073613	-0.0000000	0.0003343
46	GLOBAL	-0.0065472	0.0000023	-0.0000013
47	GLOBAL	-0.0057237	-0.0000007	0.0000024
48	GLOBAL	-0.0057152	-0.0000007	0.0002676
49	GLOBAL	-0.0033462	-0.0000006	0.0002508
50	GLOBAL	-0.0000538	-0.0000001	0.0000418
52	GLOBAL	-0.0049130	0.0000165	-0.0000010
53	GLOBAL	-0.0041021	-0.0000023	0.0000010
54	GLOBAL	-0.0040987	-0.0000023	0.0001782
55	GLOBAL	-0.0025169	-0.0000019	0.0001686
56	GLOBAL	-0.0000327	-0.0000002	0.0000257
58	GLOBAL	-0.0032991	0.0000002	-0.0000007
59	GLOBAL	-0.0024961	-0.0000024	0.0000098
60	GLOBAL	-0.0024934	-0.0000023	0.0001116
62	GLOBAL	-0.0016978	0.0000083	-0.0000005
63	GLOBAL	-0.0008991	-0.0000024	-0.0000001
64	GLOBAL	-0.0008995	-0.0000024	0.0000386
66	GLOBAL	-0.0001022	0.0000031	-0.0000003
67	GLOBAL	0.0006949	-0.0000026	-0.0000005
68	GLOBAL	0.0006930	-0.0000026	-0.0000283
70	GLOBAL	0.0014934	0.0000047	-0.0000002
71	GLOBAL	0.0022922	-0.0000029	-0.0000011
72	GLOBAL	0.0022881	-0.0000028	-0.0000849
74	GLOBAL	0.0030930	-0.0000121	-0.0000004
75	GLOBAL	0.0038933	-0.0000056	-0.0000005
76	GLOBAL	0.0038915	-0.0000056	-0.0000808
78	GLOBAL	0.0046949	0.0000017	-0.0000005
79	GLOBAL	0.0054970	-0.0000043	-0.0000010
80	GLOBAL	0.0054933	-0.0000043	-0.0001344
82	GLOBAL	0.0063008	-0.0000043	-0.0000005
83	GLOBAL	0.0071045	-0.0000032	-0.0000010
84	GLOBAL	0.0071010	-0.0000032	-0.0001696
86	GLOBAL	0.0078981	0.0000032	-0.0000005
87	GLOBAL	0.0086922	0.0000004	-0.0000013
88	GLOBAL	0.0086873	0.0000004	-0.0002334
90	GLOBAL	0.0094904	0.0000061	-0.0000003
91	GLOBAL	0.0102891	0.0000005	-0.0000018
92	GLOBAL	0.0102826	0.0000005	-0.0003001
94	GLOBAL	0.0110955	0.0000056	-0.0000001
95	GLOBAL	0.0119024	0.0000009	-0.0000022
96	GLOBAL	0.0118945	0.0000008	-0.0003372
97	GLOBAL	0.0088788	0.0000007	-0.0003294
98	GLOBAL	0.0000435	0.0000001	-0.0000322
100	GLOBAL	0.0123989	-0.0000154	-0.0000005
101	GLOBAL	0.0128939	0.0000024	0.0000000
102	GLOBAL	0.0128941	0.0000024	-0.0003729
104	GLOBAL	0.0133921	0.0000605	0.0000007
105	GLOBAL	0.0138959	-0.0000034	-0.0000080
106	GLOBAL	0.0138673	-0.0000034	-0.0004555

108	GLOBAL	0.0146356	-C.C003130	-C.CC00042
109	GLCBAL	0.0153461	0.0030138	C.CC00213
110	GLOBAL	0.0154229	C.C000136	-C.CC06472
112	GLOBAL	0.0160152	C.C013683	0.CC00202
113	GLOBAL	0.0168071	-0.C000036	-C.CC01079
114	GLOBAL	0.0164186	-C.C000035	-C.CC13792
116	GLOBAL	0.0178746	-0.0029162	-C.CC00163
117	GLOBAL	0.0187165	C.CC00100	C.CC01688
118	GLOBAL	0.0193242	C.C000099	-C.0008658
120	GLOBAL	0.0204785	-C.CC04893	C.CC02220
121	GLOBAL	0.0221946	C.C000298	C.CC02206
122	GLCBAL	0.0229842	C.0000294	-C.CC10656
124	GLOBAL	0.0231779	C.C019627	0.CC01516

VITA

Ramzi Behnam Abdul-Ahad was born in Mosul, Iraq, on October 13, 1948. He attended The University of Mosul where he received the degree of Bachelor of Science in Civil Engineering in June, 1969. Following his undergraduate study, he then worked as a teacher's assistant at The University of Mosul from 1969 to 1975.

In January, 1975, the author was awarded an academic scholarship from the Ministry of Higher Education and Scientific Research in Baghdad, Iraq. Following that he began his graduate work leading to a Master of Science in Civil Engineering at The University of Tennessee, Knoxville. He was awarded this degree in August of 1976.

He attended the University of California at Davis from September, 1976, to November, 1977. Following that, he resumed studies at The University of Tennessee, Knoxville, leading to the Doctor of Philosophy degree with a major in Civil Engineering, until the present. He was awarded this degree in June of 1981.

The author is a member of the Prestressed Concrete Institute and American Concrete Institute. He also is a registered Civil Engineer in Iraq.

He is married to Araksi Melkonian. They have two daughters, Lena and Linda.